

## Contents

### Talks

<b>1 Instruments and Methods</b>	<b>3</b>
T-1 Detection of Lithium traces in organic samples at the PGAA station . . . . .	3
T-2 Novel in situ electric field setup for studying structural aspects of ferroelectrics . . . . .	4
T-3 Concentration fluctuations in itinerant ferromagnets: Radiography with Polarized Neutrons	5
T-4 Larmor Diffraction in Antiferromagnetic and Ferromagnetic Superconductors . . . . .	6
<b>2 Magnetism and Dynamics</b>	<b>7</b>
T-5 Energy and temperature dependence of antiferromagnetic spin fluctuations in electron-doped iron arsenide superconductors . . . . .	7
T-6 Magnetic-Field-Induced Soft-Mode Quantum Phase Transition in $\text{La}_{1.855}\text{Sr}_{0.145}\text{CuO}_4$ . . . . .	8
T-7 Magnetic excitation spectra of two-dimensional weakly-frustrated $S=1/2$ antiferromagnet on a square lattice $\text{Cu}(\text{pz})_2(\text{ClO}_4)_2$ . . . . .	9
T-8 Skyrmion Lattice in $\text{MnSi}$ . . . . .	10
<b>3 Material Science</b>	<b>11</b>
T-9 In-situ neutron diffraction measurement in Co-Re alloys to study the stability of carbides at high temperatures . . . . .	11
T-10 Radiology of wood, differently seen with fast neutrons . . . . .	12
T-11 Anisotropic elastic vs. pseudoplastic deformation in uniaxially loaded NiTi . . . . .	13
T-12 Hydrogen-induced defects in Pd films . . . . .	14
<b>4 Soft Matter</b>	<b>15</b>
T-13 Structure and Dynamics of Thermoresponsive Blockcopolymer Gels . . . . .	15
T-14 Structure and Dynamics of Sugar Surfactant Based Microemulsions . . . . .	16
T-15 Dissolution of amphiphiles: a time- and space-resolved neutron imaging study . . . . .	17
T-16 Interfacial mobility and switching in polymeric brushes . . . . .	18
T-17 Correlated positron-electron emission from surfaces . . . . .	19
<b>Posters</b>	<b>21</b>
<b>5 Biology and Biophysics</b>	<b>23</b>
P-1 Reflectometry studies of supported lipid bilayers: recent progress at REFSANS . . . . .	23
P-2 X-ray and neutron reflectivity study of tethered membranes . . . . .	24
P-3 Denaturation of horse heart met-myoglobin by guanidinium hydrochloride studied by Small Angle Neutron Scattering spectroscopy . . . . .	25
<b>6 Instruments and Methods</b>	<b>27</b>
P-4 The new backscattering spectrometer SPHERES after its first year of full operation: status, highlights, perspectives . . . . .	27
P-5 Novel sample environment for activation and preparation of solid catalyst materials provided for neutron diffraction measurements at the FRM II . . . . .	28
P-6 Time-of-flight grazing incidence small angle neutron scattering on Gd nanowires . . . . .	29
P-7 J-NSE: The Jülich Neutron Spin-Echo Spectrometer at the FRM II . . . . .	30

P-8 SANS-1, the new Small-Angle Neutron Scattering instrument at Forschungs-Neutronenquelle Heinz Maier-Leibnitz (FRM II) . . . . .	31
P-9 Measurement of the full anisotropy of the elastic response of NiTi shape memory alloy . . . . .	32
P-10 Application of $^3\text{He}$ Neutron Spin Filters for neutron polarization analysis . . . . .	33
P-11 High efficient neutron diffractometer Stress-Spec for texture analysis . . . . .	34
P-12 SPODI: structural investigation of materials under special environmental conditions . . . . .	35
P-13 Feature of the PGAA instrument at FRMII . . . . .	36
P-14 3D Elemental Imaging of Cultural Heritage Objects at the PGAA Station at FRM II . . . . .	37
P-15 The N-REX <sup>+</sup> reflectometer . . . . .	38
P-16 The New Protein Single Crystal Diffractometer at the FRM II . . . . .	39
P-17 Spherical Neutron Polarimetry (SNP) on POLI-HEiDi diffractometer at FRM II . . . . .	40
P-18 The NRSE spectrometer RESEDA and first experiments . . . . .	41
P-19 NECTAR: Radiography and Tomography Using Fission Neutrons . . . . .	42
P-20 Upgrade of the Very Small Angle Neutron Scattering Instrument KWS-3 and Future Scientific Perspectives . . . . .	43
P-21 Improved focussing on RESI using neutron guides . . . . .	44
P-22 N-REX <sup>+</sup> . . . . .	45
P-23 MIRA - New options . . . . .	46
P-24 HEiDi and its Applications . . . . .	47
P-25 Surface and Bulk Investigations at the High Intensity Positron Beam Facility NEPOMUC . . . . .	48
P-26 The Time-of-Flight spectrometer TOFTOF at the FRM II . . . . .	49
<b>7 Nuclear and Particle Physics</b>	<b>51</b>
P-27 Neutron capture on Ge-76: A background in neutrinoless double beta decay experiments . . . . .	51
P-28 New experiment on the neutron radiative decay . . . . .	52
P-29 The new beamline MEPHISTO in the east neutron guide hall . . . . .	53
P-30 ROT-effect in angular distribution of prompt fission $\gamma$ rays . . . . .	54
<b>8 Material Science</b>	<b>55</b>
P-31 Influence of Secondary Extinction on Pole Figures Measurement by Neutron Diffraction . . . . .	55
P-32 Directional Coarsening in Polycrystalline Superalloys . . . . .	56
P-33 The Advancement of Work on Inert Matrix Fuel (Third Part) . . . . .	57
P-34 Global and local texture analysis at Stress-Spec . . . . .	58
P-35 The Potential of the Horizontal ToF-Neutron Reflectometer REFSANS at FRM II Munich Highlighted by Recent Experimental Results . . . . .	59
P-36 Synthesis and characterisation of nitrogen doped ZnO particles by prompt gamma activation analysis (PGAA) . . . . .	60
P-37 Application of PGAA for elemental analysis of carbonaceous sedimentary rocks . . . . .	61
P-38 Measurement of internal strain by neutron powder diffraction in core-shell $\text{Ni}_3\text{Si}(\text{Al})\text{-SiO}_x$ nanoparticles . . . . .	62
<b>9 Magnetism and Dynamics</b>	<b>63</b>
P-39 Magnetische Struktur des Kompositkristalls $\text{Ca}_2\text{Nd}_2\text{Cu}_5\text{O}_{10}$ . . . . .	63
P-40 High Resolution Spectroscopy and Diffraction at TRISP . . . . .	64
P-41 Recent results on PANDA . . . . .	65
P-42 Critical Magnetic Behaviour and Magnetocaloric Effect in $\text{PrMn}_2\text{Ge}_2$ -Based Materials . . . . .	66
P-43 Spin Torque Effects in a Helical Magnet . . . . .	67
P-44 Emergence of helimagnons bands in $\text{MnSi}$ . . . . .	68
P-45 Skyrmion Lattice in $\text{Fe}_{1-x}\text{Co}_x\text{Si}$ . . . . .	69
P-46 Ferromagnetic Quantum Phase Transition in $\text{Pd}_{1-x}\text{Ni}_x$ . . . . .	70
P-47 Spin Liquid and Spin Ice . . . . .	71
P-48 Crystallographic and magnetic study of synthetic cobalt-olivine single crystal . . . . .	72
P-49 Magnetic structure in multiferroic pyroxenes: $(\text{Na,Li})\text{FeSi}_2\text{O}_6$ . . . . .	73

<b>10 Radiography and Tomography</b>	<b>75</b>
P-50 Quantitative Neutron Radiography and Tomography at NECSA . . . . .	75
P-51 Phase-Contrast and Dark-field Imaging with Neutrons . . . . .	76
<b>11 Structure</b>	<b>77</b>
P-52 Microscopic Suppression of Training and Origin of Training Effect in Exchange Bias System	77
P-53 Aggregation of mixed surfactant system by SANS method . . . . .	78
P-54 GISANS study of sponge-like TiO <sub>2</sub> structures for photovoltaic applications . . . . .	79
P-55 Development of C-S-H Microstructure in UHPC with QENS, <sup>29</sup> Si NMR and XRD . . . . .	80
P-56 Structural investigation of Dy <sub>2</sub> CuIn <sub>3</sub> . . . . .	81
P-57 AMPOrAe A program for crystallographic, magnetic and amorphous diffraction pattern analysis . . . . .	82
P-58 Characterization of PMDEGA hydrogel films . . . . .	83
P-59 PLEPS investigation of binary Fe-Cr model alloys . . . . .	84
P-60 SANS contrast dependence on difference in thermal expansions of phases in two-phase alloys . . . . .	85
P-61 Lattice dynamics in ferromagnetic shape memory alloys . . . . .	86
P-62 Hydrogen-related defects in ZnO single crystals . . . . .	87
P-63 Temperature and composition dependence of the crystal and magnetic structures of La <sub>2-x</sub> Sr <sub>x</sub> CoIrO <sub>6</sub> (0 < x < 2) . . . . .	88
<b>12 Structural Dynamics</b>	<b>89</b>
P-64 Phonon lifetimes and superconductivity in Pb-Bi alloys . . . . .	89
P-65 Tunnelling of methyl protons in poly-substituted benzenes . . . . .	90
<b>13 Soft Matter</b>	<b>91</b>
P-66 A SANS investigation of sodium salt effects on dodecyl phosphocholine micelles . . . . .	91
P-67 Structural control of conjugated block copolymer films via addition of homopolymer . . . . .	92
P-68 Characterization and swelling kinetics of PNIPAM based block copolymer films . . . . .	93
P-69 Structural investigation of diblock copolymer thin films using TOF-GISANS . . . . .	94
P-70 Experiments at the neutron reflectometer REFSANS to study supported phospholipid bilayers systems . . . . .	95
P-71 Spinodal decomposition of PNIPAM solutions investigated with time-resolved SANS . . . . .	96
<b>Index</b>	<b>97</b>

**Talks**

## 1 Instruments and Methods

### T-1 Detection of Lithium traces in organic samples at the PGAA station.

Roman Gernhäuser<sup>1</sup>, Josef Lichtinger<sup>1</sup>

<sup>1</sup>TU München, Physik Department E12, Germany

**Abstract was obliterated by request of the authors.**

### T-2 Novel in situ electric field setup for studying structural aspects of ferroelectrics

Manuel Hinterstein<sup>1</sup>, Markus Hoelzel<sup>3</sup>, Norbert Jünke<sup>2</sup>, Hartmut Fieß<sup>1</sup>

<sup>1</sup>TU Darmstadt, Institute of Materials Science, Germany

<sup>2</sup>Universität Göttingen, Physikalische Chemie, Germany

<sup>3</sup>TU Darmstadt, Institute of Materials Science, Germany  
TU Darmstadt at Forschungs-Neutronenquelle Heinz Maier-Leibnitz (FRM II), München, Germany

Ferroelectrics play an important role for many applications like sensors and actuators. Among those materials  $\text{PbZr}_{1-x}\text{Ti}_x\text{O}_3$  (PZT) and lead free  $\text{Bi}_{0.5}\text{Na}_{0.5}\text{TiO}_3$  play a major role.

To understand the poling behaviour of ferroelectrics with respect to atomic displacement and temperature factors, full pattern powder diffraction is mandatory. This has been done for in situ studies with X-rays [1] but due to the limited geometry and low information for the oxygen atoms equivalent neutron measurements are desirable, but in literature only single reflection analysis has been reported for in situ neutron diffraction.

For the SPODI diffractometer a new setup has been built for in situ application of electric fields up to 7 kV/mm. The possible usage of large sample thickness and closed sample environments allowed the construction of a setup with no geometrical handicaps. In contrast to X-ray setups the electric field is perpendicular to the incident beam as well as the plane of diffraction avoiding angular dispersive gradients of the electric field in the diffraction pattern.

First measurements document the pronounced response to the electric field of morphotropic PZT and novel lead free ferroelectrics. The results from SPODI will be discussed together with in situ measurements conducted at the synchrotron beamlines B2 in Hamburg (DESY) and MS in Villigen (SLS). A new approach of combined refinement of X-ray and neutron data enhances the information density and combines the advantages of both techniques.

[1] K. A. Schönau, M. Knapp, H. Kungl, M. J. Hoffmann, and H. Fuess, Physical Review B 76, 144112 (2007).

### T-3 Concentration fluctuations in itinerant ferromagnets: Radiography with Polarized Neutrons

Michael Schulz<sup>1</sup>, Peter Böni<sup>1</sup>, Elbio Calzada<sup>1</sup>, Christian Franz<sup>1</sup>, Andreas Neubauer<sup>1</sup>, Martin Mühlbauer<sup>1</sup>, Christian Pfeiderer<sup>1</sup>, André Hilger<sup>2</sup>, Nikolay Kardjilov<sup>2</sup>

<sup>1</sup>TU München, Physik Department E21, Germany

<sup>2</sup>Helmholtz-Zentrum Berlin für Materialien und Energie, Germany

The depolarization of a neutron beam passing through a ferromagnet crucially depends on the magnetic properties of the sample. Combining neutron depolarisation measurements with neutron radiography allows obtaining spatially resolved information about these properties. For measuring the depolarization, we have installed a longitudinal polarized beam setup at the ANTARES beamline consisting of <sup>3</sup>He polarizers and flat coil spin flippers.

With this setup we have performed radiography with polarized neutrons in the weak itinerant ferromagnets Pd<sub>1-x</sub>Ni<sub>x</sub> in order to determine the spatial distribution of the Curie temperatures  $T_C$  in the samples. The results show that the single crystals are rather inhomogeneous showing large variations in  $T_C$ . The data allows firstly to cut out small crystals with improved homogeneity for neutron scattering experiments and secondly to provide feedback for improving the growth techniques for the crystals. In the future we hope to use the potential of this method to map out magnetic domains across large volume samples.

### T-4 Larmor Diffraction in Antiferromagnetic and Ferromagnetic Superconductors

Robert Ritz<sup>1</sup>, Dmitry Sokolov<sup>2</sup>, Philipp Niklowitz<sup>3</sup>, Thomas Keller<sup>4</sup>, Andrew Huxley<sup>2</sup>, Andrej Prokofiev<sup>5</sup>, Ernst Bauer<sup>5</sup>, Christian Pfeiderer<sup>1</sup>

<sup>1</sup>TU München, Physik Department E21, Germany

<sup>2</sup>University of Edinburgh, School of Physics and Centre for Science at Extreme Conditions, United Kingdom

<sup>3</sup>University of London, Department of Physics, United Kingdom

<sup>4</sup>MPI für Festkörperforschung, Stuttgart, Germany

<sup>5</sup>TU Wien, Fakultät für Physik, Austria

It was traditionally thought that neutron spin-echo measurements cannot be used in materials such as superconductors or ferromagnets, because they strongly depolarize a polarized neutron beam.

We have used Larmor diffraction, a novel neutron resonance spin-echo technique (see e.g. [1]), to explore the magnetic properties, lattice constants and the distribution of lattice constants in the antiferromagnetic heavy fermion superconductor CePt<sub>3</sub>Si and the ferromagnetic superconductor UGe<sub>2</sub>. In our study of CePt<sub>3</sub>Si we observe an unusually wide range of lattice parameters for the a-axis with  $\Delta a/a \approx 10^{-4}$ , revealing a possible microscopic origin of the enhanced superconducting transition temperature observed in this compound. These data also shed new light on the unusual pressure dependence of the antiferromagnetic and superconducting transition temperatures.

Further, by means of a Larmor diffraction study under high hydrostatic pressures in UGe<sub>2</sub> we are able to demonstrate that this technique may even be applied in ferromagnetic superconductors with a magnetic Ising anisotropy.

[1] C. Pfeiderer, P. Böni, T. Keller, U. K. Rößler, A. Rosch *Science* **316**, 1817 (2007).

## 2 Magnetism and Dynamics

### T-5 Energy and temperature dependence of antiferromagnetic spin fluctuations in electron-doped iron arsenide superconductors

Dmytro Inosov<sup>1</sup>, Jitae Park<sup>1</sup>, Philippe Bourges<sup>2</sup>, Yvan Sidis<sup>2</sup>, Dunlu Sun<sup>1</sup>, Astrid Schneidewind<sup>3</sup>, Klaudia Hradil<sup>3</sup>, Daniel Haug<sup>1</sup>, Chengtian Lin<sup>1</sup>, Bernhard Keimer<sup>1</sup>, Vladimir Hinkov<sup>1</sup>

<sup>1</sup>MPI für Festkörperforschung, Stuttgart, Germany

<sup>2</sup>CEA Saclay, Laboratoire Léon Brillouin, Gif-sur-Yvette, France

<sup>3</sup>Forschungs-Neutronenquelle Heinz Maier-Leibnitz (FRM II), München, Germany

The phase diagram of layered iron arsenides is dominated by the immediate vicinity or even coexistence of superconductivity and antiferromagnetism. In addition, a “resonance peak” was recently observed – a pile-up of antiferromagnetic spectral weight in the superconducting state. This apparent similarity to the cuprate high-temperature superconductors has fostered speculations about a far-reaching analogy of the underlying physics and a common origin of superconductivity in both families.

Using inelastic neutron scattering (INS), we have studied the spin-excitation spectrum of the high-quality electron-doped  $\text{BaFe}_{2-x}\text{Co}_x\text{As}_2$  single crystals in a broad energy and temperature range. Unlike in the cuprates, the temperature evolution of the resonance peak and the shape of the normal-state spectrum of antiferromagnetic spin fluctuations are in good agreement with those expected for a weak itinerant antiferromagnet, without any signatures of strong electron correlations.

### T-6 Magnetic-Field-Induced Soft-Mode Quantum Phase Transition in $\text{La}_{1.855}\text{Sr}_{0.145}\text{CuO}_4$

Niels Bech Christensen<sup>1</sup>, Johan Chang<sup>2</sup>, Christof Niedermayer<sup>2</sup>, Kim Lefmann<sup>3</sup>, Henrik Rønnow<sup>4</sup>, Des McMorrow<sup>5</sup>, Astrid Schneidewind<sup>6</sup>, Peter Link<sup>6</sup>, Arno Hiess<sup>7</sup>, Martin Boehm<sup>7</sup>, Rafael Mottl<sup>2</sup>, Stephane Pailhes<sup>2</sup>, Naoki Momono<sup>8</sup>, Migaku Oda<sup>8</sup>, Masayuki Ido<sup>8</sup>, Joel Mesot<sup>2</sup>

<sup>1</sup>Risø National Laboratory, Materials Research Division, Denmark

<sup>2</sup>PSI, Laboratory for Neutron Scattering, Villigen, Switzerland

<sup>3</sup>University of Copenhagen, Niels Bohr Institute, Nano-Science Center, Denmark

<sup>4</sup>Ecole Polytechnique Federale de Lausanne, Laboratory for Quantum Magnetism, Switzerland

<sup>5</sup>University College London, London Centre for Nanotechnology and Department of Physics and Astronomy, UK

<sup>6</sup>Forschungs-Neutronenquelle Heinz Maier-Leibnitz (FRM II), München, Germany

<sup>7</sup>ILL, Grenoble, France

<sup>8</sup>Hokkaido University, Department of Physics, Sapporo, Japan

Inelastic neutron-scattering experiments - conducted in part at the PANDA triple-axis spectrometer at FRM II - on the high-temperature superconductor  $\text{La}_{1.855}\text{Sr}_{0.145}\text{CuO}_4$  reveal a magnetic excitation gap that decreases continuously upon application of a magnetic field perpendicular to the  $\text{CuO}_2$  planes. The gap vanishes at the critical field required to induce long-range incommensurate antiferromagnetic order, providing compelling evidence for a field-induced soft-mode driven quantum phase transition. We discuss the relation of our results to experiments performed on other cuprate high-temperature superconductors as well as their relation to theory and numerical work [1].

[1] J.Chang et al, <http://arxiv.org/abs/0902.1191> and references therein. Accepted in Phys. Rev. Letters (2009).

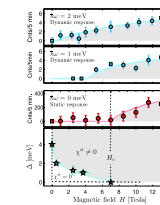


Figure 2.1: Magnetic field dependence of incommensurate inelastic [(a)-(b)] and elastic [(c)] scattering in  $\text{La}_{1.855}\text{Sr}_{0.145}\text{CuO}_4$ . (d) Field dependence of the excitation gap, falling off with increasing field and dropping to zero at the onset field for static magnetic order, coexisting with superconductivity.

## T-7 Magnetic excitation spectra of two-dimensional weakly-frustrated S=1/2 antiferromagnet on a square lattice $\text{Cu}(\text{pz})_2(\text{ClO}_4)_2$

Nikolay Tsyulin<sup>1</sup>, Fan Xiao<sup>2</sup>, Astrid Schneidewind<sup>3,4</sup>, Peter Link<sup>4</sup>, Matthew Woodward<sup>2</sup>, Henrik Rønnow<sup>5</sup>, Christopher Landee<sup>2</sup>, Mark Turnbull<sup>6</sup>, Michel Kenzelmann<sup>7</sup>

<sup>1</sup>PSI, Laboratory for Neutron Scattering, Villigen, Switzerland; ETH Zurich, Laboratory for Solid State Physics, Switzerland

<sup>2</sup>Clark University, Department of Physics, Worcester, USA

<sup>3</sup>TU Dresden, Institut für Festkörperphysik, Germany

<sup>4</sup>Forschungs-Neutronenquelle Heinz Maier-Leibnitz (FRM II), München, Germany

<sup>5</sup>Ecole Polytechnique Fédérale de Lausanne, Switzerland

<sup>6</sup>Clark University, Carlson School of Chemistry and Biochemistry, Worcester, USA

<sup>7</sup>ETH Zurich, Laboratory for Solid State Physics, Switzerland; PSI, Laboratory for Developments and Methods, Villigen, Switzerland

We present a neutron scattering study of spin dynamics in a weakly frustrated S=1/2 two-dimensional (2D) antiferromagnet (AF) on a square lattice  $\text{Cu}(\text{pz})_2(\text{ClO}_4)_2$ . The measurements were performed using the cold-neutron three-axes spectrometer PANDA. A gapped one-magnon mode at the AF zone center was observed and explained with the presence of a small XY exchange anisotropy. The gap energy was studied as a function of the applied magnetic field up to H=12T and showed a linear dependence. Measurements of the magnetic excitation spectra along the AF zone boundary revealed 10.7(4)% dispersion of a one-magnon mode and a magnetic continuum scattering. Both features originate from a resonating valence bond quantum fluctuations between nearest neighbor spins. The observed dispersion is slightly larger than expected from calculations for 2D Heisenberg AF on a square lattice with nearest neighbor interactions. We interpret the experimental results with a presence of a small AF next nearest neighbor interaction that enhances quantum fluctuations in the system. An applied magnetic field renormalizes the excitation spectra and suppresses the energy of magnon. The excitation spectrum at H=12T features two well defined magnetic modes: a gapped one-magnon mode and a Goldstone mode, that indicates unbroken rotational spin symmetry. Our results show that quantum fluctuations are supported by 2D S=1/2 AF on a square lattice and enhanced by a small additional interaction.

[1] N. Tsyulin, T. Pardini, R. R. P. Singh, F. Xiao, P. Link, A. Schneidewind, A. Hiess, C. P. Landee, M. M. Turnbull, and M. Kenzelmann, accepted by Phys. Rev. Lett. [2] F. M. Woodward, P. J. Gibson, G. B. Jameson, C. P. Landee, M. M. Turnbull and R. D. Willett, Inorg. Chem., 46, 4256-4266 (2007).

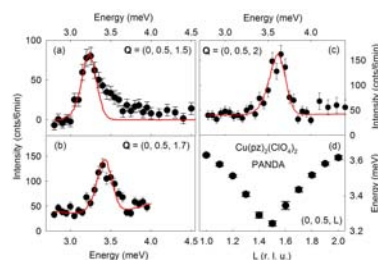


Figure 2.2: (a-c) The constant wave-vector scans performed at the AF zone boundary. The red curves are the fits of a Gaussian function convoluted with the instrumental resolution function. Subplot (a) shows the magnetic continuum scattering above the magnon mode. (d) The AF zone boundary dispersion measured at zero magnetic field.

## T-8 Skyrmion Lattice in MnSi

Sebastian Mühlbauer<sup>1</sup>, Florian Jonietz<sup>1</sup>, Benedikt Binz<sup>2</sup>, Christian Pfleiderer<sup>1</sup>, Achim Rosch<sup>2</sup>, Andreas Neubauer<sup>1</sup>, Robert Georgii<sup>3</sup>, Peter Böni<sup>1</sup>

<sup>1</sup>TU München, Physik Department E21, Germany

<sup>2</sup>Universität zu Köln, Institut für Theoretische Physik, Germany

<sup>3</sup>Forschungs-Neutronenquelle Heinz Maier-Leibnitz (FRM II), München, Germany

Skyrmions represent topologically stable field configurations with particle-like properties.

We use neutron scattering at MIRA, FRM II, to observe the spontaneous formation of a two-dimensional lattice of skyrmion lines, a type of magnetic vortices, in the chiral itinerant-electron magnet MnSi [1]. The skyrmion lattice stabilizes at the border between paramagnetism and long-range helimagnetic order perpendicular to a small applied magnetic field – regardless of the direction of the magnetic field relative to the atomic lattice.

Our study experimentally establishes magnetic materials lacking inversion symmetry as an arena for new forms of crystalline order composed of topologically stable spin states.

[1] Mühlbauer, S., Binz, B., Jonietz, F., Pfleiderer, C., Rosch, A., Neubauer, A., Georgii, R., Böni, P. Science, 323(5916), (2009), 915-919.

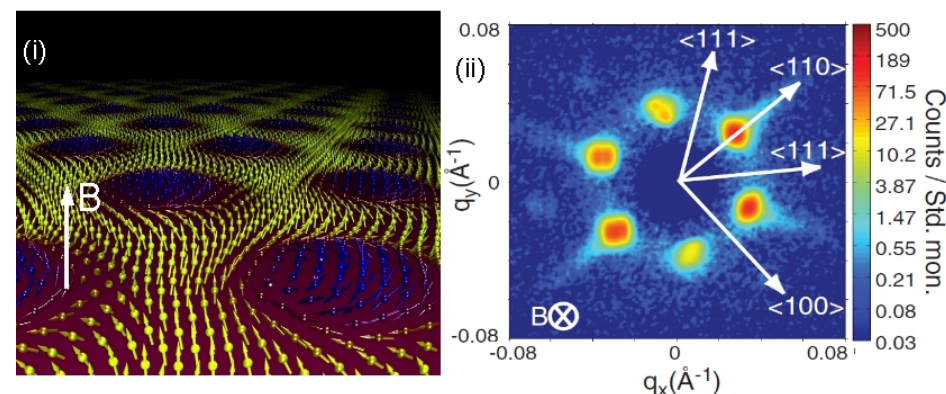


Figure 2.3: Panel (i): Real space depiction of the spin structure of the skyrmion line lattice. Note that the depiction shows a cut through the skyrmion line lattice in a plane perpendicular to the applied magnetic field. Panel (ii) Typical neutron scattering pattern of MnSi, obtained at MIRA, FRM II. A scattering pattern obtained in the A-Phase, characterized by the skyrmion line lattice is shown.

### 3 Material Science

#### T-9 In-situ neutron diffraction measurement in Co-Re alloys to study the stability of carbides at high temperatures

Debashis Mukherji<sup>1</sup>, Pavel Strunz<sup>2</sup>, Michael Hofmann<sup>3</sup>, Ralph Gilles<sup>3</sup>, Joachim Rösler<sup>1</sup>

<sup>1</sup>TU Braunschweig, Institut für Werkstoffe, Germany

<sup>2</sup>Nuclear Physics Institute, Neutron Physics Laboratory, Rez, Czech Republic

<sup>3</sup>Forschungs-Neutronenquelle Heinz Maier-Leibnitz (FRM II), München, Germany

New high temperature materials are needed to substitute Ni-base superalloys above 1200°C. Co-Re based alloys are being developed at IfW, TU Braunschweig as a new generation high temperature alloy. Re (high melting point) forms a continuous solid solution with Co and increases melting point of Co-alloys. Various hardening mechanisms are being explored in Co-Re-Cr-C system; in which precipitation strengthening by carbides is an important one. Microstructural characterization of experimental Co-Re alloys shows presence of various carbides depending on the alloy composition. In the quaternary alloy Co-Re-Cr-C (alloy CoReL1), Cr<sub>23</sub>C<sub>6</sub> was identified. Amongst other morphologies the carbides also form as fine plates, like the pearlite structure in carbon-steels. Unlike that in the conventional Co-alloys (where the matrix is fcc), in Co-Re alloy the matrix is hcp phase. When Ta is added to the alloy (alloy CoReL2), additionally, TaC (MC type) carbides also form as a fine dispersion (100 nm cubes) between the lamellar Cr-carbides. For application in gas turbine the long term stability of the microstructure and the mechanical property are important. The microstructural stability, particularly the stability of carbides at high temperatures, was studied through in-situ diffraction measurements at the Stress-Spec instrument at FRM II. The main aim of the present measurement was to observe the evolution of phases, particularly TaC, at 1200°C in CoReL2 alloy. A standard furnace was used for high temperature measurement. The preliminary evaluation shows that the amount of Cr<sub>23</sub>C<sub>6</sub> carbide decreases while sigma phase appears and increases its amount quickly after 1200°C is reached. TaC carbide is relatively stable but also its volume fraction seems slowly to increase with the exposure time.

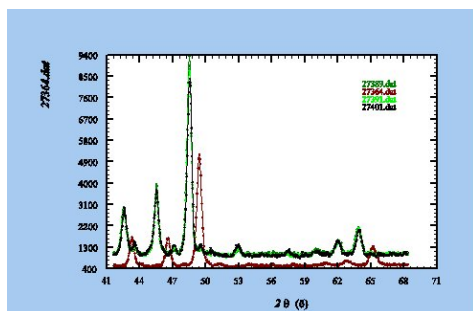


Figure 3.1: 27364=RT measurement; 27389, 27391 and 27401= measurement at 1200°C and after 0h, 2h and 15h respectively.

#### T-10 Radiology of wood, differently seen with fast neutrons

Kurt Osterloh<sup>1</sup>, Mirko Jechow<sup>1</sup>, Uwe Zscherpel<sup>1</sup>, Uwe Ewert<sup>1</sup>, Thomas Bücherl<sup>2</sup>, Andreas Hasenstab<sup>3</sup>

<sup>1</sup>BAM Federal Institute for Materials Research and Testing, Berlin, Germany

<sup>2</sup>TU München, Institut für Radiochemie, Germany

<sup>3</sup>Remmers Fachplanung GmbH, Lönningen, Germany

Wood is a material with distinct and individual features, highly structured depending on the particular origin, its exposure to environmental conditions and its usage. As compared to more homogenous, mostly man-made materials, damages impairing the mechanical stability may be disguised underneath the natural structures. Moreover, certain indications such as cracks have to be interpreted individually in position and dimensions if their detection requires further actions or not. Even worse, some kind of damages may be hardly detected while reducing the mechanical stability by more than 80 %, i. e. in cases of fungal rot or microbial degradation of glued layers. The common denominator in the course of such impairments is moisture because water is a prerequisite of any biological degradation. Unless a cavity is formed, there are problems to identify non-destructively rotten areas by their altered matrix structures.

The fact that neutrons are efficiently interacting with hydrogen was the rationale to consider using them for radiological imaging particularly contrasting the hydrogen content. Image artefacts occurring as white spots were successfully removed with an own dedicated algorithm. Employing the fast neutron beam of the NECTAR facility of the FRM II, samples of up to nearly 50 cm layer thickness of wood have been successfully penetrated. Certain structural features appeared with a different contrast as compared to images generated with X-rays. Further digital refinement procedures such as applying filtering with automatic noise recognition revealed more structural details indicating putative changes in the wooden matrix. Tomography allowed studying certain features more in detail which appear only faintly in a plain radiographic image (see figure). Heterogeneities within the glued layers of gluelam could be detected even in large specimens. As a consequence, neutrons reveal different details than other radiological methods and should therefore be regarded as a complementary one rather than a replacement.

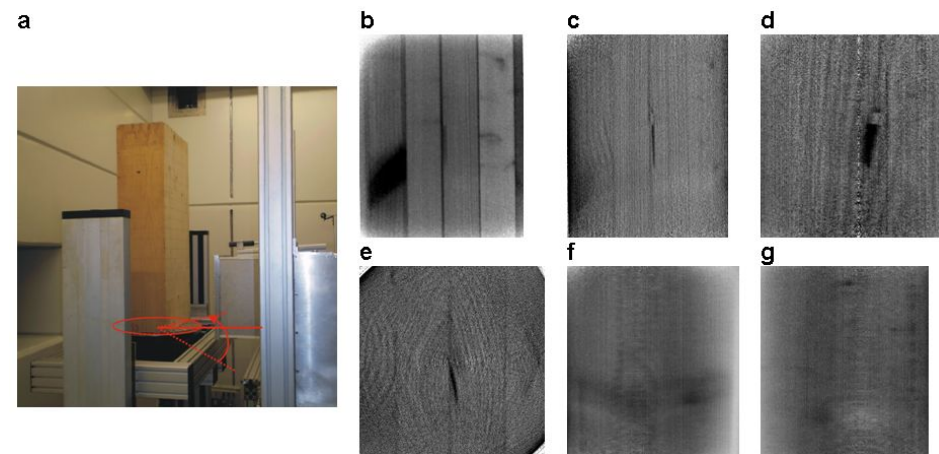


Figure 3.2: Tomography of a gluelam specimen with restricted projections (-45° to +45°). a) experimental setup indicating the angle covered by the directions of projections, b) plane radiography from the central position, i.e. perpendicular to the surface, c) central inclusion viewed parallel to the beam direction, d) same perpendicular to the beam direction, e) view from top, f) glued layer left to the centre with heterogeneities, g) glued layer right to the centre, again with signs of heterogeneity.

## T-11 Anisotropic elastic vs. pseudoplastic deformation in uniaxially loaded NiTi

Wolfgang Schmahl<sup>1</sup>

<sup>1</sup>LMU München, Geo-Department, Sektion Kristallographie, Germany

## T-12 Hydrogen-induced defects in Pd films

Jakub Cizek<sup>1</sup>, Ivan Prochazka<sup>1</sup>, Oksana Melikhova<sup>1</sup>, Gerhard Brauer<sup>2</sup>, Wolfgang Anwand<sup>2</sup>, Werner Egger<sup>3</sup>, Peter Sperr<sup>3</sup>, Christoph Hugenschmidt<sup>4</sup>, Ryota Gemma<sup>5</sup>, Astrid Pundt<sup>5</sup>, Reiner Kirchheim<sup>5</sup>

<sup>1</sup>Charles University in Prague, Faculty of Mathematics and Physics, Czech Republic

<sup>2</sup>FZ Dresden-Rossendorf, Germany

<sup>3</sup>Universität der Bundeswehr München, Institut für Angewandte Physik und Messtechnik, Neubiberg, Germany

<sup>4</sup>Forschungs-Neutronenquelle Heinz Maier-Leibnitz (FRM II), München, Germany

<sup>5</sup>Universität Göttingen, Fakultät für Physik, Germany

Hydrogen loading causes a significant volume expansion, which is isotropic in free-standing bulk materials. Contrary to bulk samples, thin films are clamped to an elastically stiff substrate which prevents the in-plane expansion. Hence, hydrogen loaded thin film may expand only in the out-of-plane direction. Hence, hydrogen-induced expansion of thin films is strongly anisotropic and very high compressive in-plane stresses (in the GPa range) are introduced by hydrogen loading. As a consequence, lattice defects may be created in thin films loaded with hydrogen.

This work reports about defects created by hydrogen loading in epitaxial Pd films deposited on Al<sub>2</sub>O<sub>3</sub> substrates by cold cathode beam sputtering. Hydrogen-induced defects are characterized by positron annihilation spectroscopy performed on variable energy slow positron beams. Extended studies of defect depth profile and its development with increasing concentration of hydrogen were performed by measurement of Doppler broadening of annihilation profile using a continuous positron beam. Selected states were subsequently investigated by positron lifetime spectroscopy on a pulsed positron beam PLEPS. Firstly, the microstructure of virgin films is characterized. Subsequently, the hydrogen concentration in the films was increased step-by-step by electrochemical charging. The development of the film microstructure and the evolution of defects were investigated.

It was found that virgin films contain already a high density of defects: positrons are trapped at misfit dislocations located mainly close to the interface with the substrate. In addition, larger vacancy clusters were found. Hydrogen loading introduces new defects identified as dislocations created by plastic deformation initiated by hydrogen-induced stresses or by growing hydride particles.

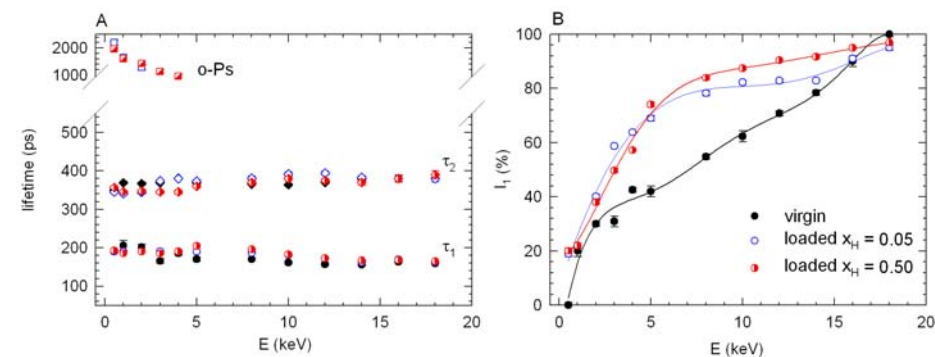


Figure 3.3: Results of positron lifetime (LT) investigations of Pd films: (A) positron lifetimes resolved in LT spectra, (B) intensity of the shorter component attributed to misfit dislocations as a function of positron energy. The following states were measured: virgin film (full symbols) and films loaded with hydrogen up to concentration  $x_H = 0.05$  (open symbols) and  $x_H = 0.50$  (half filled symbols). Solid lines are polynomial fits to guide the eye only

## 4 Soft Matter

### T-13 Structure and Dynamics of Thermoresponsive Blockcopolymer Gels

Joseph Adelsberger<sup>1</sup>, Andreas Meier-Koll<sup>1</sup>, Weinan Wang<sup>1</sup>, Thomas Hellweg<sup>2</sup>, Olaf Holderer<sup>3</sup>, Peter Busch<sup>3</sup>, Vitaliy Pipich<sup>3</sup>, Achille Mayelle Bivigou Koumba<sup>4</sup>, André Laschewsky<sup>4</sup>, Peter Müller-Buschbaum<sup>1</sup>, Christine M. Papadakis<sup>1</sup>

<sup>1</sup>TU München, Physik Department E13, Germany

<sup>2</sup>Universität Bayreuth, Physikalische Chemie I, Germany

<sup>3</sup>Jülich Centre for Neutron Science, Outstation at FRM II, München, Germany

<sup>4</sup>Universität Potsdam, Institut für Chemie, Germany

Thermoresponsive polymer gels display strong changes in volume when heated above the lower critical solution temperature (LCST). They are thus attractive candidates as sensors or actuators. We investigate triblock copolymers consisting of two hydrophobic polystyrene (PS) end blocks and a hydrophilic, thermoresponsive poly-N-isopropyl-acrylamide (PNIPAM) middle block. In aqueous solution, these copolymers form core-shell micelles or micellar networks. Physically crosslinked thermoresponsive gels constitute an attractive alternative to chemically crosslinked networks [1]. The structure of the micelles and their correlation has been determined using small-angle neutron scattering (SANS) at KWS 2 [2]. Both for 5 wt% and 17 wt% solutions, the micellar radius shows a sudden decrease at the LCST due to the shrinkage of the thermoresponsive shell. Above the LCST, the collapsed micelles form clusters. Neutron spin-echo spectroscopy (NSE) at J-NSE and dynamic light scattering have been used to study the segmental dynamics of the thermoresponsive shell block and the micellar diffusion coefficient in the same solutions. Below the LCST, the averaged diffusion coefficient of the PNIPAM block is temperature-independent and decreases with increasing polymer concentration. Above the LCST, for both concentrations, the same values for the diffusion coefficient of segmental dynamics are observed. SANS and NSE thus allow a detailed characterization of self-organized thermoresponsive networks.

[1] K. Troll, C. M. Papadakis et al., *Colloid Polym. Sci.* 286, 1079 (2008); W. Wang, C. M. Papadakis, P. Müller-Buschbaum et al., *Macromolecules* 41, 3209 (2008); W. Wang, C. M. Papadakis, P. Müller-Buschbaum et al., *Macromol. Rapid Commun.* 30, 140 (2009); A. Bivigou Koumba, A. Laschewsky, *Macromol. Chem. Phys.* 210, 565 (2009) [2] A. Jain, C. M. Papadakis et al., *Macromol. Symp.*, submitted

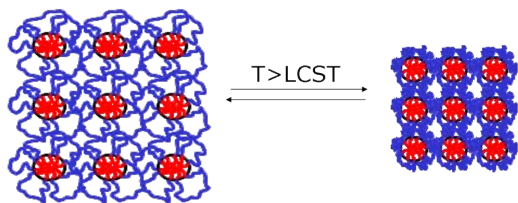


Figure 4.1: Schematics of network formation by self-assembly of the triblock copolymers and the network collapse.

### T-14 Structure and Dynamics of Sugar Surfactant Based Microemulsions

Thomas Hellweg<sup>1</sup>

<sup>1</sup>Universität Bayreuth, Physikalische Chemie I, Germany

Sugar surfactant based microemulsions are environment friendly and exhibit only rather low temperature dependence of the phase behavior. In these systems the curvature of the interfacial film can be tuned using the addition of alcohols like e.g. pentanol [1]. Hence, these systems are well suited to follow the change of the bending dynamics of the surfactant film as a function of the temperature  $T$ . In the present contribution SANS and neutron spin echo data for this kind of microemulsion are presented.  $T$  is varied in the range from 283,15 K to 315 K. The outcome is compared to predictions of the Zilman-Granek model for undulation dynamics of surfactant films.

[1] Wellert, S.; Karg, M.; Imhof, H.; Steppin, A.; Altmann, H.-J.; Richardt, A.; Tiersch, B.; Koetz, J.; Hellweg, T.; Structure of biodiesel based bicontinuous microemulsions for environmentally compatible decontamination: A small angle neutron scattering and freeze fracture electron microscopy study, *J. Colloid and Interf. Sci.* 325:250-258 (2008)

## T-15 Dissolution of amphiphiles: a time- and space-resolved neutron imaging study

Helen E. Hermes<sup>1</sup>, Stefan U. Egelhaaf<sup>1</sup>, Burkhard Schillinger<sup>2</sup>, Michael Schulz<sup>2</sup>, Anders Kästner<sup>3</sup>, Gabriel Frei<sup>3</sup>, Eberhard Lehmann<sup>3</sup>

<sup>1</sup>Universität Düsseldorf, Physik der weichen Materie, Germany

<sup>2</sup>Forschungs-Neutronenquelle Heinz Maier-Leibnitz (FRM II), München, Germany

<sup>3</sup>PSI, Laboratory for Neutron Scattering, Villigen, Switzerland

In solution, amphiphiles such as lipids and copolymers can self-assemble into a variety of structures. When a droplet of such an amphiphile is contacted with water, the osmotic pressure difference results in an influx of water which causes a dynamic change in the concentration-dependent structure. Currently, our main interest in this process is to develop a fundamental experimental picture of how solvent diffuses into and dissolves a droplet. To date, much information has been obtained using optical techniques. However, the optical transmission of a sample is dependent on both concentration and structure so that it is not possible to differentiate between changes in these. Recently, it has become possible to quantitatively determine the evolution of the microscopic concentration profiles using neutron imaging. Due to latest technical improvements in this method, time- and space-resolved water profiles can now be determined in-situ with a resolution of a few tens of micrometers and seconds.

In this presentation, we will discuss some of our data from lipid and copolymer systems obtained using neutron imaging.

## T-16 Interfacial mobility and switching in polymeric brushes

Sebastian Lenz<sup>1</sup>, Adrian Rühm<sup>2</sup>, Rüdiger Berger<sup>1</sup>, Jochen S. Gutmann<sup>1</sup>

<sup>1</sup>MPI für Polymerforschung, Mainz, Germany

<sup>2</sup>MPI für Metallforschung, Stuttgart, Germany

End tethered polymer brushes can be used to create switchable surfaces. The properties of such surfaces are dependent from the solvent quality. Polymer brushes are collapsed in bad solvents and swollen in good solvents. Brush thicknesses and related polymer brush solvent uptake can be measured in situ with Neutron Reflectivity (NR). We focused on the swelling behavior poly-methyl-meth-acrylate (PMMA) brushes. To tune the solvents swelling quality towards the PMMA several mixtures of a deuterated bad solvent (d4-MeOH) and a deuterated good solvent (d6-THF) were chosen in the performed studies. As expected the PMMA brush thickness and fraction of total solvent in the brush phase increased with an increase in solvent quality. However, comparing NR results with theory [1] showed that the PMMA brush could include about 2 times the amount of bad solvent than predicted by theory. It was previously shown [2] that the solvents quality on PMMA brushes also influence the brushes surface stress, which can be related to the systems Gibbs energy. Surface stresses can be monitored, when the PMMA brushes are synthesized on thin flexible Nano Mechanical Cantilever (NMC) substrates. NMC bending experiments showed that the surface stress in the PMMA brush is decreases proportional to the inverse of the total solvent fraction in the PMMA brush

[1] T. M. Birshtein and Y. V. Lyatskaya, *Macromolecules* 27, 1256-1266 (1994). [2] G. G. Bumbu, M. Wolkenhauer, G. Kircher, J. S. Gutmann, and D. Berger, *Langmuir* 23, 2203-2207 (2007).

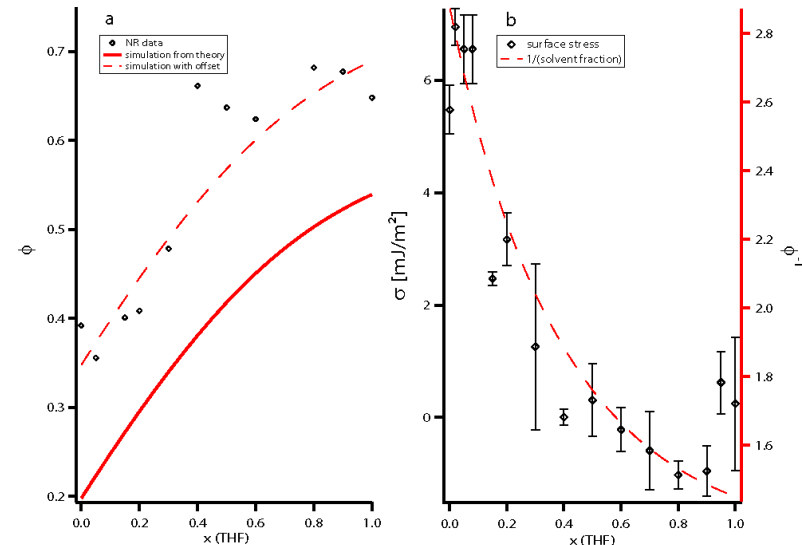


Figure 4.2: a) solvent fraction  $\phi$  in PMMA brush; comparison of NR data with theory (red straight line), red dashed line shows an offset of  $\sim 0.15$ ; b) comparison of surface stresses  $\sigma$  in PMMA brush with  $\phi - 1$

## T-17 Correlated positron-electron emission from surfaces

**Frank Oliver Schumann<sup>1</sup>, Grant van Riessen<sup>1</sup>, Michael Birke<sup>1</sup>, Carsten Winkler<sup>1</sup>, Jürgen Kirschner<sup>1</sup>**

<sup>1</sup>MPI für Mikrostrukturphysik, Halle, Germany

Electrons in a solid do not move independent from each other. The Pauli principle demands that two electrons with parallel spins can not be at the same location. The Coulomb interaction makes it energetically unfavorable for electrons to be close to each other. This constitutes the concept of the exchange-correlation (xc) hole.

Our electron pair emission studies demonstrate that this concept is an experimental reality. In these experiments a primary electron or photon hits a surface and emits an electron pair. In order to disentangle the different contributions to the xc-hole, one should use as primary particle a positron and study the positron-electron pair emission. In this case one does not need to consider the Pauli principle. Because of this motivation we performed the first experiment, which demonstrates that the impact of a positron causes indeed the emission of a positron-electron pair. We used the NEPOMUC facility together with a pair of hemispherical analyzers operated with a coincidence circuit. As target we selected a LiF(100) surface, which was hit with 85 eV primary positrons.

We find that the emission of positron-electron pairs is time correlated. The energy distributions show that we also have a contribution where the ejected valence band electron originates from the valence band.

**Posters**

## 5 Biology and Biophysics

### P-1 Reflectometry studies of supported lipid bilayers: recent progress at REFSANS

**Bert Nickel<sup>1</sup>, Stefan Stanglmaier<sup>1</sup>, Samira Hertrich<sup>1</sup>, Kirstin Fritz<sup>1</sup>, Joachim Rädler<sup>1</sup>**  
<sup>1</sup>LMU München, Fakultät für Physik, Experimentalphysik, Germany

We have employed Refsans at FRM II to study the nanostructure of supported lipid bilayers. In order to find the optimal experimental setting, various chopper configurations have been tested to compare resolution and flux with the expected values. Using contrast variation, spontaneous insertion of glycolipids from micellar phase into SLBs could be observed, as well as an asymmetric distribution of charged lipids on a SiO<sub>2</sub> surface. These experiments show that Refsans is able to yield insight into subtle structural changes in lipid bilayers. Experiments have been performed with strong support from M. Haese-Seiller and R. Kampmann, GKSS.

### P-2 X-ray and neutron reflectivity study of tethered membranes

**Samira Hertrich<sup>1</sup>, Bert Nickel<sup>1</sup>**

<sup>1</sup>LMU München, Fakultät für Physik, Experimentalphysik, Germany

Tethered membranes, i.e. lipid bilayers which are chemically grafted to an interface, are a versatile way to add biofunctionality to a biologically passive surface. In order to provide a biomimetic environment for membrane proteins, the tethered membrane should provide a certain degree of mechanical softness and diffusivity, which is usually tuned by the proper choice of the cushion layer interfacing the lipid bilayer with the inert interface.

Here, we employ a multi-step chemical reaction to fabricate tethered membranes [1]. First, the silicon oxide surface is functionalized with silanes (VTS). This VTS monolayer is oxidized and PEG2000-lipids are added to this layer using NHS chemistry. Then these PEG2000-lipids are embedded in a lipid bilayer which is deposited by spin coating and subsequent hydration.

The diffusivity of the lipid bilayer is verified by fluorescence microscopy techniques. It is possible to determine layer thicknesses and scattering length densities of the sample from x-ray and neutron reflectivity measurements. Three different techniques are performed that complement each other: synchrotron x-ray reflectivity provides high flux and high resolution, the x-ray reflectometer setup in the lab offers flexibility to vary pH and ionic concentrations systematically, and neutron reflectivity measurements at FRM II give additional information about the hydration of the interlayer and protein insertion efficiency.

Synchrotron measurements performed at selected pH (pH = 4, 7, and 10) show a compression of the PEG interlayer at pH 10 from 7 nm to 5 nm, indicating that the interlayer is highly deformable.

[1] C. Daniel, K.E. Sohn, T.E. Mates, E.J. Kramer, J.O. Rädler, E. Sackmann, B. Nickel, L. Andruzzi, Structural Characterization of an Elevated Lipid Bi-Layer Obtained by Stepwise Functionalization of a Self-Assembled Alkenyl Silane Film, *Biointerphases* 2 109 (2007)

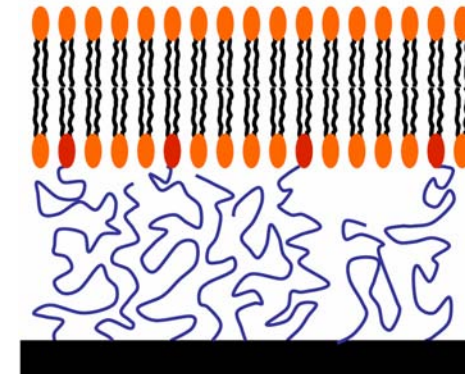


Figure 5.1: Lipid bilayer on a PEG cushion grafted to the silicon oxide surface.

### **P-3 Denaturation of horse heart met-myoglobin by guanidinium hydrochloride studied by Small Angle Neutron Scattering spectroscopy**

**Marie-Sousai Appavou<sup>1</sup>, Dieter Richter<sup>2</sup>**

<sup>1</sup>Jülich Centre for Neutron Science, Outstation at FRM II, München, Germany

<sup>2</sup>FZ Jülich GmbH, Institut für Festkörperforschung, Germany

A protein can be assumed as a heteropolymer composed by a sequence of amino acid residues which have different chemical properties.

According to their position along the main backbone, they induce a specific folding into secondary (alpha helix, beta sheet, turns ...) and tertiary structures related to the function of the protein [1]. Proteins acquire this tridimensional native structure in few seconds probably because they do not explore all the space conformations. Indeed, some parts of the proteins fold more quickly than others and lead to folding intermediates.

In the frame of understanding the folding of proteins, we have investigated the unfolding of a model system: the horse heart myoglobin which is essentially composed by helical structures. Guanidinium hydrochloride was used as denaturing agent at several concentrations in order to get some of the folding intermediates of this protein. Denaturation studies have already been performed on this system since 1968 by visible spectroscopy studies and circular dichroism [2].

It was shown that myoglobin denaturation lead to several intermediates with specific characteristics in terms of heme release and partial helical structures conservation. By using Small Angle Neutron Scattering techniques, we play with the contrast between the hydrogenated protein and the deuterated solvent. The SANS spectroscopy can allow to access these folding intermediate by applying polymer physics theory [3, 4].

These folding intermediates are characterized at low q values by the radius of gyration extrapolated at null concentration in the Guinier regime [5] and by intermolecular interactions using the Zimm approximation [6] and at higher q-values using the Kratky representation [7] of the scattered intensity and on which we apply models describing the behavior of the protein under different denaturing conditions [8].

[1] C.B. Anfinsen, Science, 181, 273 (1973) [2] A.N. Schechter et C.J. Epstein J Mol Biol. 35, 567 (1968) [3] P.J. Flory, J Chem. Phys. 17, 303 (1949) [4] C. Tandford, Adv. Prot. Chem., 23, 121-282 (1968) [5] A. Guinier et G. Fournet, Small Angle Scattering of X-Rays (1955) [6] B.H.Zimm J. Chem. Phys., 16, 1093-1099 (1948) [7] J.S. Pedersen and P. Schurtenberger, Macromol., 29, 7602-7612 (1996) [8] M. Kataoka et al, Protein Sci. 6, 422-430 (1997)

## 6 Instruments and Methods

### P-4 The new backscattering spectrometer SPHERES after its first year of full operation: status, highlights, perspectives

Joachim Wuttke<sup>1</sup>, Gerald J. Schneider<sup>1</sup>

<sup>1</sup>Jülich Centre for Neutron Science, Outstation at FRM II, München, Germany

SPHERES is a third-generation backscattering spectrometer. Focussing optics and a phase-space transform chopper give us high flux, a very good signal-to-noise ratio (SNR=600:1 since fall 2008), and an excellent resolution (<650neV). Since winter 2007/8, SPHERES is available to external users. Successful experiments have been performed in quite different fields: hydrogen storage, confined water, polymer and protein dynamics, molecular rotations, nuclear spin excitations.

Further optimization of the instrument is currently being prepared by extensive calculations. In particular, a new chopper will bring a considerable improvement of flux and SNR.

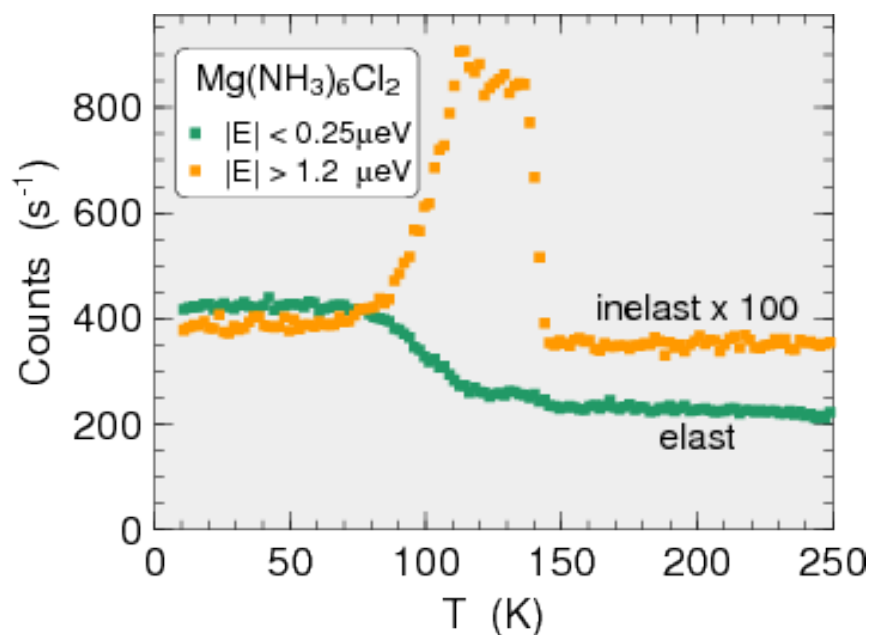


Figure 6.1: Traditionally, during temperature scans at backscattering spectrometers only the elastic scattering is recorded. The high flux at SPHERES allows us to monitor the inelastic intensity as well. In this example, a phase transition shows up much more clearly in the inelastic than in the elastic signal. By the same token, SPHERES can be used for kinetic experiments.

### P-5 Novel sample environment for activation and preparation of solid catalyst materials provided for neutron diffraction measurements at the FRM II

Stephan J. Reitmeier<sup>1</sup>, Oliver C. Gobin<sup>1</sup>, Andreas Janus<sup>1</sup>, Andreas Jentys<sup>1</sup>, Markus Hoelzel<sup>2</sup>, Hartmut Fueß<sup>3</sup>, Wolfgang Schmahl<sup>4</sup>, Johannes A. Lercher<sup>1</sup>

<sup>1</sup>TU München, Department Chemie, Technische Chemie 2, Germany

<sup>2</sup>TU Darmstadt at Forschungs-Neutronenquelle Heinz Maier-Leibnitz (FRM II), München, Germany

<sup>3</sup>TU Darmstadt, Materialwissenschaft, Germany

<sup>4</sup>LMU München, Lehrstuhl für anorganische und biogene Geomaterialien, Germany

A novel sample environment for either ex-situ or in-situ preparation of catalytically active materials and sorbents which are designated for neutron diffraction measurements at the SPODI has been designed. The designed apparatus is planned to be used for experiments aiming to provide a more general understanding of the catalytic structure activity relations using industrially relevant catalyst samples in contact with organic sorbate molecules and reactants. The system (see Figure) is equipped with UHV vacuum pumps (2 turbomolecular drag pumps and a rotary vane pump) and an optional mass spectrometer unit (Pfeiffer Prisma QMS200). A separate sorbate dosing unit with three independent valve lines allows for activation and preparation procedures at low sorbate coverages with partial pressures below  $10^{-2}$  mbar as well as at elevated pressures up to 1.0 bar. Six pressure gauges are installed to monitor and maintain accurately the sorbate partial pressures.

The system can additionally be used to prepare a series of five samples ex-situ in parallel under controlled conditions, which will be sequentially analyzed, but can also be directly connected to the existing SPODI experimental setup thus enabling the study of sorption processes under reaction conditions in situ. Herein, we want to give an overview on this novel developed sample environment by shortly sketching possible future applications, especially when combined with the already existing SPODI facility at the FRM II for in-situ neutron scattering experiments. First experiments with activated HZSM-5 as standard reference material were already carried. Additional experiments are planned and will comprise the commissioning of the whole system in both operation modes and the testing of new types of sample containers and, the implementation of the novel experimental procedure at the SPODI using zeolite catalyst materials.

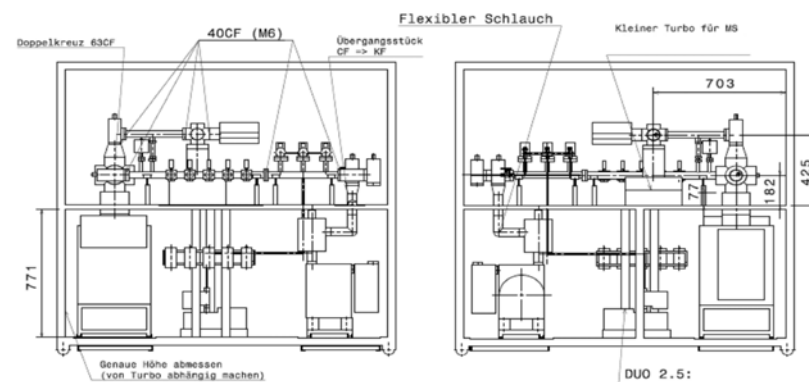


Figure 6.2: Scheme showing front and back view of the novel instrument for activation and preparation of solid catalyst materials for neutron diffraction measurements.

## P-6 Time-of-flight grazing incidence small angle neutron scattering on Gd nanowires

Wolfgang Kreuzpaintner<sup>1</sup>, Jean-François Moulin<sup>1</sup>, Dieter Lott<sup>1</sup>, Reinhard Kampmann<sup>1</sup>, Martin Haese-Seiller<sup>1</sup>, Michael Störmer<sup>1</sup>, Andreas Schreyer<sup>1</sup>

<sup>1</sup>GKSS-Forschungszentrum Geesthacht, Germany

A Gd nanowire grating with a periodicity of approximately 225nm prepared on a faceted sapphire substrate was investigated by Time-Of-Flight Grazing Incidence Small Angle Neutron Scattering using REFSANS at the FRM II neutron source.

The technique and its advantage of faster data acquisition by use of a continuous neutron wavelength spectrum over a single wavelength setup in investigating a periodically laterally structured sample by GISANS are presented.

The measurements allowed to obtain information on the critical wavelength, the reflected and transmitted intensities and also allowed a reconstruction of large portions of the grating truncation rods in reciprocal space. Results were obtained for various orientations around the sample normal and compared with a theoretical model, showing good agreement.

[1] W. Kreuzpaintner, J.-F. Moulin, D. Lott, R. Kampmann, M. Haese-Seiller, M. Störmer, and A. Schreyer, Eur. Phys. J. Special Topics 167, 73-79 (2009); and references therein

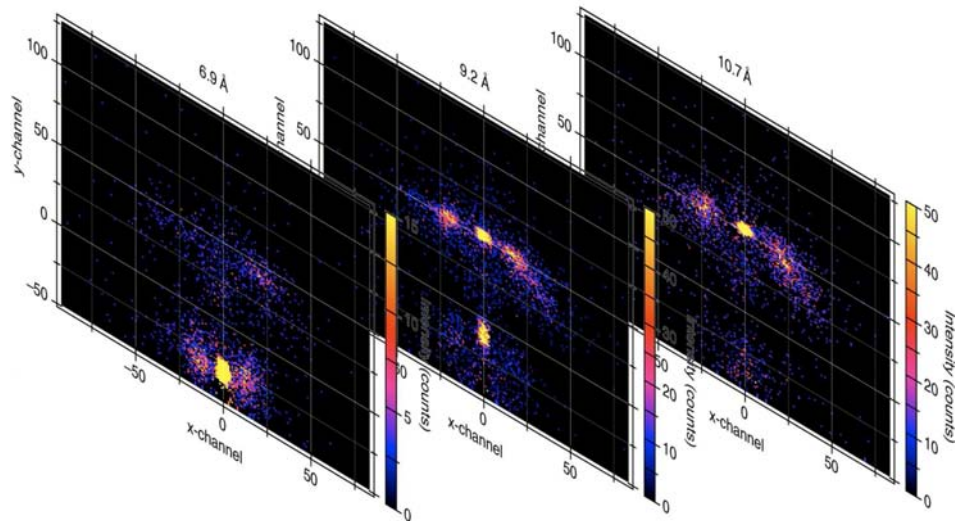


Figure 6.3: Detector images for a single wavelength slice which are extractable by the Time-Of-Flight information collected for each neutron. Shown are the detector images for wavelengths of  $\lambda = 6.9\text{\AA}$  (below the critical wavelength),  $9.2\text{\AA}$  (at the critical wavelength) and  $10.7\text{\AA}$  (above the critical wavelength).

## P-7 J-NSE: The Jülich Neutron Spin-Echo Spectrometer at the FRM II

Olaf Holderer<sup>1</sup>, Nicolas R. de Souza<sup>1</sup>, Michael Monkenbusch<sup>2</sup>, Dieter Richter<sup>1</sup>

<sup>1</sup>Jülich Centre for Neutron Science, Outstation at FRM II, München, Germany

<sup>2</sup>FZ Jülich GmbH, Institut für Festkörperforschung, Germany

Neutron spin echo (NSE) spectroscopy is due to its high energy resolution a well-suited method for studying slow dynamics, such as the dynamics of soft matter systems (glasses, polymers and complex liquids), or paramagnetic properties of e.g. spin glasses.

After the relocation from the FRJ-2 to the new FRM II reactor, the Jülich Neutron Spin-Echo Spectrometer J-NSE recommenced operation in 2007 and is accessible for external users since.

The spectrometer is positioned at the end of a neutron guide, giving access to a broad band of incident wavelengths between 4.5 and 19 Å. This, together with new correction elements in the two main precession coils, results in a significant increase in dynamic range [1,2]. The high incident flux of polarized neutrons provided by the neutron guide system leads to a gain in intensity compared to the setup in Jülich of a factor of 15 for the same wavelength of 8 Å as in Jülich.

A paramagnetic setup has been installed which allows separating magnetic and nuclear scattering in paramagnetic experiments. We will present the new characteristics of the instrument and first experiments in different fields of physics carried out at J-NSE spectrometer.

[1] O. Holderer et al., Nucl.Instr.Meth.A, 586, 90 (2008) [2] O. Holderer et al., Meas. Sci. Technol. 19, 034022 (2008)

## P-8 SANS-1, the new Small-Angle Neutron Scattering instrument at Forschungs-Neutronenquelle Heinz Maier-Leibnitz (FRM II)

Ralph Gilles<sup>1</sup>, Andreas Schreyer<sup>2</sup>, Winfried Petry<sup>1</sup>

<sup>1</sup>Forschungs-Neutronenquelle Heinz Maier-Leibnitz (FRM II), München, Germany

<sup>2</sup>GKSS-Forschungszentrum Geesthacht, Germany

The new small-angle scattering instrument SANS-1, a project of the Technische Universität München and the GKSS in Geesthacht is currently build at the new Forschungsneutronenquelle Heinz Maier-Leibnitz, FRM II. This contribution describes the concept, the technical features, and the currently status of the instrument. To optimise the SANS-1 instrument with the claim to be at the “state of the art” many calculations and variations of instrument parameters were performed by Monte Carlo simulations in advance. Results of these simulations are a vertical S-shaped neutron guide with extreme suppression of fast background neutrons optimized for complementary wavelength packages, a tower with two eligible selectors, one for medium resolution at high intensity and one for high resolution (optional) and two optimised Fe/Si transmission polarizers. After passing the selector tower a collimation system with four parallel horizontal tracks is installed, one track is occupied with a neutron guide, another one with apertures for improving resolution, one position is for a laser system to support alignment and the last one is equipped with background apertures and could be used for lenses. The detector tube of around 2.4 m inner diameter allows to use an area detector of 1 x 1 m<sup>2</sup> with lateral movement of more than 0.5 m. The detector is equipped with 128 position sensitive detectors to provide 8 mm x 8 mm pixel resolution. It is planned to install a second detector behind this large area detector for measurements simultaneously at low q-values.

[1] R. Gilles, A. Ostermann, C. Schanzer, B. Krimmer, W. Petry, 2006, Physica B, 385-386, 1174. [2] R. Gilles, A. Ostermann, W. Petry, 2007, J. Appl. Cryst., 40, s428.



Figure 6.4: Fig. 1: The magenta coloured detector tank of SANS-1 in preparation for the vacuum test.

## P-9 Measurement of the full anisotropy of the elastic response of NiTi shape memory alloy

Casjen Merkel<sup>1</sup>, Wolfgang Schmahl<sup>1</sup>, Markus Hoelzel<sup>2</sup>, Günther Seidl<sup>2</sup>, Michael Hofmann<sup>2</sup>

<sup>1</sup>LMU München, Kristallographie, Germany

<sup>2</sup>Forschungs-Neutronenquelle Heinz Maier-Leibnitz (FRM II), München, Germany

We constructed a mechanical loading frame in which the stress-axis can be rotated in a chi-circle and on the omega-circle of the instrument, in such a way that longitudinal, transverse and intermediate relations between stress-axis and observed lattice planes can be realized.

Martensitic twin reorientations allow deformed NiTi alloys to recover their pristine shape by thermal treatment. This shape memory effect is based on deformation by ferroelastic switching of the twin domain structure of the monoclinic phase under stress. This twin structure remains stable when the stress is released. Heating transforms the material into the cubic B2 phase. This phase transforms to the monoclinic phase with random twinning, recovering the original shape upon cooling in a stress-free environment.

High resolution neutron diffraction is required to access the crystallographic properties and textures of these alloys. Rietveld refinement using the spherical harmonics description for the texture adjustment allows us to obtain the phase state and lattice parameters of coarse grained polycrystalline samples as used in industrial applications with high accuracy. We used the newly constructed loading frame and obtained stress related lattice parameter variations in the  $1 \times 10^{-3}$  range while the macroscopic tensile strain along the load axis is up to 4.5%.

## P-10 Application of $^3\text{He}$ Neutron Spin Filters for neutron polarization analysis

Sergey Masalovich<sup>1</sup>

<sup>1</sup>Forschungs-Neutronenquelle Heinz Maier-Leibnitz (FRM II), München, Germany

Polarized  $^3\text{He}$  Neutron Spin Filters (NSF) make a great impact on the instrumentation for neutron polarization and polarization analysis since polarized nuclei of  $^3\text{He}$  possess very high spin-dependent neutron absorption efficiency over a wide range of neutron energies. The straight-line passage of a neutron beam through a NSF with no change of a neutron trajectory enables one to measure a neutron polarization for nearly any divergent scattered beam.

Furthermore, the NSFs offer homogeneous analyzing efficiency with a predictable value, predictable transmission, a negligible small angle scattering from a  $^3\text{He}$  cell and a low gamma-ray background produced. Taken together these features make NSF technique extremely useful in applications such as neutron imaging with polarization analysis, small-angle neutron scattering, off-specular reflectometry and large solid angle polarization analysis. When necessary, NSF allows for a very precise measurement of a neutron beam polarization either with an opaque spin filter or with a recently proposed 2x1 NSF.

Experiments performed with the use of  $^3\text{He}$  NSFs at FRM II and other neutron centers will be presented.

## P-11 High efficient neutron diffractometer Stress-Spec for texture analysis

Christian Randau<sup>1</sup>, Heinz-Günter Brokmeier<sup>1</sup>, Michael Hofmann<sup>2</sup>, William Tekouo<sup>3</sup>, W.M. Gan<sup>4</sup>, Martin Müller<sup>4</sup>, Andreas Schreyer<sup>4</sup>

<sup>1</sup>TU Clausthal, Institut für Werkstoffkunde und Werkstofftechnik, Germany

<sup>2</sup>Forschungs-Neutronenquelle Heinz Maier-Leibnitz (FRM II), München, Germany

<sup>3</sup>TU München, Produktionstechnisches Anwenderzentrum für den Mittelstand, Germany

<sup>4</sup>GKSS-Forschungszentrum Geesthacht, Germany

The materials science diffractometer Stress-Spec, which is operated by a joint cooperation among GKSS, HZB, TU München and TU Clausthal, is configured either for stress or texture analysis. A combining analysis on global texture, local texture, strain pole figure and FWHM pole figure can be performed by flexible configuration and sample environment. Especially, the high neutron flux makes it more attractive for local texture analysis.

The new instrument control environment "openInspire" provides data detection time synchronously to move of all axes. This allows the newly developed continuous pole figure measurement method, which can eliminate the positioning time and reduce the measuring time down to 40%. Secondly, 100% measurement of grains in the gauge volume can be obtained. A newly developed robot and laser tracker system is under construction, which can realize automatic sample changing and its precise positioning. Hence, Stress-Spec is now in a good stand for high efficient and precise texture analysis.

## P-12 SPODI: structural investigation of materials under special environmental conditions

Markus Hoelzel<sup>1</sup>, Anatoliy Senyshyn<sup>1</sup>, Norbert Jünke<sup>2</sup>, Hans Boysen<sup>3</sup>, Wolfgang Schmahl<sup>3</sup>, Hartmut Fueß<sup>4</sup>

<sup>1</sup>TU Darmstadt at Forschungs-Neutronenquelle Heinz Maier-Leibnitz (FRM II), München, Germany

<sup>2</sup>Uni Göttingen at Forschungs-Neutronenquelle Heinz Maier-Leibnitz (FRM II), München, Germany

<sup>3</sup>LMU München, Kristallographie, Germany

<sup>4</sup>TU Darmstadt, Institute of Materials Science, Germany

The high-resolution powder diffractometer SPODI is designed to refine structural parameters in complex systems. During 2008, the efficiency of the instrument was improved by upgrades of the monochromator unit and data evaluation procedure. Beyond high angular resolution and excellent profile shape the diffractometer SPODI provides also a variety of environmental conditions. The standard sample environment of FRM II, namely closed-cycle cryostat, high-temperature furnace and closed-cycle-5T-magnet is available. In addition, special environment conditions for materials characterisation are developed in collaborations between the project team of SPODI, our co-operation partners and FRM II.

A rotatable loading frame has been constructed and set into operation which enables an orientation of the load axis with respect to the scattering plane. Mechanical hysteresis loops on nickel-titanium shape memory alloys have been applied at different orientations to study texture development and the strain tensor elements.

To understand the poling mechanisms in ferroelectrics, a device for high electric fields was developed and used for lead titanate zirconate  $\text{PbZr}_{1-x}\text{Ti}_x\text{O}_3$  (PZT) samples (up to 7 kV/mm). A multi channel potentiostat is available, allowing to study a lithium battery in-operando. The phase transformation behaviour of hydrogen storage materials during uptake and release of deuterium has been investigated at different deuterium pressures up to 70 bar and temperatures up to 250 °C. A device for the gas loading of catalysers was set into operation and will be available on SPODI in the near future.

In addition to the tools for special environmental conditions and examples of materials characterisation, we report on upgrades of the instrument and statistics in the user operation.

## P-13 Feature of the PGAA instrument at FRMII

Lea Canella<sup>1</sup>, Petra Kudejova<sup>2</sup>, Ralf Schulze<sup>3</sup>, Jan Jolie<sup>3</sup>, Andreas Türler<sup>1</sup>

<sup>1</sup>TU München, Institut für Radiochemie, Germany

<sup>2</sup>Forschungs-Neutronenquelle Heinz Maier-Leibnitz (FRM II), München, Germany

<sup>3</sup>Universität zu Köln, Institut für Kernphysik, Germany

The NL4b neutron guide at the Forschungsneutronenquelle Heinz-Maier Leibnitz (FRM II) in Garching is dedicated to a new Prompt Gamma-ray Activation Analysis (PGAA) instrument. PGAA is a non-destructive radioanalytical technique for the determination of the elemental composition of samples under analysis. The main characteristic of this facility is the elliptical tapered cold neutron beam that allows to reach high neutron flux values at the sample position. Moreover, at the facility two different kind of set-up are available:

- A set-up for standard PGAA, with a wide choice of irradiation conditions;
- A set-up for Prompt Gamma-ray Activation Imaging, i.e. position sensitive PGAA, and Neutron Tomography (PGAI-NT).

The first set-up allows the determination of the elemental composition in a bulk sample, while with the second set-up the three dimensional distribution of elements inside a solid object can be studied and correlated to the internal structure of the sample thanks to the NT instrumentation.

First comprehensive analysis with PGAA, PGAI and NT techniques at the research reactor FRM II was tested on a piece of the Allende meteorite. With the PGAA method the bulk elemental composition of the heterogeneous meteorite was determined. Due to the small dimension of the sample, only the 2D elemental distribution of the object was derived with position sensitive PGAI analysis. Neutron tomography of the meteorite was carried out with the same cold neutron beam.

[1] Kudejova P., Meierhofer G., Zeitelhack K., Jolie J., Schulze R., Türler A., Materna T., 2008. The new PGAA and PGAI facility at the research reactor FRM II in Garching near Munich. *J. Radioan. Nucl. Chem.* 278. [2] Canella L., Kudejova P., Schulze R., Türler A., Jolie J.. PGAA, PGAI and NT with cold neutrons: test measurement on a meteorite sample. Accepted paper on Applied Radiation and Isotopes.

## P-14 3D Elemental Imaging of Cultural Heritage Objects at the PGAA Station at FRM II

Ralf Schulze<sup>1</sup>, Petra Kudejova<sup>2</sup>, Lea Canella<sup>2</sup>, Tamás Belgya<sup>3</sup>, Zoltan Kis<sup>3</sup>, László Szentmiklósi<sup>3</sup>, Martin Eberth<sup>1</sup>, Giulia Festa<sup>4</sup>, Jan Jolie<sup>1</sup>, Andreas Türler<sup>2</sup>

<sup>1</sup>Universität zu Köln, Institut für Kernphysik, Germany

<sup>2</sup>TU München, Institut für Radiochemie, Germany

<sup>3</sup>Hungarian Academy of Sciences, Institute of Isotopes, Budapest, Hungary

<sup>4</sup>Università degli Studi di Roma Tor Vergata, Dipartimento di Fisica and Centro NAST, Italy

The interest in the elemental compositions of cultural heritage objects was driving the development of a new 3D elemental imaging method based on Prompt Gamma-ray Activation Analysis (PGAA). This new method, called Prompt Gamma-ray Activation Imaging (PGAI) [1] in combination with Neutron Tomography (NT), has been developed in the frame of the european ANCIENT CHARM project [2] and should be useful not only for cultural heritage studies but also for the investigation of other samples from different fields.

At the existing PGAA facility at the research reactor Heinz Maier-Leibnitz (FRM II), [3] a PGAI/NT setup has been installed and tested. Several valuable cultural heritage objects have been measured with 2D and 3D PGAI, e.g. a full grid scan of an ancient fibula has been done to deliver the first complete elemental map utilizing this new method. For bulky samples the possibilities of measuring surfaces up to depths to about 250µm have been checked which gave important informations for the restoration and conservation of the analyzed objects [4].

Procedures for the alignment and calibration of the facility have been developed. These procedures make it possible to combine the acquired data sets with data from other facilities delivering other properties of the samples, e.g. structural information. They also provide reliable navigation inside the analysed samples. The combination of these different measurements will give supplementary informations of the sample properties.

The financial support of EU FP6 ANCIENT CHARM project (contract no. 15311) is gratefully acknowledged.

[1] Zsolt Kasztovszky and Tamás Belgya. From PGAA to PGAI: From Bulk Analysis to Elemental Mapping. *Archeometriai Műhely*, (2):16-21, 2006. [2] G. Gorini. Ancient Charm: A research Project for Neutron-based Investigation of Cultural-heritage Objects. *Il Nuovo Cimento*, 30(1):47-58, 2007. [3] P. Kudejová, et al., On the construction of a new instrument for cold-neutron prompt gamma-ray activation analysis at the FRM II. *Journal of Radioanalytical and Nuclear Chemistry*, 265(2):221-227, 2005. [4] G. Festa et al., A non destructive stratigraphic and radiographic neutron study of Lorenzo Ghiberti's reliefs from Paradise and North doors of Florence Baptistery, submitted to *Journal of Applied Physics*,



Figure 6.5: Gold Fibula (Hungarian Nationan Museum)

## P-15 The N-REX<sup>+</sup> reflectometer

Adrian Rühm<sup>1</sup>, Thomas Keller<sup>2</sup>, Janos Major<sup>1</sup>, Joergen Franke<sup>1</sup>, Kathrin Buchner<sup>1</sup>, Helmut Dosch<sup>1</sup>, Bernhard Keimer<sup>2</sup>

<sup>1</sup>MPI für Metallforschung, Stuttgart, Germany

<sup>2</sup>MPI für Festkörperforschung, Stuttgart, Germany

The Max-Planck-Institut für Metallforschung operates the combined neutron/X-ray reflectometer N-REX<sup>+</sup> at the FRM II. This project is part of the joint initiative of several Max-Planck-Institutes for a focused research program exploiting the unique properties of neutrons for the investigation of advanced materials and condensed matter phenomena. The first standard user experiments have been conducted in May 2007.

The instrument is located in the neutron guide hall at the cold guide NL1. In the standard operating mode the sample geometry is horizontal (e.g. for liquid surfaces), but a vertical geometry is also possible. N-REX<sup>+</sup> is equipped with a 2D position sensitive detector (<sup>3</sup>He wire chamber) and an X-ray diffractometer allowing for simultaneous in-situ neutron/X-ray reflectometry (neutron X-ray contrast variation).

Currently the instrument is upgraded and optimized for polarization analysis optimized for the study of magnetism in thin layers, such as superconductor heterostructures. The current upgrade aims to increase the flux (new monochromator design and focusing elements), lower the background (optimized detector shielding, vacuum or He-4 flight paths), provide high fields at the sample (superconducting horizontal magnet) and increase the beam polarization (polarizing neutron guide).

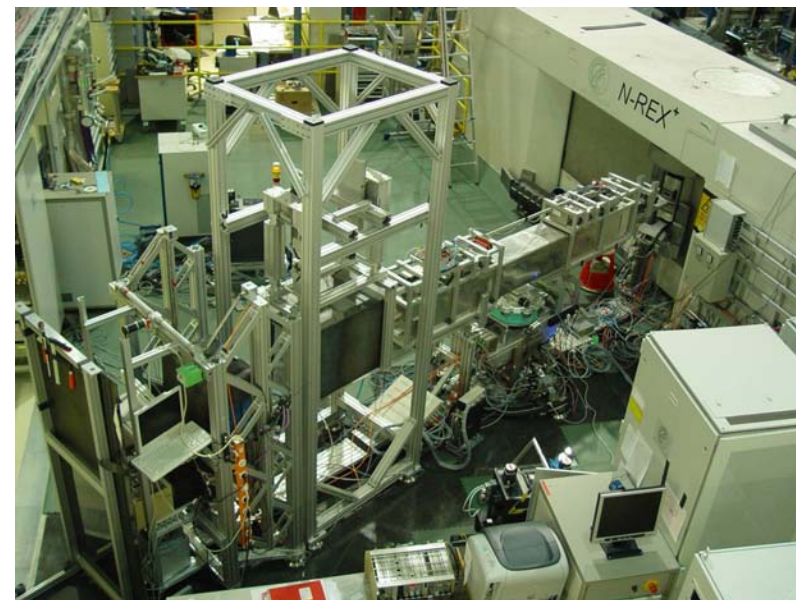


Figure 6.6: The N-REX<sup>+</sup> reflectometer at the FRM II

## P-16 The New Protein Single Crystal Diffractometer at the FRM II

Andreas Ostermann<sup>1</sup>, Michael Monkenbusch<sup>2</sup>, Winfried Petry<sup>1</sup>, Dieter Richter<sup>2</sup>

<sup>1</sup>Forschungs-Neutronenquelle Heinz Maier-Leibnitz (FRM II), München, Germany

<sup>2</sup>FZ Jülich GmbH, Institut für Festkörperforschung, Germany

The Forschungszentrum Jülich (JCNS) in collaboration with the Forschungsneutronenquelle Heinz Maier-Leibnitz (FRM II) will construct and build a monochromatic single crystal diffractometer dedicated to the structure determination of biological macromolecules.

The diffractometer will be installed at the cold guide NL1 in front of the instrument N-REX<sup>+</sup>. Neutrons are reflected out of the lower part (height 25mm) of the neutron guide by a pyrolytic graphite crystal (PG002). The wavelength can be varied between 2.4 and 5.6 Å thereby enabling optimization of the number of measurable reflections and the spatial resolution. Higher order contaminations are removed by a velocity selector. To cover a large solid angle the detector consists of an online neutron imaging plate system in a cylindrical geometry. An additional ZnS:Li scintillator CCD camera (detection area 200mm x 200mm) is foreseen for additional detection abilities for and crystal alignment.

The main advantage of this instrument is the possibility to adapt the wavelength to the size of the unit cell of the sample crystal while operating with a monochromatic beam that keeps the background level low. Operation of the instrument is planned to start summer 2010.

## P-17 Spherical Neutron Polarimetry (SNP) on POLI-HEiDi diffractometer at FRM II

Vladimir Hutanu<sup>1,2</sup>, Martin Meven<sup>1</sup>, Andrew Sazonov<sup>1,2</sup>, Gernot Heger<sup>2</sup>

<sup>1</sup>Forschungs-Neutronenquelle Heinz Maier-Leibnitz (FRM II), München, Germany

<sup>2</sup>RWTH Aachen, Institut für Kristallographie, Germany

New polarised neutron single crystal diffractometer POLI-HEiDi (Polarisation Investigator) is now under construction at the Heinz Maier-Leibnitz neutron source (FRM II). The new instrument at the hot source is designed for the ability to perform magnetic structure investigations using different polarised neutron diffraction techniques. Both classical Polarised Neutron Diffraction (PND), known also as flipping ratiion method, and Spherical Neutron Polarimetry (SNP) will be implemented. SNP technique using zero-field sample environment will be commissioned in 2009. Two zero-field polarimeters Cryopad and MuPAD are available. The number of specific instrumentation as non-magnetic goniometer, 3He spin filter polariser and analyser cells and magnetostatic chambers, polarisation manipulation devices, etc. have been constructed and successful tested. The construction of the whole instrument focused on the SNP option will be presented. The results of the first SNP test experiment using MuPAD are discussed.



Figure 6.7: POLI-HEiDi instrument on beam line SR 9B during the last test measurements in March 2009.



## P-20 Upgrade of the Very Small Angle Neutron Scattering Instrument KWS-3 and Future Scientific Perspectives

Guenter Goerigk<sup>1</sup>, Emmanuel Kentzinger<sup>2</sup>

<sup>1</sup>Jülich Centre for Neutron Science, Outstation at FRM II, München, Germany

<sup>2</sup>FZ Jülich GmbH, Institut für Festkörperforschung, Germany

KWS-3 is a very small angle neutron scattering instrument running on the focusing mirror principle. In Jülich it allowed performing scattering experiments with a wave vector transfer resolution between  $10^{-4}$  and  $10^{-3} \text{ \AA}^{-1}$ , bridging a gap between Bonse-Hart and pinhole cameras.

After the transfer into the guide hall of the FRM II neutron source in Garching a major upgrade became necessary, with the aim to make proper use of the enhanced neutron flux, which was nearly one order of magnitude larger compared to Jülich. Especially the neutron mirror was refurbished with a new <sup>65</sup>Cu-coating. After mirror refurbishment and optical alignment the upgrade activities are going on at the end of the dedicated neutron guide.

The beam line will be back to commissioning in the reactor cycle of June 2009. Subsequently first scientific projects will be implemented to the beam line operation, which will make complementary use of Small-Angle Neutron Scattering (SANS), Light Scattering (LS) and Anomalous Small-Angle X-ray Scattering (ASAXS).

## P-21 Improved focussing on RESI using neutron guides

Bjoern Pedersen<sup>1</sup>, Wilhelm Klein<sup>1</sup>, Fritz Frey<sup>2</sup>, Andreas Ostermann<sup>1</sup>

<sup>1</sup>Forschungs-Neutronenquelle Heinz Maier-Leibnitz (FRM II), München, Germany

<sup>2</sup>LMU München, Kristallographie, Germany

To increase the signal-to-noise ratio we installed a channelled focusing guide after the monochromator. First results will be presented, showing a signal-to-noise gain of approx. 2.

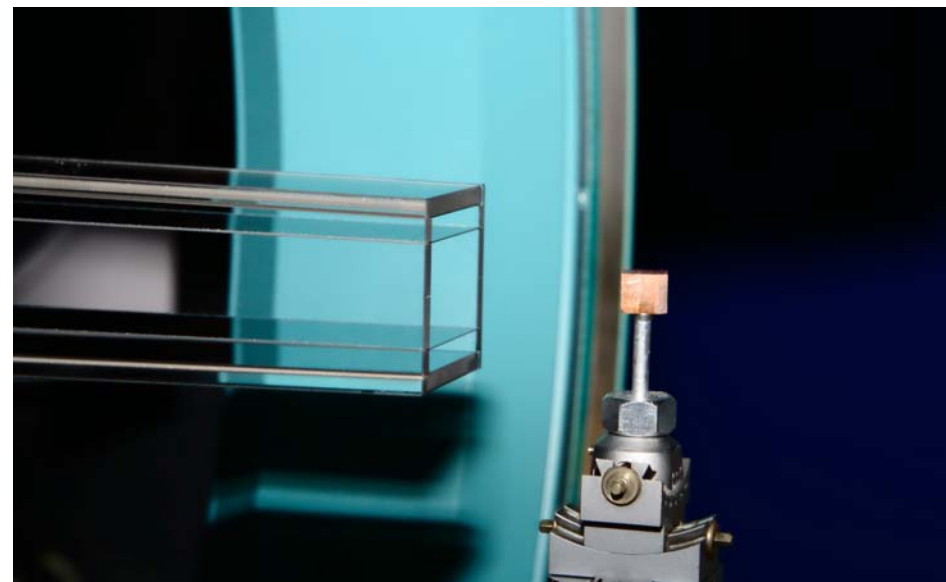


Figure 6.10: Frontend of the focussing guide, the inner channel is clearly visible.

## P-22 N-REX<sup>+</sup>

Adrian Rühm<sup>1,2</sup>, Mathias Schmidt<sup>2</sup>, Max Nülle<sup>2</sup>, Marton Major<sup>1,2</sup>, Janos Major<sup>2</sup>, Helmut Dosch<sup>2</sup>

<sup>1</sup>Forschungs-Neutronenquelle Heinz Maier-Leibnitz (FRM II), München, Germany

<sup>2</sup>MPI für Metallforschung, Stuttgart, Germany

The reflectometer N-REX<sup>+</sup> is running in regular user operation mode. While the main field of application has so far been soft matter science on interfaces, proposals for experiments on magnetism in layered systems have now become about equal in number.

We will present several examples of data obtained at N-REX<sup>+</sup>. On solid samples against air reflectivities down to  $1e^{-6}$  can be routinely recorded in 10 to 14 hours, depending on the required  $q$ -resolution. For solid-liquid interfaces the dynamic range of reflectivity data is limited to  $1e^{-5}$ , due to absorption losses and intrinsic background from the sample cells. The two-dimensional <sup>3</sup>He detector allows to simultaneously record off-specular data. Both polarized neutron reflectivity and off-specular scattering experiments can be performed. <sup>3</sup>He spin filters for wide-angle polarization analysis can be accommodated.

To improve the overall instrument performance and data quality, N-REX<sup>+</sup> is currently being upgraded in several aspects. The upgrade aims at a reduction of the background level as well as an enhancement of the primary neutron flux. This will be achieved by the installation of an evacuated or gas-filled detector shielding which acts as a neutron flight tube and can also accommodate components for polarization analysis. To improve signal and background of experiments with polarized neutrons, spin flippers so far operated in transmission will be replaced by RF flippers. Furthermore the monochromator will be upgraded to a larger number of crystal layers, and a horizontally focusing neutron guide will be installed between monochromator and sample, which will in particular facilitate experiments on smaller samples. It is also discussed to convert the neutron guide NL-1 into a polarized guide by the insertion of two V-shaped polarizing mirrors. This in principle is detrimental to unpolarized experiments, but as a result of all planned improvements we expect a net gain in instrument performance also for unpolarized experiments.



Figure 6.11: The reflectometer N-REX<sup>+</sup> in polarized neutron reflectometry configuration

## P-23 MIRA - New options

Robert Georgii<sup>1</sup>, Georg Brandl<sup>2</sup>, Reinhard Schwikowski<sup>1</sup>, Peter Böni<sup>2</sup>

<sup>1</sup>Forschungs-Neutronenquelle Heinz Maier-Leibnitz (FRM II), München, Germany

<sup>2</sup>TU München, Physik Department E21, Germany

MIRA is a versatile instrument for cold neutrons using neutrons with a wavelength  $\lambda > 3 \text{ \AA}$ . Below  $6 \text{ \AA}$  a new monochromator offers now significantly larger intensity. The instrument is situated at the cold neutron guide NL6 in the neutron guide hall of the FRM II.

As the instrument set-up can be changed quickly, MIRA is ideally suited as a testing platform for realizing new instrumental set-ups and ideas. In particular, MIRA is unique in its possibilities of combining different neutron scattering methods as:

- Polarized or non-polarised small angle scattering (SANS)
- A MIEZE spin echo option for quasi-elastic measurements
- Cold diffraction for large structures
- Polarized or non-polarised reflectometry.
- Spherical Polarimetry

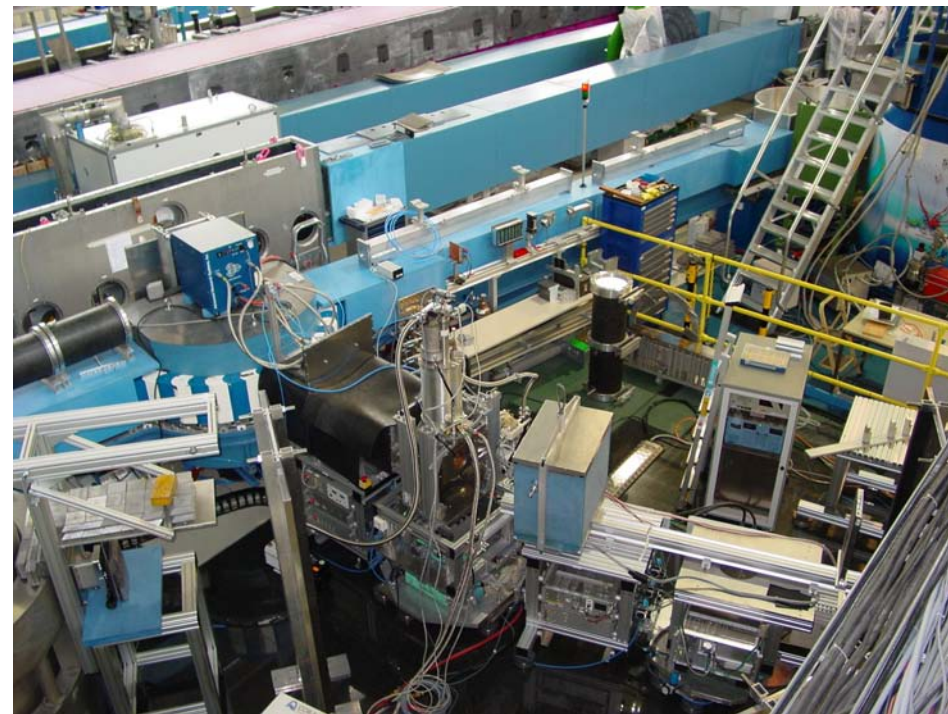


Figure 6.12: MIRA with its new monochromator option. The sample position is equipped with a magnet and a cryostat. The old monochromator (on the left) can still be used.

## P-24 HEiDi and its Applications

**Martin Meven**<sup>1</sup>, **Andrew Sazonov**<sup>2</sup>, **Vladimir Hutanu**<sup>2</sup>, **Gernot Heger**<sup>2</sup>

<sup>1</sup>Forschungs-Neutronenquelle Heinz Maier-Leibnitz (FRM II), München, Germany

<sup>2</sup>RWTH Aachen, Institut für Kristallographie, Germany

The instrument HEiDi at the neutron source Heinz Maier-Leibnitz (FRM II) uses hot neutrons for single crystal diffraction analysis of structural and magnetic properties of samples for which other methods are not applicable.

The hot topic of multiferroic compounds like REMnO<sub>3</sub> (RE=Dy, Gd) whose highly absorbing and heavy rare earth elements make it normally extremely difficult to get accurate structural and magnetic diffraction data is a good example for the unique capabilities of this instrument using both large penetration depth and large q range [1]. Also other compounds with complex magnetic properties were successfully studied [2].

This contribution will give an overview of the instrument (like the gain factor from the hot source, see also [3]) and its applications in different fields of solid state physics, chemistry and crystallography concerning structural details (highly accurate atomic positions and anisotropic mean square displacements, phase transitions, local disorder, magnetism, etc.).

[1] Magnetic Structure of GdMnO<sub>3</sub>. A. Möchel; J. Voigt; M. Meven, J.-W. Kim; and T. Brückel; Verhandlungen der Deutschen Physikalischen Gesellschaft, R. 6, Bd. 43, MA 29.2 (2008). [2] Structural behaviour of synthetic Co<sub>2</sub>SiO<sub>4</sub> at low Temperatures; A. Sazonov, M. Meven, V. Hutanu, V. Kaiser, G. Heger, D. Trots, M. Merz; Acta Cryst. B 64, 661 (2008). [3] HEiDi: Single Crystal Diffractometer at the Hot Source of the FRM II; Meven M., Hutanu, V.; Heger, G.; Neutron News 18, 19-21 (2007).

## P-25 Surface and Bulk Investigations at the High Intensity Positron Beam Facility NEPOMUC

**Christoph Hugenschmidt**<sup>1,2</sup>, **Hubert Ceeh**<sup>1,2</sup>, **Günther Dollinger**<sup>3</sup>, **Werner Egger**<sup>3</sup>, **Gottfried Kögel**<sup>3</sup>, **Benjamin Löwe**<sup>3</sup>, **Jakob Mayer**<sup>1,2</sup>, **Philip Pikart**<sup>1,2</sup>, **Christian Piochacz**<sup>1,2</sup>, **Karin Hain**<sup>1,2</sup>, **Peter Sperr**<sup>3</sup>, **Klaus Schreckenbach**<sup>1,2</sup>

<sup>1</sup>Forschungs-Neutronenquelle Heinz Maier-Leibnitz (FRM II), München, Germany

<sup>2</sup>TU München, Physik Department E21, Germany

<sup>3</sup>Universität der Bundeswehr München, Institut für Angewandte Physik und Messtechnik, Neubiberg, Germany

The high intensity NEutron induced POsitrone source MUniCh (NEPOMUC) at the research reactor FRM II delivers a low-energy positron beam ( $E = 1\text{keV}$ ) of  $9 \cdot 10^8$  moderated positrons per second.

At present four experimental facilities are in operation at NEPOMUC:

A coincident Doppler-broadening spectrometer (CDBS) for defect spectroscopy and investigations of the chemical vicinity of defects, the pulsed low-energy positron system (PLEPS) for depth dependent positron lifetime spectroscopy within short measurement time, a positron annihilation induced Auger-electron spectrometer (PAES) for surface studies and an apparatus for the production of the negatively charged positronium ion  $\text{Ps}^-$ . A positron remoderation unit which is operated with a tungsten single crystal in back reflection geometry has been implemented in order to improve the beam brilliance.

An overview of NEPOMUC and experimental results is given.

## P-26 The Time-of-Flight spectrometer TOFTOF at the FRM

### II

Giovanna Giulia Simeoni<sup>1,2</sup>, Christoph Smuda<sup>3,1,2</sup>, Sebastian Busch<sup>1,2</sup>, Martin Schmiele<sup>1,2</sup>, Jürgen Neuhaus<sup>1,2</sup>, Winfried Petry<sup>1,2</sup>, Tobias Unruh<sup>1,2</sup>

<sup>1</sup>Forschungs-Neutronenquelle Heinz Maier-Leibnitz (FRM II), München, Germany

<sup>2</sup>TU München, Physik Department E13, Germany

<sup>3</sup>ETH Zürich, Institut für Pharmazeutische Wissenschaften, Zürich, Switzerland

TOFTOF is a multi-disc chopper time-of-flight spectrometer, working in direct geometry, installed at the neutron source Heinz Maier-Leibnitz (FRM II). It is fed with neutrons from the undermoderated cold source operated with D<sub>2</sub> at 25 K.

Features characterizing the TOFTOF performance are an extreme high signal-to-background ratio, a high intensity also at low incident neutron wavelengths and the possibility of achieving a very high energy resolution. The excellent signal-to-background ratio of the instrument is due to its remote position in the neutron guide hall, an elaborated shielding concept and an s-shaped curved primary neutron guide. Typical of TOFTOF is the very low background count rate provided by the 600 detectors, of about 3.0 counts/s (reactor in operation, instrument shutter closed). In addition to that, the spectrometer is characterized by a high flux which exceeds 1010 n/cm<sup>2</sup>s (white beam at sample position).

The s-shaped primary neutron guide is also responsible for the high intensity at low wavelengths and for its continuous distribution over a broad range of incident neutron wavelengths, from 1.4 Å up to 16 Å thus bridging the wavelength gap between thermal and traditional cold TOF spectrometers. Moreover, the low background and perfect symmetric resolution function allow standard measurements up to an elastic energy resolution of 2 µeV (FWHM) (see figure). Exploiting this high resolution TOFTOF configuration, it is possible to perform experiments typical for backscattering spectrometers. Given the complementarity of the dynamic ranges of the two techniques at high resolution, the employment of TOFTOF in this case contributes to extend the accessible knowledge about the system.

Among all the successful experiments already carried out throughout the last four years of operation, we address our attention to some significant scientific highlights obtained in the fields of disordered systems, pharmaceutical technology and magnetism.

Further development concerning the extension of the detector bank, the upgrade of the chopper system, the improvement of the secondary neutron guide as well as new sample environments are discussed.

[1] C. Smuda, S. Busch, R. Schellenberg, T. Unruh, J.Phys. Chem. B 113 (2009) 916

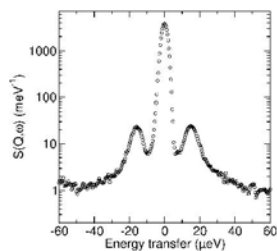


Figure 6.13: Tunneling spectrum of Q0 at  $T = 4$  K and  $Q = 0.5 \pm 0.05$  Å<sup>-1</sup> obtained at TOFTOF with instrument resolution of 4 µeV

## 7 Nuclear and Particle Physics

### P-27 Neutron capture on Ge-76: A background in neutrinoless double beta decay experiments

Georg Meierhofer<sup>1</sup>, Lea Canella<sup>2</sup>, Peter Grabmayr<sup>1</sup>, Josef Jochum<sup>1</sup>, Jan Jolie<sup>3</sup>, Petra Kudejova<sup>4</sup>

<sup>1</sup>Universität Tübingen, Physikalisches Institut, Germany

<sup>2</sup>TU München, Institut für Radiochemie, Germany

<sup>3</sup>Universität zu Köln, Institut für Kernphysik, Germany

<sup>4</sup>Forschungs-Neutronenquelle Heinz Maier-Leibnitz (FRM II), München, Germany

The Majorana nature of the neutrino can be proved by the observation of the neutrinoless double beta decay [1]. From the measured half-life the effective neutrino mass can be derived, if theory provides precise nuclear matrix elements. The half-lives for these decays are very long (for  $^{76}\text{Ge}$ :  $> 10^{25}$  y), therefore reducing the background is the major task for double beta experiments.

The GERDA (GERmanium Detector Array) experiment [2] at the Gran Sasso Laboratory (LNGS) in Italy searches for the neutrinoless double beta decay in  $^{76}\text{Ge}$ . The isotope  $^{76}\text{Ge}$  is an ideal candidate as it can be source and detector at the same time.

A main contribution to the background arises from the prompt gamma cascades after neutron capture by  $^{76}\text{Ge}$  and the following  $\beta^-$ -decay of  $^{77}\text{Ge}$ . As the energies of this gamma cascade are poorly known, measurements with isotopically enriched Germanium samples were carried out using the PGAA facility at the FRM II. Additional data from a coincidence measurement allow to reconstruct the decay scheme. The cross section for the  $^{76}\text{Ge}(n,\gamma)^{77}\text{Ge}$  reaction was determined using the decay gammas of  $^{77}\text{Ge}$  in a separate experiment.

The results achieved with the measurements at the FRM II will help to reduce the remaining background in the GERDA experiment.

This work is supported by a grant from BMBF.

[1] F.T. Avignone, S.R. Elliott and J. Engel, Rev. Mod. Phys. **80**, 481 (2008). [2] GERDA, "The germanium detector array for the search of neutrinoless double beta decays of  $^{76}\text{Ge}$  at Gran Sasso", Proposal to the LNGS, (2004) <http://www.mpi-hd.mpg.de/gerda>.

### P-28 New experiment on the neutron radiative decay

Rashid Khafizov<sup>1</sup>, Ivan Kolesnikov<sup>1</sup>, Sergey Tolokonnikov<sup>1</sup>, Vladimir Torokhov<sup>1</sup>, Valery Solovoi<sup>2</sup>, Madlen Kolkhidashvili<sup>2</sup>, Igor Konorov<sup>3</sup>

<sup>1</sup>RRC Kurchatov Institute, Institute of Nuclear and General Physics, Moscow, Russia

<sup>2</sup>Russian Academy of Science, Petersburg Nuclear Physics Institute, Russia

<sup>3</sup>TU München, Physik Department E18, Germany

The report is dedicated to the preparation of the new experiment on the neutron radiative decay what is conducted for the last years.

We started the experimental research of this neutron decay branch with the experiment conducted at ILL in 2002 [1] and continued in another experiment at the second and third cycles at the FRM II reactor of the Technische Universität München [2] in 2005.

In the first experiment we succeeded in measuring only the upper limit on the relative intensity (B.R.) of the radiative neutron decay and in the second we succeeded in discovering events of radiative neutron decay and measure its B.R.  $= (3.2 \pm 1.6) \cdot 10^{-3}$  (with C.L. = 99.7% and gamma quanta energy over 35 keV). The obtained average B.R. value was approximately twice the theoretical value calculated earlier within the framework of the standard electroweak model [3].

However, due to significant experimental error it would be preliminary to deduce that based on this finding a deviation from the standard model has been observed. To prove or disprove the existence of a deviation it is necessary to conduct a new experiment that would allow to measure the radiative peak in timing spectra [2] with precision in the order of 1%. By the present time we have prepared a new experiment the main result of which would be the measurement of B.R. for the radiative branch of neutron decay with this precision.

[1] M. Beck et al., JETP Letters v. 76(6), 2002, p. 332 [2] R.U. Khafizov et al. JETP Letters, v. 83(1), 2006, p. 5 [3] Yu.V. Gaponov, R.U. Khafizov, Phys. Lett. B 379(1996), p. 7.

## P-29 The new beamline MEPHISTO in the east neutron guide hall

Jens Klenke<sup>1</sup>

<sup>1</sup>Forschungs-Neutronenquelle Heinz Maier-Leibnitz (FRM II), München, Germany

The white beamline MEPHISTO at the FRM II is dedicated to precision experiments in the field of fundamental and particle physics. These experiments with neutrons, electrons, ions and gamma rays give valuable data for the tests of the basic assumptions of the Standard Model. The Standard Model itself the starting point for nearly all theories in particle physics, cosmology and astronomy.

The beamline, now situated in the west neutron guide hall will be moved in the new east guide hall during the next years. The demand for more space, a undisturbed guide and high flux arise from new planned experiments.

The poster will present the status of the work including the calculations of the new guide from the cold source to the experiment area. The new MEPHISTO will be a very attractive beamline for further instruments in the framework of international nuclear and particle physics at the FRM II.

## P-30 ROT-effect in angular distribution of prompt fission $\gamma$ rays

Gevorg Danilyan<sup>1</sup>

<sup>1</sup>Alikhanov Institute for Technical and Experimental Physics, Moscow, Russia

We have found a small inclination of the symmetry axis of the prompt fission gamma-rays angular distribution relative to the "fission axis" in binary fission of  $^{235}\text{U}$  induced by cold polarized neutrons. The sign of the shift depends on the direction of cold neutron beam polarization and it can be explained only by the quasi-classical rotation of the fissile nucleus at the scission point. The observed effect is similar to the ROT-effect found in light charged particles distribution in ternary fission.

The ROT-effect in experiment is expressed as the asymmetry of counts rate:

$$R = N_1(\Theta) - N_2(\Theta) / N_1(\Theta) + N_2(\Theta).$$

Here  $N_i(\Theta)$  is the coincidence counts rate between pulses from the gamma-rays detector and fragment detector;  $\Theta$  is the angle between them;  $i = 1$  and  $2$  corresponds to the measurements at two opposite polarization direction of longitudinally polarized neutron beam.

Angular dependence of the asymmetry  $R$  over the angle between the fission axis and gamma-ray direction is shown in the figure.

The energy dependence of the ROT-asymmetry  $R$  roughly follows the energy dependence of prompt fission gamma-rays anisotropy. This is an evidence that the ROT-effect is essential to all gamma-rays. Prompt fission gamma-rays emitted by excited fission fragments may contribute to the  $R$  due to orientation of spins of the fragments.

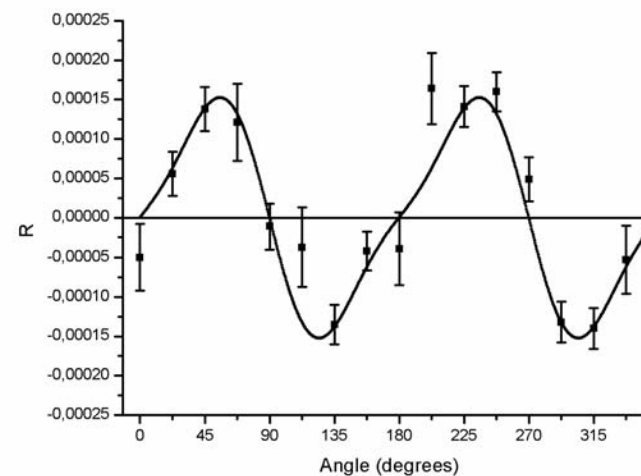


Figure 7.1:

## 8 Material Science

### P-31 Influence of Secondary Extinction on Pole Figures Measurement by Neutron Diffraction

Jesús Palacios Gómez<sup>1</sup>

<sup>1</sup>National Polytechnic Institute, Escuela Superior de Física y Matemáticas, Mexico City, Mexico

Previous pole figures of high textured high purity copper samples measured with neutron diffraction with three different wavelengths to study the influence of secondary extinction [1] have revealed that reflection 222 exhibited between 8% to 43% higher pole density maxima than reflection 111. Since measuring conditions were the same for both reflections this difference was attributed to extinction. Pole density maxima of strong reflections revealed also a light tendency to lower values with decreasing wavelength. This was attributed to the fact that for shorter wavelengths more reflections exist competing for intensity, increasing secondary extinction. However, the short wavelengths could be obtained only as secondary contamination and new measurements with better conditions are needed to improve quantitative results.

A self consistent approach is presented here to measure the influence of secondary extinction on the whole pole figure. Since extinction corrections require the orientation distribution of crystallites, an iterative procedure is devised in which measured CODF is used as a starting function, which is subjected to secondary extinction influence. A point by point comparison of initial and resulting ODFs should give the behavior of secondary extinction on the Euler space, and this is expected to give a good approximation to the true ODF, which again, under extinction correction should give the experimentally obtained CODF. Extinction should be determined by calculating the diffracted power lost in its way to the detector, through differential equations involving incident and diffracted intensities, and the diffracting power of all participating planes.

[1] J. Palacios G., J. M. Walter, E. Jansen, T. Kryshtab, submitted to J. Appl. Cryst.

### P-32 Directional Coarsening in Polycrystalline Superalloys

Fabian Schmitz<sup>1</sup>, Joachim Rösler<sup>1</sup>, Debashis Mukherji<sup>1</sup>

<sup>1</sup>TU Braunschweig, Institut für Werkstoffe, Germany

Nanoporous membranes showing very fine and regular porosity are desired for a great variety of functional applications such as filters in hospitals or as structures in miniature heat exchangers. In a new method the porous metal is produced from binary or multi-component alloys containing second phase precipitates. In the so called rafting process the cubic  $\gamma'$ -precipitates start to coarsen and finally create a network within the  $\gamma$ -matrix. The initial precipitate arrangement and its morphology in the bulk alloy are important factors which guide their self assembly. In a following electrochemical leaching process one of the phases can be removed leaving the nanoporous membrane.

So far, we have used commercially available single crystalline nickel-base superalloys for producing thin nanoporous membranes in a creep type process under unidirectional external loading at elevated temperature. Now research is in progress to produce the nanoporous membranes from polycrystalline alloys. Starting from the commercially available wrought alloy Nimonic 115 two different alloys have been found. As an alternative production route the material is predeformed in a rolling process. A subsequent annealing step leads to directional coarsening of the precipitates.

To find suitable values for the deformation required and the optimum temperature for the process neutron diffraction at SPODI and Stress-Spec was used.

During tensile deformation at Stress-Spec the change in the coherency strains between matrix and precipitates was monitored. These coherency strains strongly influence the coarsening behaviour.

High temperature measurements at SPODI monitored the change in misfit with rising temperature. The transmission geometry enables us to get a full spectrum showing superlattice peaks as well as fundamental peaks even in textured specimen. Additionally a large volume of bulk material is measured, so that an overall misfit value is determined.

[1] Pollock, T.M. And A.S. Argon. 1994. Acta metal. mater, 42, 1859 [2] Kuhn, H.-A., H. Biermann, T. Ungar, and H. Mughrabi. 1991. Acta Metall. Mater., 39, 2783. [3] Rösler, J., O. Näth, S. Jäger, F. Schmitz, and D. Mukherji. 2005. Acta Mater., 53, 1397. [4] Rösler, J., and D. Mukherji. 2003. Adv. Eng. Mater., 5, 916. [5] Rösler, J., O. Näth, S. Jäger, F. Schmitz, and D. Mukherji. 2005. Journal of Metals, 57, 52. [6] Veron, M., Y. Brechet, F. Louchet. 1996. Scripta mater., 34, 1883

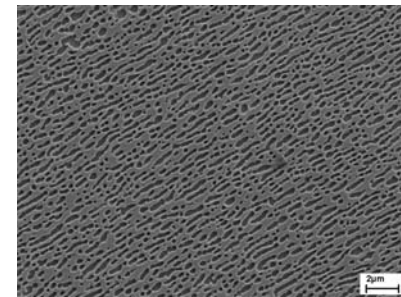


Figure 8.1: Microstructure of alloy 115 NC after four steps of deformation and intermittent annealing at 1273K/24h.

### P-33 The Advancement of Work on Inert Matrix Fuel (Third Part)

Ashraf Elsayed Mohamed<sup>1</sup>

<sup>1</sup>Institute of Energy, Alexandria, Egypt

Recent aims to destroy plutonium in the most effective way have led to the development of a uranium free fuel based on zirconia. Concepts for this so-called "inert matrix fuel-IMF": IMF is a non-fertile oxide fuel consisting of PuO<sub>2</sub> diluted in inert oxides such as stabilised ZrO<sub>2</sub>, its main advantage is that it does not produce new plutonium during irradiation, as it does not contain uranium (U-free fuel). An addition of thoria in the matrix (thoria-doped fuel) may be required for coping with reactivity feedback needs.

Several ceramers (ceramic+ceramic) and cermets (ceramic+metal) are good candidates for plutonium fuels without uranium or for the target related to the heterogeneous recycling of minor actinides. Those ceramers are actinide compounds (PuO<sub>2</sub> or AmO<sub>2</sub>) dispersed in inert matrix such as MgO or MgAl<sub>2</sub>O<sub>4</sub>.

All U-free fuels are envisaged to be operated under a once-through cycle scheme - the spent fuel is supposed to be spent directly to the final disposal in deep geological formations without requiring any further reprocessing treatment.

The objective of this paper is to discuss the advancement of work on inert matrix fuels and discuss the damage sources of inert matrix fuels for transmutation of minor actinides or for burning excess Pu, which are the following:

- thermal or fast neutrons;
- $\alpha$ -decay (5-6 MeV He-ions, > 100 keV daughter recoil atoms);
- fission fragment impact(70-100 MeV heavy ions of elements between Ga and Dy);
- intense  $\beta$ - and  $\gamma$  - radiation.

### P-34 Global and local texture analysis at Stress-Spec

Weimin Gan<sup>1</sup>, Heinz-Günter Brokmeier<sup>2</sup>, Christian Randau<sup>2</sup>

<sup>1</sup>GKSS-Forschungszentrum Geesthacht, Germany

<sup>2</sup>TU Clausthal, Institut für Werkstoffkunde und Werkstofftechnik, Germany

Thermal neutron diffraction is the leading method for non-destructive global texture measurement in metals, alloys, composites, ceramics and rocks up to sample volumes in the cm<sup>3</sup> range. Neutron diffraction is also an efficient tool for multi-phased system or weak texture analysis. In addition, due to its high flux and flexible configuration Stress-Spec diffractometer takes more advantages for local or gradient texture analysis.

A series of selected nice texture measurements which have done at Stress-Spec, such as Mg-Al or Mg-Pb multi-phased extruded bar, natural calcite sample, will be presented. Moreover, an example of gradient texture measurement on an extruded bone-like AZ31 Mg alloy profile is highlighted. Texture evolution from the center to edge part in this profile indicates a transition zone in the way of different extrusion model, which will be described in detail.

### **P-35 The Potential of the Horizontal ToF-Neutron Reflectometer REFSANS at FRM II Munich Highlighted by Recent Experimental Results**

**Reinhard Kampmann<sup>1</sup>, Martin Haese-Seiller<sup>1</sup>, Jean-François Moulin<sup>1</sup>, Matthias Pomm<sup>1</sup>, Bert Nickel<sup>2</sup>, Peter Müller-Buschbaum<sup>3</sup>, Wolfgang Kreuzpaintner<sup>1</sup>, Dieter Lott<sup>1</sup>, Martin Müller<sup>1</sup>, Andreas Schreyer<sup>1</sup>**

<sup>1</sup>GKSS Forschungszentrum Geesthacht, Germany

<sup>2</sup>LMU München, Fakultät für Physik, Experimentalphysik, Germany

<sup>3</sup>TU München, Physik Department E13, Germany

The horizontal neutron reflectometer REFSANS allows to perform comprehensive analyses of vertical and lateral surface and interface structures by means of specular and off-specular neutron reflectivity as well as small-angle neutron scattering at grazing incidence (GI-SANS), both on solid and free liquid interfaces. The performance of this novel instrument is highlighted by means of recent measurements of weak off-specular scattering, GI-SANS and extremely low specular reflectivity including the case of a strong incoherent substrate scattering.

### **P-36 Synthesis and characterisation of nitrogen doped ZnO particles by prompt gamma activation analysis (PGAA)**

**Stefan Söllradl<sup>1</sup>, Lea Canella<sup>2</sup>, Petra Kudejova<sup>3</sup>, Andreas Türler<sup>2</sup>, Rainer Niewa<sup>1</sup>**

<sup>1</sup>TU München, Department Chemie, Germany

<sup>2</sup>TU München, Institut für Radiochemie, Germany

<sup>3</sup>Forschungs-Neutronenquelle Heinz Maier-Leibnitz (FRM II), München, Germany

Small, nitrogen doped ZnO particles were synthesised by solution combustion from aqueous solution. As precursor  $Zn(NO_3)_2 \cdot 6H_2O$  and urea were completely dissolved in DI water and heated to 500°C in a muffle furnace. After synthesis the samples were investigated and characterised mainly by powder x-ray diffraction, raman spectroscopy and prompt gamma activation analysis (PGAA) at FRM II.

[1] Mapa M.; Gopinath C. S. Chem. Mater. 2009, 21 (2), 351-359

### P-37 Application of PGAA for elemental analysis of carbonaceous sedimentary rocks

Anke Jurisch<sup>1</sup>, Bernhard M. Krooss<sup>1</sup>, Sabine Heim<sup>1</sup>  
<sup>1</sup>RWTH Aachen, Lehrstuhl für Erdöl und Kohle, Germany

A set of test experiments was conducted to assess the suitability of the PGAA method in geosciences for the characterisation of the composition of carbonaceous sedimentary rocks. The aim of this study was to assess whether PGAA can improve the characterisation of heterogeneous mineral assemblies by common techniques (X-ray fluorescence analysis, XRF) and if it can be used for routine measurements in the future.

Fifteen test samples which had previously been characterized comprehensively with regard to their elemental composition were analyzed at the PGAA instrument of the FRM II. The primary target element was nitrogen which was known to occur in organic and inorganic compounds of these sedimentary rocks. Correlations with S, P, V and Ni would provide hints on the origin and the geochemical cycling of the nitrogen in Palaeozoic sedimentary rocks. The conventional determination of nitrogen (Elementar-Analyzer) affords the quantification of nitrogen with detection limits as low as 100 ppm. The practical detection limit of the PGAA instrument for nitrogen was 1000 ppm. Only a few of the selected samples had nitrogen contents above this limit. Thus, a correlation with conventional methods could not be achieved.

The bulk elemental compositions obtained from PGAA and XRF are now being compared and examined for their compatibility with the mineral compositions derived from X-ray diffraction analysis (XRD). The XRF data indicated lower K<sub>2</sub>O values than XRD analysis implying that significant proportions of K<sup>+</sup> in clay minerals have been replaced by NH<sub>4</sub><sup>+</sup>.

The common interpretation of PGAA results for nitrogen and other elements in terms of oxides (element/oxide-ratios) and "most likely" oxidation states may not be adequate for carbonaceous rocks which were mostly deposited under anoxic (reducing) conditions. Therefore, at the present stage of investigations the primary PGAA element/element-ratios (el/el) are considered to be more useful for the study of carbonaceous rocks.

### P-38 Measurement of internal strain by neutron powder diffraction in core-shell Ni<sub>3</sub>Si(Al)-SiO<sub>x</sub> nanoparticles

Giancarlo Pigozzi<sup>1</sup>, Debashis Mukherji<sup>2</sup>, Ralph Gilles<sup>3</sup>  
<sup>1</sup>ETH Zurich, Laboratorium für Nanometallurgie, Switzerland  
<sup>2</sup>TU Braunschweig, Institut für Werkstoffe, Germany  
<sup>3</sup>Forschungs-Neutronenquelle Heinz Maier-Leibnitz (FRM II), München, Germany

Internal defects and strain in nanoparticles can influence their properties and therefore measuring these values is relevant. Powder diffraction technique (neutron and synchrotron) are successfully used to characterize internal strain in the core-shell Ni<sub>3</sub>Si(Al)-SiO<sub>x</sub> nanoparticles having mean diameter of about 80 nm [1]. The nanoparticles, which are strain-free after extraction from the bulk alloys, develop internal strain on heating (see figure, left). Both micro- and macro-strains can be measured from the analysis of Bragg peak shift and broadening (see figure, right). It is identified that differences in thermal expansion coefficient of the metallic core and the amorphous shell of the nanoparticles, as well as partial disordering of the L12 ordered core phase are the main causes for the strain evolution. Synchrotron measurements can also detect partial crystallization of the amorphous silica shell.

[1] G. Pigozzi, D. Mukherji, R. Gilles, P. Jencus and C. Siemers, Measurement of internal strain in core-shell Ni<sub>3</sub>Si(Al)-SiO<sub>x</sub> nanoparticles To appear in Nanotechnology (May 2009)

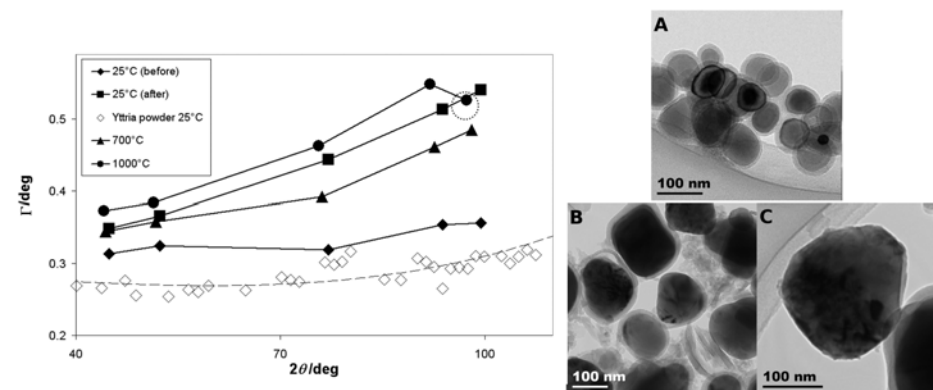


Figure 8.2: Left: Plot of the Gaussian full width at half maximum (FWHM) of the main lattice peaks as a function of  $2\theta$  calculated from the diffraction peaks of Ni<sub>3</sub>Si(Al) phase. Right: Bright-field TEM images of the core-shell nanoparticles. (A) As synthesized and before heating. (B and C) After in-situ heating at SPODI. Shell rupture and loss of adhesion are clearly visible as signs of mechanical damage.

## 9 Magnetism and Dynamics

### P-39 Magnetische Struktur des Kompositkristalls



**Karine Sparta**<sup>1</sup>, **Georg Roth**<sup>1</sup>, **Martin Meven**<sup>2</sup>, **Nadja Wizen**<sup>3</sup>, **Jorge Hamann Borrero**<sup>3</sup>, **Norman Leps**<sup>3</sup>, **Christian Hess**<sup>3</sup>, **Bernd Büchner**<sup>3</sup>

<sup>1</sup>RWTH Aachen, Institut für Kristallographie, Germany

<sup>2</sup>Forschungs-Neutronenquelle Heinz Maier-Leibnitz (FRM II), München, Germany

<sup>3</sup>Leibniz-Institut für Festkörper- und Werkstofforschung, Dresden, Germany

The composite crystal  $\text{Ca}_2\text{Nd}_2\text{Cu}_5\text{O}_{10}$  belongs to the dopable spin chains series  $\text{Ca}_{2+x}\text{Ln}_{2-x}\text{Cu}_5\text{O}_{10}$  with  $\text{Ln} = \text{La}^{3+}, \text{Y}^{3+}, \text{Nd}^{3+}, \text{Gd}^{3+}$ . . . [1,2], in which the formal oxidation state for Cu can in principle be varied from  $2+$  ( $x = 0$ ) to  $2.4+$  ( $x = 2$ ). We have shown in the case of the Y and Nd compounds that the  $\text{CuO}_2$  chains of edge-sharing  $\text{CuO}_4$  squares are highly distorted, with an incommensurately modulated polyhedral deformation for  $\text{Cu}^{2+}$  (spin 1/2) between square planar and flattened tetrahedron [3].

The nuclear and magnetic structure of the composite crystal  $\text{Ca}_2\text{Y}_2\text{Cu}_5\text{O}_{10}$  has been recently studied as a function of temperature by means of single crystal neutron diffraction [4]. We present in this contribution our latest results on the magnetic structure of  $\text{Ca}_2\text{Nd}_2\text{Cu}_5\text{O}_{10}$ , measured on the four-circle neutron diffractometer HEIDI.

[1] P.K. Davies et al., J. Am. Ceram. Soc. 74 (1991), 569-573. [2] P.K. Davies, J. Solid State Chem. 95 (1991), 365-387. [3] J. Thar, Diploma thesis, Aachen (2005). [4] G. Roth et al., FRM II experimental report, experiment No. 932 (2008).

### P-40 High Resolution Spectroscopy and Diffraction at TRISP

**Thomas Keller**<sup>1</sup>, **Pegor Aynajian**<sup>1</sup>, **Nathalie Munnikes**<sup>1</sup>, **Sibel Bayrakci**<sup>1</sup>, **Christian Pfleiderer**<sup>2</sup>, **Kathrin Buchner**<sup>1</sup>, **Manfred Ohl**<sup>1</sup>, **Bernhard Keimer**<sup>1</sup>

<sup>1</sup>MPI für Festkörperforschung, Stuttgart, Germany

<sup>2</sup>TU München, Physik Department E21, Germany

TRISP is a novel high-resolution neutron spectrometer combining the triple axis and neutron resonance spin echo (NRSE) techniques. The design of TRISP is optimized for the study of intrinsic line widths of elementary excitations (phonons, magnons) with an energy resolution in the  $\mu\text{eV}$  region over a broad range of momentum and energy transfers. Compared to conventional triple axis spectrometers (TAS), this corresponds to an improvement of the energy resolution of one to two orders of magnitude. We present a summary of highlight experiments on TRISP, including spin excitations in 3D Heisenberg antiferromagnets [1], phonons in elemental superconductors [2] and high resolution diffraction (Larmor diffraction) [3].

[1] S. P. Bayrakci, T. Keller, K. Habicht, B. Keimer, 'Spin-Wave Lifetimes Throughout the Brillouin Zone', Science 312, 1926 (2006). [2] P. Aynajian, T. Keller, L. Boeri, S. M. Shapiro, K. Habicht, B. Keimer, 'Energy Gaps and Kohn Anomalies in Elemental Superconductors', Science 319, 1519 (2008). [3] C. Pfleiderer, P. Böni, T. Keller, U. K. Rößler, A. Rosch, 'Non-Fermi Liquid Metal Without Quantum Criticality', Science 316, 1871 (2007).



Figure 9.1: The TRISP (TRiple axis SPin echo) spectrometer at the FRM II

## P-41 Recent results on PANDA

Astrid Schneidewind<sup>1</sup>, Peter Link<sup>2</sup>, Enrico Faulhaber<sup>1</sup>, Oliver Stockert<sup>3</sup>, Michael Loewenhaupt<sup>4</sup>

<sup>1</sup>TU Dresden at Forschungs-Neutronenquelle Heinz Maier-Leibnitz (FRM II), München, Germany

<sup>2</sup>Forschungs-Neutronenquelle Heinz Maier-Leibnitz (FRM II), München, Germany

<sup>3</sup>MPI of Molecular Cell Biology and Genetics, Dresden, Germany

<sup>4</sup>TU Dresden, Institut für Festkörperphysik, Germany

After a short introduction on some technical specialities of the cold neutron triple axis spectrometer PANDA at the Forschungsneutronenquelle Heinz Maier-Leibnitz (FRM II) I will discuss recent results obtained by our group at IFP (Institut für Festkörperphysik, TU Dresden) in collaboration with e.g. IFW-Dresden, MPI-CPfS and others and by external users.

Our investigations comprise magnetic structures, phase diagrams, crystal field and collective excitations in frustrated systems like  $R_2PdSi_3$  with  $R$  = heavy rare earths [1], in heavy-fermion superconductors like  $CeCu_2Si_2$  [2] or the newly discovered FeAs-based superconductors [3,4].

[1] D.S. Inosov et al., Phys. Rev. Lett. 102, 046401 (2009) [2] O. Stockert et al., Physica B 403, 973 (2008) [3] Y. Su et al., Phys. Rev. B 79, 064504 (2009) [4] Songxue Chi et al., Phys. Rev. Lett. 102, 107006 (2009)

## P-42 Critical Magnetic Behaviour and Magnetocaloric Effect in $PrMn_2Ge_2$ -Based Materials

Stewart Campbell<sup>1</sup>, Jianli Wang<sup>2</sup>

<sup>1</sup>School of Physical, Environmental and Mathematical

<sup>2</sup>UNSW@ADFA, Canberra, ACT; Bragg Institute, ANSTO, NSW Australia

The discovery of a giant magnetocaloric effect (GMCE) near room temperature in  $Gd_5Si_2Ge_2$  has led to heightened interest in materials that exhibit magnetic transitions which offer potential for enhanced magnetocaloric behaviour (see [1] and references therein). Magnetostructural coupling and/or magnetovolume effects have been found to play significant roles in governing the magnetocaloric effect in several materials which exhibit first order magnetic transitions [e.g. 1, 2]. Here we present our investigation of the critical magnetic behaviour in three systems -  $Pr_{1-x}R_xMn_2Ge_2$ , ( $R=Y,Lu$ ),  $PrMn_{2-x}Fe_xGe_2$  and  $PrMn_2Ge_{2-x}Si_x$  - where strong magnetovolume effects have been detected (e.g.  $\Delta V/V = 0.34\%$  and  $0.23\%$  for  $Pr_{0.5}Y_{0.5}Mn_2Ge_2$  and  $PrMn_{1.4}Fe_{0.6}Ge_2$ , respectively).

By selecting atoms of reduced sizes (Y, Lu, Fe and Si) to substitute the corresponding 2a-, 4d- and 4e-site atoms for the Pr-, Mn- and Ge-layers respectively in  $PrMn_2Ge_2$ , we have modified dMn-Mn, the Mn-Mn intra-planar distance. This has allowed us to design re-entrant ferromagnetic transitions in  $Pr_{0.5}Y_{0.5}Mn_2Ge_2$ ,  $Pr_{0.6}Lu_{0.4}Mn_2Ge_2$ ,  $PrMn_{1.4}Fe_{0.6}Ge_2$  and  $PrMn_2Ge_{0.8}Si_{1.2}$  which are expected to exhibit first order magnetic transitions and to be accompanied with large magnetovolume effects. The relationships between magnetic phase transitions and structural changes resulting from the decrease in dMn-Mn with temperature have been investigated by magnetisation, differential scanning calorimetry and neutron diffraction measurements. Full details on the magnetic structures and magnetic phase transitions and their interplay with the magnetovolume effects will be presented.

[1] K A Gschneider Jr, V K Pecharsky and A O Tsokol, Rep Prog Phys 68 1479 (2005) [2] J D Zou, B G Shen, B Gao, J Shen, and J R Sun, Adv Mater 21 693 (2009)

## P-43 Spin Torque Effects in a Helical Magnet

**Florian Jonietz<sup>1</sup>, Sebastian Mühlbauer<sup>1</sup>, Christian Pfleiderer<sup>1</sup>, Rembert Duine<sup>2</sup>, Achim Rosch<sup>3</sup>, Peter Böni<sup>1</sup>**

<sup>1</sup>TU München, Physik Department E21, Germany

<sup>2</sup>Utrecht University, Institute for Theoretical Physics, The Netherlands

<sup>3</sup>Universität zu Köln, Institut für Theoretische Physik, Germany

Spin torque interactions in soft ferromagnets are a promising route to novel spintronics devices. In these systems the spin torque is due to changes of the orientation of the spin-polarization of the conduction electrons in non-colinear spin structures, notably Bloch domain walls. A major constraint of these studies is the extrinsic nature of magnetic pinning in soft ferromagnets requiring very large current densities of order  $10^{12}$  A/m<sup>2</sup>.

We report AC susceptibility and neutron scattering measurements in the A-Phase of MnSi, a two-dimensional skyrmion lattice [1], as a function of electric DC currents. The non-colinear spin structure is here intrinsic and due to Dzyaloshinsky-Moriya interactions, resulting in a very small pinning.

We find distinct features that suggest spin torque effects at current densities that are 5 to 6 orders of magnitude smaller than those observed in soft ferromagnets. This identifies helical magnets as a new route to exploiting spin torque effects in novel spintronic applications.

[1] S. Mühlbauer, B. Binz, F. Jonietz, C. Pfleiderer, A. Rosch, A. Neubauer, R. Georgii, P. Böni, Science 323, 915 (2009)

## P-44 Emergence of helimagnons bands in MnSi

**Marc Janoschek<sup>1</sup>, Florian Bernlochner<sup>2</sup>, S.R. Dunsiger<sup>2</sup>, Christian Pfleiderer<sup>2</sup>, Peter Böni<sup>2</sup>, Bertrand Roessli<sup>3</sup>, Peter Link<sup>4</sup>, Achim Rosch<sup>5</sup>**

<sup>1</sup>Universität zu Köln, II. Physikalisches Institut, Germany

<sup>2</sup>TU München, Physik Department E21, Germany

<sup>3</sup>PSI, Laboratory for Neutron Scattering, Villigen, Switzerland

<sup>4</sup>Forschungs-Neutronenquelle Heinz Maier-Leibnitz (FRM II), München, Germany

<sup>5</sup>Universität zu Köln, Institut für Theoretische Physik, Germany

Recent theoretical studies [1,2] predict that the broken inversion symmetry in the helimagnetic phase of MnSi will lead to a rich spectrum of Goldstone modes, also referred to as helimagnons, for wave vectors that are small compared to the helical propagation vector  $k$ . However, for wave vectors that are large compared to  $k$ , and thus correspond to length scales over which the magnetic moments are coupled almost ferromagnetically, a nearly ferromagnetic dispersion was generally expected, even in the helical phase.

We have performed extensive inelastic neutron scattering experiments by means of triple-axis spectroscopy in order to explore the nature of these excitations in the helical phase. We observed broad dispersive excitations that are not in agreement with the expected ferromagnetic behavior in large wave vector limit. Using a parameter free model that extends [1] to the regime of large wave vectors, we quantitatively establish that these excitations represent broad and intense spin wave bands that are purely caused by the tiny magnetic propagation vector. The long-period of the helix implies a small magnetic Brillouin zone leading to multiple Umklapp interactions and thus many helimagnon modes in a magnetic reduced zone schema.

Our study provides a tractable show-case how collective spin excitations may be radically modified even in simple systems by seemingly harmless small magnetic propagation vectors.

[1] D. Belitz, T. R. Kirkpatrick and A. Rosch Phys. Rev. B 73, 054431 (2006) [2] S. V. Maleyev, Phys. Rev. B 73, 174402 (2006)

## P-45 Skyrmion Lattice in $\text{Fe}_{1-x}\text{Co}_x\text{Si}$

Tim Adams<sup>1</sup>, Wolfgang Münzer<sup>1</sup>, Christian Franz<sup>1</sup>, Andreas Neubauer<sup>1</sup>, Sebastian Mühlbauer<sup>1</sup>, Florian Jonietz<sup>1</sup>, Christian Pfeleiderer<sup>1</sup>, Benedikt Binz<sup>2</sup>, Achim Rosch<sup>2</sup>, Robert Georgii<sup>3</sup>, Peter Böni<sup>1</sup>, Martin Schmid<sup>4</sup>, Juri Grin<sup>4</sup>

<sup>1</sup>TU München, Physik Department E21, Germany

<sup>2</sup>Universität zu Köln, Institut für Theoretische Physik, Germany

<sup>3</sup>Forschungs-Neutronenquelle Heinz Maier-Leibnitz (FRM II), München, Germany

<sup>4</sup>MPI für Chemische Physik fester Stoffe, Dresden, Germany

The recent identification of the A-phase in MnSi as a hexagonal lattice of anti-skyrmions raises the question, if skyrmion lattice ground states exist in further members of the series of B20 transition metal compounds. We have grown single crystals of selected compositions in the series  $\text{Fe}_{1-x}\text{Co}_x\text{Si}$  by means of vapor transport and optical float zoning. Our samples are consistent with the previously reported temperature versus composition phase diagram. Comprehensive neutron scattering and magneto-transport measurements establish an extremely rich magnetic phase diagram of skyrmion phases as a function of magnetic field strength, temperature and direction.

## P-46 Ferromagnetic Quantum Phase Transition in $\text{Pd}_{1-x}\text{Ni}_x$

Christian Franz<sup>1</sup>

<sup>1</sup>TU München, Physik Department E21, Germany

Growing experimental evidence suggests that ferromagnetic quantum criticality in pure compounds, quite generally, is pre-empted by a first order transition or the emergence of complex modulated order. Recently a ferromagnetic quantum critical point has been reported in Ni-doped Pd for a Ni concentration  $x_c \approx 2.5\%$ . This QCP appears to be consistent with the marginal Fermi liquid state of a pure three-dimensional ferromagnet. We have revisited this issue in detailed measurements of the magnetization, specific heat and magneto-transport as well as neutron depolarization tomography, a new technique to map out variations of ferromagnetic components. For concentrations far from  $x_c$  we find the behavior expected of a marginal Fermi liquid. However, as the critical concentration is approached strong inconsistencies with the predictions of a marginal Fermi liquid are observed, indicating a trend to a first order quantum phase transition.

## P-47 Spin Liquid and Spin Ice

S.R. Dunsiger<sup>1</sup>, R.F. Kiefl<sup>2</sup>, S.T. Bramwell<sup>3</sup>, K.H. Chow<sup>4</sup>, J.P. Clancy<sup>5</sup>, J.R.D. Copley<sup>6</sup>, H.A. Dabkowska<sup>5</sup>, J.S. Gardner<sup>7</sup>, B.D. Gaulin<sup>5</sup>, T. Jenkins<sup>6</sup>, G.D. Morris<sup>8</sup>, A.N. Price<sup>9</sup>, Y. Qiu<sup>6</sup>, J.P. Ruff<sup>5</sup>, J.E. Sonier<sup>10</sup>

<sup>1</sup>TU München, Physik Department E21, Germany

<sup>2</sup>University of British Columbia, Vancouver, Canada

<sup>3</sup>University College London, United Kingdom

<sup>4</sup>University of Alberta, Edmonton, Canada

<sup>5</sup>McMaster University, Hamilton, Canada

<sup>6</sup>NIST Center for Neutron Research, Gaithersburg, USA

<sup>7</sup>Indiana University, Bloomington, USA

<sup>8</sup>TRIUMF, Vancouver, Canada

<sup>9</sup>Universität Erlangen-Nürnberg, Germany

<sup>10</sup>Simon Fraser University, Vancouver, Canada

Due to the geometry of their underlying crystal structure, many magnetic materials form networks such that it may not be possible to energetically satisfy all interactions simultaneously: the system is said to be frustrated. The curiosity about these systems stems from the possibility that if conventional magnetic order is highly frustrated then one may find novel low temperature behaviour. There is now considerable evidence that the ground state is „fragile,, or extremely sensitive to a variety of factors such as anisotropy, the range of the spin-spin interactions, thermal and quantum fluctuations, as well as disorder.

The pyrochlore oxides, of general formula  $A_2B_2O_7$  are comprised of networks of corner sharing tetrahedra. In particular, the geometrically frustrated pyrochlore  $Tb_2Ti_2O_7$  remains an enigma - combined neutron scattering and  $\mu$ SR results point to a cooperative paramagnetic or spin liquid state with persistent spin dynamics down to the millikelvin regime in zero applied magnetic field, even though antiferromagnetic correlations develop as high as 50 K. Indeed, such an example of a geometrically frustrated system which does not magnetically order at low temperature is extremely rare. By contrast, in the isostructural compound  $Ho_2Ti_2O_7$ , there is a gradual freezing of the spin fluctuations at low temperatures. Two of the spins on the vertices of any tetrahedron are constrained by anisotropy to point in toward the centre of the tetrahedron, while the remaining two point outwards. The statistical mechanics governing the low temperature spin configuration in this so called spin ice material mimics that of proton disorder in water ice and as such, it is a model magnetic system.

I will describe our recent progress using the complementary techniques of  $\mu$ SR and neutron scattering to explore the phase diagram of these unusual magnetic systems, as well as their low energy excitations.

## P-48 Crystallographic and magnetic study of synthetic cobalt-olivine single crystal

Andrew Sazonov<sup>1,2</sup>, Martin Meven<sup>1</sup>, Vladimir Hutanu<sup>1,2</sup>, Gernot Heger<sup>2</sup>

<sup>1</sup>Forschungs-Neutronenquelle Heinz Maier-Leibnitz (FRM II), München, Germany

<sup>2</sup>RWTH Aachen, Institut für Kristallographie, Germany

Orthosilicate olivine ( $Mg_{1-x}Fe_x)_2SiO_4$  is a major phase of the earth's upper mantle. Knowledge of its thermodynamic properties is crucial for undertaking many mineralogical, petrological and geo-physical investigations. Besides the importance for geologists and mineralogists, olivines display a surprising variety of chemical and physical properties.

$M_2SiO_4$  compounds crystallizing in the olivine structure are characterized by a distorted hexagonal close-packed array of oxygen anions in which one-eighth of the tetrahedral interstices are filled by silicon and one-half of the octahedral interstices are occupied by the divalent metal cation  $M$ . The olivine-type silicates have an orthorhombic crystal structure with the space group  $Pnma$ , in which four formula units are contained in the unit cell ( $Z = 4$ ). The Si atoms are coordinated by four O atoms to form isolated  $SiO_4$  tetrahedra connected via divalent cations  $M$ . These cations are surrounded by six O atoms and occupy two distinct octahedral sites;  $M1$  is located on a center of symmetry and  $M2$  on a mirror plane.

Most of the studies provided on the olivine-type oxides have been performed at or above room temperature and at high pressure. In spite of these investigations, uncertainties and gaps in knowledge still persist. One of the less-studied olivine-type silicates is the synthetic cobalt olivine,  $Co_2SiO_4$ .

The main goal of the present study is to determine precisely the changes in the crystal and magnetic structures of  $Co_2SiO_4$  in the temperature range from 2.5 K to 300 K by means of single crystal neutron diffraction measurements. The high accuracy in the determination of the atomic positions and the atomic displacement parameters (ADPs) in this study was essential to correctly interpret the experimental electron and spin density maps obtained in our experiments with synchrotron radiation and polarized neutrons. Moreover, the magnetic properties of  $Co_2SiO_4$  have been investigated now in more detail. We also present the result of a complete symmetry analysis of the possible magnetic structures for  $Co_2SiO_4$  which have not been discussed before in detail, while the different magnetic structure models were already proposed earlier [1-3].

[1]. S. Nomura, R. Santoro, J. Fang and R.J. Newnham. J. Phys. Chem. Solids 25, 901 (1964). [2]. H. Kondo and S. Miyahara. J. Phys. Soc. Jpn. 21, 2193 (1966). [3]. W. Lottermoser and H. Fuess. Phys. Stat. Sol. A 109, 589 (1988).

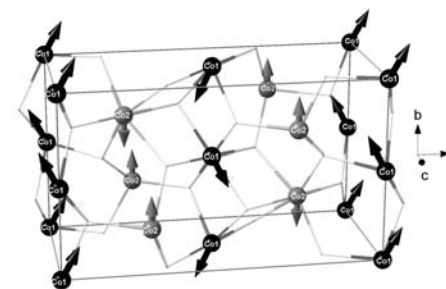


Figure 9.2: A schematic representation of  $Co_2SiO_4$  magnetic structure

## P-49 Magnetic structure in multiferroic pyroxenes: (Na,Li)FeSi<sub>2</sub>O<sub>6</sub>

**Max Baum**<sup>1</sup>, **Alexander C. Komarek**<sup>1</sup>, **Navid Qureshi**<sup>1</sup>, **Petra Becker-Bohaty**<sup>2</sup>, **Ladislav Boharty**<sup>2</sup>, **Martin Meven**<sup>3</sup>, **Astrid Schneidewind**<sup>3</sup>, **Peter Link**<sup>3</sup>, **M. Teresa Fernandez-Diaz**<sup>4</sup>, **Markus Braden**<sup>1</sup>

<sup>1</sup>Universität zu Köln, II. Physikalisches Institut, Germany

<sup>2</sup>Universität zu Köln, Institut für Geologie und Mineralogie, Germany

<sup>3</sup>Forschungs-Neutronenquelle Heinz Maier-Leibnitz (FRM II), München, Germany

<sup>4</sup>ILL, Grenoble, France

(Na,Li)FeSi<sub>2</sub>O<sub>6</sub> exhibit multiferroic properties. Previous neutron diffraction experiments on powder samples of both compounds were interpreted in a commensurate model with antiferromagnetically coupled FeO<sub>6</sub> chains of anti- or ferromagnetic character. Our tripleaxis result of a single crystal is at odds with the former published commensurate model for magnetic ordering: magnetic ordering is incommensurate in (Na,Li)FeSi<sub>2</sub>O<sub>6</sub> with a temperature independent modulation.

Magnetic satellites appear at q-positions corresponding to an incommensurate modulation vector (0,0.78,0). Based on powder neutron diffraction data, Redhammer et al. propose the Shubnikov group P21/c as the magnetic space group for LiFeSi<sub>2</sub>O<sub>6</sub>. This corresponds in antiferromagnetic ordering within and between the FeO<sub>6</sub> chains. Our measurement on a single crystal reveals the Shubnikov group P21/c' which is equivalent to ferromagnetic coupling within the chains and antiferromagnetic coupling between the chains.

## 10 Radiography and Tomography

### P-50 Quantitative Neutron Radiography and Tomography at NECSA

Mabuti Radebe<sup>1</sup>, Frikkie De Beer<sup>1</sup>

<sup>1</sup>NECSA, Radiation Service, Pretoria, South Africa

The SANRAD ( SOUTH AFRICAN NEUTRON RADIOGRAPHY) facility consist of one infrastructural facility based on two sources of penetrating radiation, i.e. SAFARI-1 research nuclear reactor as thermal neutron source and a 100kV x-ray generator. This facility, which hosts the only operational neutron tomography R&D facility in the Southern Hemisphere and in Africa, are being extensively utilized by post graduate students and industry. The facility sees application in a wide range of scientific and engineering disciplines, amongst which is nuclear science and technology, geosciences, palaeontology, civil, mechanical, chemical, etc. The SANRAD facility upgrade towards the SANCRAT (SOUTH AFRICAN NATIONAL CENTRE FOR RADIOGRAPHY AND TOMOGRAPHY) is underway. The centre is envisaged to host thermal neutron-, x-ray micro focus-, higher energy x-ray- and gamma ray penetrating radiation imaging infrastructures.

This presentation focuses on the implementation and utilization of QNI (Quantitative Neutron Imaging) software package for the correction of neutron radiographs for the scattering component from the radiation containment environment and multiple scatter of the sample. It entails the determination of experimental water attenuation coefficient and comparison to the theoretical value, as well as the characterisation and quantification of porous media using neutron radiography at the SANRAD facility. Recent results obtained through QNI will be discussed and supplementary experiments to be conducted at FRM II and PSI during the IAEA fellowship will be outlined.

[1] F.C. de Beer, "Characteristics of the neutron/X-ray tomography system at the SANRAD facility in South Africa", NIM-A, 542 (2005), p1-8.

### P-51 Phase-Contrast and Dark-field Imaging with Neutrons

Franz Pfeiffer<sup>1</sup>

<sup>1</sup>TU München, Physik Department E17, Germany

Imaging with visible light today uses numerous contrast mechanisms, including bright- and dark-field contrast, phase-contrast schemes and confocal and fluorescence-based methods. Neutron (and X-ray) imaging, on the other hand, has only recently seen the development of an analogous variety of contrast modalities.

In this presentation I will describe our recently developed novel approach for phase-contrast and dark-field imaging with neutron sources. I will first describe the basic principles, advantages, and limitations of phase-contrast and dark-field imaging based on a grating interferometer. Then, I present several novel application examples to material science. I will particularly focus on recent work, in which neutron dark-field imaging has been used to visualize the bulk magnetization behaviors of thick ferromagnetic specimens.

[1] F. Pfeiffer, C. Gruenzweig, O. Bunk, G. Frei, E. Lehmann, and C. David, Physical Review Letters 96, 215505 (2006)

[2] C. Gruenzweig, C. David, O. Bunk, M. Dierolf, G. Frei, G. Kuehne, J. Kohlbrecher, R. Schaefer, P. Lejcek, H.M.R. Rønnow, and F. Pfeiffer, Physical Review Letters 101, 025504 (2008)

[3] M. Strobl, C. Grünzweig, A. Hilger, I. Manke, N. Kardjilov, C. David, and F. Pfeiffer, Physical Review Letters 101, 123902 (2008)

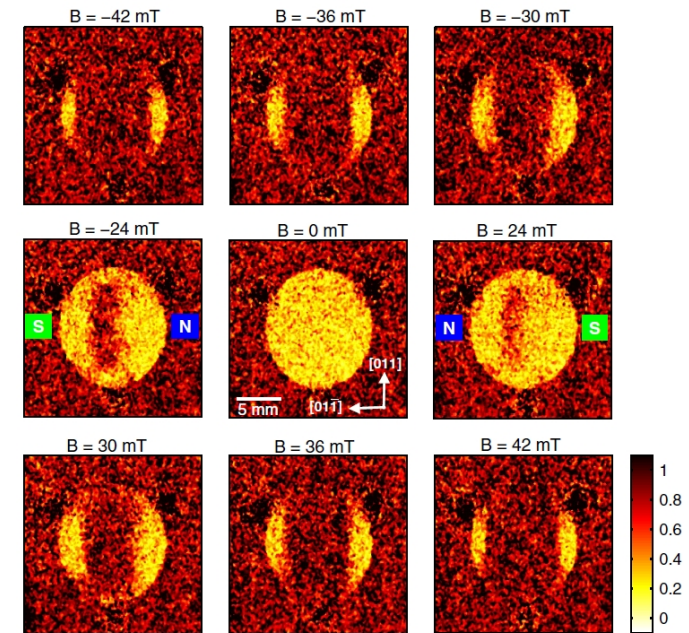


Figure 10.1: Neutron dark-field imaging visualizes the magnetization process in a bulk ferromagnetic test sample (here a single-crystalline FeSi disc)

## 11 Structure

### P-52 Microscopic Suppression of Training and Origin of Training Effect in Exchange Bias System

Amitesh Paul<sup>1</sup>

<sup>1</sup>Helmholtz-Zentrum Berlin für Materialien und Energie, Germany

Difference between subsequent (partial) magnetization reversal loops is called the “training effect”. Even though the microscopic origin of the training effect is still under debate, it is generally agreed to be due to rearrangement of interfacial antiferromagnetic spin structure, which can be considered as rotatable hysteretic grains (rotatable anisotropy) particularly in exchange biased polycrystalline specimens. It has been a challenge to understand the origin as well as to overcome the training response. There have been attempts in that direction but mainly by manipulating the field (external) strengths or the direction. Here we report of regaining the untrained state, neither by using the temperature variation nor by modifying the field and this makes this finding unique.

We have observed earlier that cooling the system in a remanent state (rendering spontaneous exchange bias), may even lead to a suppression of the training effect, whereas the same sample being field-cooled exhibits a clear training response.

By using a depth-sensitive polarized neutron scattering technique in specular and off-specular mode, we observe that cooling an exchange bias system in a remanent state (without an external magnetic field) results in a microscopic suppression of training.

Such untrained state with spontaneous exchange bias provides a unique basis in understanding the training effect in general – an interplay between uniaxial anisotropy and rotating grains in polycrystalline antiferromagnetic layer. Coupling remains unaffected for similar population of rotating grains, favouring symmetric reversal of FM layer with similar exchange bias, independent of number of field cycles. This results therefore pave the way for technological exploitation.

### P-53 Aggregation of mixed surfactant system by SANS method

Aldona Rajewska<sup>1</sup>

<sup>1</sup>Institute of Atomic Energy, Swierk-Otwock, Poland

Mixtures of surfactants: classic nonionic heptaethylene glycol monodecyl ether (C<sub>10</sub>E<sub>7</sub>) and anionic fluorosurfactant potassium perfluorooctane sulfonate (KFOS) in D<sub>2</sub>O (heavy water) were investigated with small angle neutron scattering method at KWS-2 instrument.

Samples were investigated in two series:

I serie (main part):

10 samples: KFOS+D<sub>2</sub>O only (1 sample) for concentration 25mM/l, C<sub>10</sub>E<sub>7</sub>+D<sub>2</sub>O only (1 sample) 25mM/l, [KFOS+C<sub>10</sub>E<sub>7</sub>+D<sub>2</sub>O] (8 samples) for concentrations: 2.5mM/l KFOS / 22.5mM/l C<sub>10</sub>E<sub>7</sub>, 5mM/l KFOS / 20 mM/l C<sub>10</sub>E<sub>7</sub>, 7.5mM/l KFOS / 17.5 mM/l C<sub>10</sub>E<sub>7</sub>, 10mM/l KFOS / 15mM/l C<sub>10</sub>E<sub>7</sub>, 12.5mM/l KFOS / 12.5 mM/l C<sub>10</sub>E<sub>7</sub>, 15 mM/l KFOS / 10 mM/l C<sub>10</sub>E<sub>7</sub>, 17.5 mM/l KFOS / 7.5mM/l C<sub>10</sub>E<sub>7</sub>, 22.5 mM/l KFOS / 2.5mM/l C<sub>10</sub>E<sub>7</sub>.

II serie (contrast variation):

8 samples - for 0.3 KFOS+0.7 C<sub>10</sub>E<sub>7</sub> e.g 7.5mM/l KFOS / 17.5 mM/l C<sub>10</sub>E<sub>7</sub> (4 samples) 1cv - only in H<sub>2</sub>O, 2cv (0.5ml H<sub>2</sub>O+1.5ml D<sub>2</sub>O), 3cv (1ml H<sub>2</sub>O+1ml D<sub>2</sub>O), 4cv (1.5ml H<sub>2</sub>O+0.5ml D<sub>2</sub>O) and for 0.7 KFOS+0.3 C<sub>10</sub>E<sub>7</sub> e.g. 17.5mM/l KFOS / 7.5 mM/l C<sub>10</sub>E<sub>7</sub> (4 samples) 5cv – only H<sub>2</sub>O, 6cv (0.5ml H<sub>2</sub>O+1.5ml D<sub>2</sub>O), 8cv (1mlH<sub>2</sub>O+1ml D<sub>2</sub>O), 9cv (1.5ml H<sub>2</sub>O+0.5ml D<sub>2</sub>O).

All of surfactants solutions in part I of experiment were prepared using D<sub>2</sub>O as a solvent (99.9% deuterated) but for part II with H<sub>2</sub>O, too. The nonionic C<sub>10</sub>E<sub>7</sub> and anionic KFOS surfactants were purchased in Sigma - Aldrich and were used without further purification. All SANS measurements were performed on KWS-2 SANS spectrometer at FRM II, Garching.

Neutrons were used of wavelength 7 Å<sup>-1</sup>. For the measurements quartz cells of thickness 2mm (part I experiment) and 1 mm (part II experiment) were used.

## P-54 GISANS study of sponge-like TiO<sub>2</sub> structures for photovoltaic applications

Gunar Kaune<sup>1</sup>, Qi Zhong<sup>1</sup>, Reinhard Kampmann<sup>2</sup>, Martin Haese-Seiller<sup>2</sup>, Peter Müller-Buschbaum<sup>1</sup>

<sup>1</sup>TU München, Physik-Department E13, Germany

<sup>2</sup>GKSS-Forschungszentrum Geesthacht, Germany

Photovoltaic energy conversion systems based on an inorganic semiconductor and an organic hole transporting material, so called hybrid solar cells, have emerged to a promising alternative technology for solar light harvesting [1]. In a common device, a nanosized structure with a large interface between the two components is necessary to separate efficiently excitons generated by incoming light. This can be achieved by application of a nanostructured inorganic semiconducting material, whose interspaces are filled with a polymeric hole transporting material.

In our model system we use nanostructured titanium dioxide (TiO<sub>2</sub>) films with a sponge-like morphology, which is prepared by application of a sol-gel process [2]. To further structure the films on micrometer scale colloidal particles are added to the sol-gel solution as a secondary template and subsequently removed from the spin coated films by calcination [3]. The resulting structure in the films is studied with grazing incidence small angle neutron scattering (GISANS) at the REFSANS instrument.

To qualify the penetration of the polymeric hole transport material into the TiO<sub>2</sub> morphology a thin film of poly(N-vinylcarbazole) (PVK) is spin coated on top of the TiO<sub>2</sub> layer and the resulting hybrid film structure probed again with GISANS. Since PVK matches the scattering contrast of TiO<sub>2</sub> from the GISANS data conclusions on the degree of pore filling can be drawn. For additional structural characterisation scanning electron microscopy and atomic force microscopy are used.

[1] U. Bach, D. Lupo, P. Comte, J. E. Moser, F. Weissörtel, J. Salbeck, H. Spreitzer, M. Grätzel, Nature 395, 583 (1998) [2] M. Memesa, S. Weber, S. Lenz, J. Perlich, R. Berger, P. Müller-Buschbaum, J. S. Gutmann, Energy Environ. Sci. 2009, DOI: 10.1039/b902754h [3] G. Kaune, M. Memesa, R. Meier, M. A. Ruderer, A. Diethert, J. S. Gutmann, P. Müller-Buschbaum, in preparation

## P-55 Development of C-S-H Microstructure in UHPC with QENS, <sup>29</sup>Si NMR and XRD

Tobias Gutberlet<sup>1</sup>, Harald Hilbig<sup>1</sup>, Robin E. Beddoe<sup>1</sup>

<sup>1</sup>TU München, Centrum Baustoffe und Materialprüfung, Germany

For the optimization of the mechanical and chemical properties of Ultra High Performance Concrete (UHPC), a scientific working knowledge of microstructure formation depending on temperature and composition is necessary. The strength-giving phase of UHPC is C-S-H (Calcium Silicate Hydrate) formed by the hydration of Ca<sub>3</sub>SiO<sub>5</sub> with SiO<sub>2</sub>. At present, the development of C-S-H microstructure is not well understood and current models are inadequate.

Therefore the quasi-elastic neutron scattering technique will be used to study the kinetics of water-bonding in different Ca<sub>3</sub>SiO<sub>5</sub>-SiO<sub>2</sub>-H<sub>2</sub>O systems at temperatures varying from 10 to 90°C. Parallel investigations are being performed with <sup>29</sup>Si NMR to observe the structure (polymerisation) of the silicates and with XRD to examine the formation of Ca(OH)<sub>2</sub> and the consumption of Ca<sub>3</sub>SiO<sub>5</sub> in the hydration process. After preparing the paste samples, the QENS, XRD (both in situ) and NMR data are taken in short intervals during the first day of hydration. Afterwards the intervals are continuously increased up to two weeks. The presented results of preliminary investigations are promising.

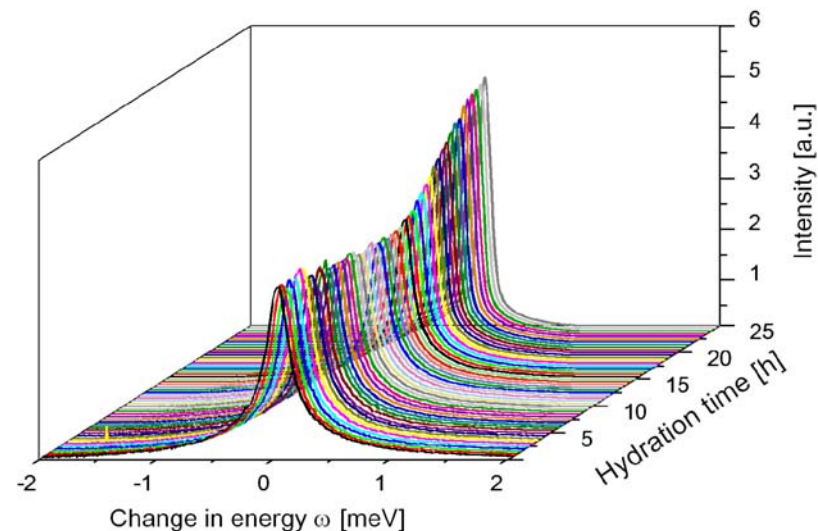


Figure 11.1: Quasi-elastic neutron scattering of a Ca<sub>3</sub>SiO<sub>5</sub>-SiO<sub>2</sub>-H<sub>2</sub>O system at 20°C in the first 25 hours of hydration



## P-58 Characterization of PMDEGA hydrogel films

Qi Zhong<sup>1</sup>, Weinan Wang<sup>1</sup>, Achille Mayelle Bivigou Koumba<sup>2</sup>, André Laschewsky<sup>2</sup>, Christine M. Papadakis<sup>1</sup>, Martin Haese-Seiller<sup>3</sup>, Reinhard Kampmann<sup>3</sup>, Peter Müller-Buschbaum<sup>1</sup>

<sup>1</sup>TU München, Physik Department E13, Germany

<sup>2</sup>Universität Potsdam, Institut für Chemie, Germany

<sup>3</sup>GKSS-Forschungszentrum Geesthacht, Germany

Stimuli-sensitive hydrogels exhibit interesting properties which attract increasing attention due to a large variety of applications. The novel thermo-responsive homopolymer poly(monomethoxy diethyleneglycol acrylate) (PMDEGA) exhibits a higher lower critical solution temperature (LCST) as compared to the frequently investigated thermoresponsive polymer poly(N-isopropylacrylamide) (PNIPAM).

Thus PMDEGA can be an interesting alternative to the use of PNIPAM. In order to create an internal ordering in the thin hydrogel films of PMDEGA, the homopolymer is replaced by a PMDEGA based triblock copolymer with polystyrene end-block, P(S-b-MDEGA-b-S). Thin films are prepared out of solution on Si substrates. To investigate the swelling behaviour dry and wet films are compared. The wet films are achieved by placing the PMDEGA based samples in a saturated atmosphere of deuterated water. The internal structure is investigated with grazing incidence small-angle neutron scattering (GISANS). As a consequence, the incorporated water is detected.

These measurements were performed at the REFSANS instrument in time-of flight mode (TOF). A sample-to-detector distance of 8.75 m and an incident angle of  $0.5^\circ$  are applied during the measurement. In addition, the thin dry films are probed with X-ray reflectivity.

## P-59 PLEPS investigation of binary Fe-Cr model alloys

Vladimir Slugen<sup>1</sup>, Stanislav Sojak<sup>1</sup>, Vladimir Krsjak<sup>1</sup>, Werner Egger<sup>2</sup>

<sup>1</sup>Slovak University of Technology, Department of Nuclear Technology, Bratislava, Slovakia

<sup>2</sup>Universität der Bundeswehr München, Institut für Angewandte Physik und Messtechnik, Neubiberg, Germany

Reduced activation ferritic/martensitic (RAFM) steels are due to very good stress resistance (radiation, temperature, mechanical stress) considered as the structural materials for the application in future nuclear facilities. In laboratory conditions is neutron radiation damage experimentally simulated by high energy ions (helium, hydrogen, etc.).

The Pulsed Low Energy Positron System (PLEPS) at the research reactor FRM II was used to study the depth profiling of binary Fe-Cr alloys. Fe-Cr model alloys with different chromium content were investigated in as-received state as well as after 250 keV helium ions implantation (doses up to  $6.24 \times 10^{17} \text{ cm}^{-2}$ ). PLEPS allows us to observe large void defects in layer close to the surface (500 nm). These results correspond well with helium profile maxima calculated by SRIM software and also with results gained by Scanning Electron Microscope (SEM) [1]. Influence of increasing chromium content in binary Fe-Cr alloys was registered in the change of the size and distribution of vacancy type defects for both, implanted and as-received specimens.

[1] Krsjak V., Sojak S., Slugen V., Petriska M., Troev T.: Ion implantation induced defects in Fe-Cr alloys studied by conventional positron annihilation lifetime spectroscopy; Positron studies of defects (PSD), Czech republic - Prague, 1-5.september 2008 (in print)

## P-60 SANS contrast dependence on difference in thermal expansions of phases in two-phase alloys

Pavel Strunz<sup>1</sup>, Ralph Gilles<sup>2</sup>, Debashis Mukherji<sup>3</sup>, Michael Hofmann<sup>2</sup>, Dominique del Genovese<sup>3</sup>, Joachim Rösler<sup>3</sup>, Markus Hoelzel<sup>5</sup>, Vadim Davydov<sup>4</sup>

<sup>1</sup>Nuclear Physics Institute, Neutron Physics Laboratory, Rez, Czech Republic

<sup>2</sup>Forschungs-Neutronenquelle Heinz Maier-Leibnitz (FRM II), München, Germany

<sup>3</sup>TU Braunschweig, Institut für Werkstoffe, Germany

<sup>4</sup>Nuclear Physics Institute ASCR, Husinec-Rez, Czech Republic

<sup>5</sup>TU Darmstadt at Forschungs-Neutronenquelle Heinz Maier-Leibnitz (FRM II), München, Germany

Theoretical expressions describing SANS scattering contrast dependence on temperature in the region where no phase-composition changes occur were derived for two-phase Ni superalloys.

The theory is based on the difference in thermal expansion of the two primary phases,  $\gamma$  and  $\gamma'$ . The simulations show that the scattering-contrast temperature evolution is significant enough to be considered in in-situ SANS experiments with superalloys at elevated temperatures. The performed simulations show that the magnitude of the scattering contrast at room temperature is firmly connected with the particular shape of the scattering-contrast temperature dependence. This fact can be used for the determination of the scattering contrast without a knowledge of the compositions of the individual phases.

The derived theoretical expressions for scattering contrast were proven experimentally on a Ni-Fe-base alloy DT706. The evolution of lattice parameters of both the matrix and the precipitate phases was obtained from the in-situ wide angle neutron diffraction experiment (StressSpec and SPOD). The theoretical scattering contrast dependence was then successfully fitted to the measured SANS (V4, HZB) integral intensity.

## P-61 Lattice dynamics in ferromagnetic shape memory alloys

Jürgen Neuhaus<sup>1</sup>, Semih Ener<sup>2</sup>, Winfried Petry<sup>1</sup>, Klaudia Hradil<sup>3</sup>, Peter Link<sup>1</sup>, Richard A. Mole<sup>1</sup>

<sup>1</sup>Forschungs-Neutronenquelle Heinz Maier-Leibnitz (FRM II), München, Germany

<sup>2</sup>TU München, Physik Department E13, Germany

<sup>3</sup>Universität Göttingen, Institut für Physikalische Chemie, Germany

Ferromagnetic shape memory alloys with chemical composition close to the stoichiometric Ni<sub>2</sub>MnGa composition have received great interest due to their unique physical properties like magnetic shape memory effect (MSM), giant magnetic field induced strain (MFIS) and giant magnetocaloric effect (MCE) [1,2].

In recent years, much attention has been given to phonon measurements relating anomalies in specific branches to the phase transitions observed in Ni<sub>2</sub>MnGa [3-5]. First principle calculations in Ni-Mn-X alloys with stoichiometric composition relate Fermi nesting effects and the magnetic order to the observed anomalies.

In this work we investigated the whole phonon dispersion for a Ni<sub>49</sub>Mn<sub>32</sub>Ga<sub>19</sub> alloy in the high temperature Austenite (L21 structure) as well as in the low temperature Martensite phase with a 5M modulation in comparison to the stoichiometric composition. Phonon anomalies have been studied in detail along the ( $\zeta, \zeta, 0$ ) TA2 branch with [1 -1 0] polarization with using the three-axis instruments PUMA and PANDA.

The measurements revealed that both systems show strong temperature dependent phonon softening in the TA2 branch. The observed temperature dependence in the optical branches do not follow the prediction from first principle calculations.

[1] A. Sozinov, A.A. Likhachev, N. Lanska and K. Ullakko, Appl. Phys. Lett. 80 (2002) 1746. [2] L. Pareti, M. Solzi, F. Albertini and A. Paoluri, Eur. Phys. J. B 32 (2003) 303. [3] A. Zheludev, S.M. Shapiro and P. Wochner, Phys. Rev. B 51 (1995) 11310. [4] U. Stuhr, P. Vorderwisch and V.V. Kokorin, J. Phys.: Condens. Matter 12 (2000) 7541. [5] L. Mañosa, A. Planes, J. Zarestky, T. Lograsso, D.L. Schlagel and C. Stassis, Phys. Rev. B 64 (2001) 024305. [6] A.N. Vasil'ev, A.D. Bozhko, V.V. Khovailo, i.e. Dikshtein, V.G. Shavrov, V.D. Buchelnikov, M. Matsumoto, S. Suzuki, T. Takagi and J. Tani, Phys. Rev. B 59 (1999) 1113.

## P-62 Hydrogen-related defects in ZnO single crystals

Jakub Cizek<sup>1</sup>, Ivan Prochazka<sup>1</sup>, Oksana Melikhova<sup>1</sup>, Gerhard Brauer<sup>2</sup>, Wolfgang Anwand<sup>2</sup>, Werner Egger<sup>3</sup>, Peter Sperr<sup>3</sup>, Christoph Hugenschmidt<sup>4</sup>, Vladimir Havranek<sup>5</sup>

<sup>1</sup>Charles University in Prague, Faculty of Mathematics and Physics, Czech Republic

<sup>2</sup>FZ Dresden-Rossendorf, Germany

<sup>3</sup>Universität der Bundeswehr München, Institut für Angewandte Physik und Messtechnik, Neubiberg, Germany

<sup>4</sup>Forschungs-Neutronenquelle Heinz Maier-Leibnitz (FRM II), München, Germany

<sup>5</sup>Nuclear Physics Institute of the ASCR, Husinec-Rez, Czech Republic

ZnO is a wide band gap semiconductor with a variety of applications. Properties of ZnO single crystals are significantly influenced by lattice defects. A detailed characterization of lattice defects in ZnO crystals is, therefore, of a great importance. Hydrothermally (HT) grown ZnO single crystals with (0001) orientation were investigated on high-resolution conventional positron lifetime (LT) spectrometer and on pulsed positron beam PLEPS. The following specimens were studied: (i) virgin as-grown crystal, (ii) ZnO crystal implanted at room temperature with 2.5 MeV H<sup>+</sup> ions, and (iii) ZnO crystal covered with 30 nm thick Pd over-layer and electrochemically loaded with hydrogen. The virgin crystal exhibits (a) a single component spectrum with lifetime 182 ps, which is remarkably longer than the bulk ZnO lifetime obtained from the first principles theoretical calculations [1] and also from experiment [2], (b) a very short positron diffusion length. This indicates that virgin HT grown crystal contains already significant concentration of defects which trap positrons. By comparison with theoretical calculations these defects were identified as Zn-vacancies surrounded by hydrogen atoms. The mean positron lifetime in H<sup>+</sup> implanted crystal converges to a higher value compared to the virgin sample. It testifies that H<sup>+</sup> implanted crystal contains additional defects created by bombardment of energetic protons. The crystal electrochemically doped with hydrogen exhibits significantly higher positron lifetime measured by slow positron beam. However, at the same time there is only a moderate change of the lifetime measured by conventional LT spectroscopy. It was found that electrochemical hydrogen loading causes plastic deformation of the crystal and a slip in the direction of c-axis [3]. A high value of mean positron lifetime measured on the beam indicates that small vacancy clusters or voids have been introduced into a subsurface layer by hydrogen-induced plastic deformation.

[1] G. Brauer et al., Phys. Rev. B 74, 045208 (2006). [2] G. Brauer et al., Phys. Rev. B 79, 115212 (2009). [3] J. Cizek et al., J. Appl. Phys. 103, 053508 (2008).

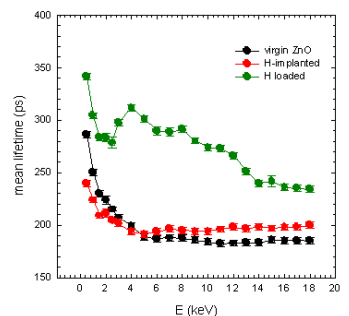


Figure 11.4: Mean positron lifetime measured on ZnO crystals as a function of energy of incident positrons.

## P-63 Temperature and composition dependence of the crystal and magnetic structures of La<sub>2-*x*</sub>Sr<sub>*x*</sub>CoIrO<sub>6</sub> (0 < *x* < 2)

Narendirakumar Narayanan<sup>1</sup>, Daria Mikhailova<sup>1</sup>, Helmut Ehrenberg<sup>2</sup>, Dmytro Trots<sup>3</sup>, Anatoliy Senyshyn<sup>4</sup>, Hartmut Fueß<sup>1</sup>

<sup>1</sup>TU Darmstadt, Fachbereich Materialwissenschaft, Germany

<sup>2</sup>Leibniz-Institut für Festkörper- und Werkstoffforschung Dresden, Institut für Komplexe Materialien, Germany

<sup>3</sup>HASYLAB at DESY, Hamburg, Germany

<sup>4</sup>Forschungs-Neutronenquelle Heinz Maier-Leibnitz (FRM II), München, Germany

In recent years double perovskites (DP) A<sub>2</sub>BB'O<sub>6</sub> with 3d transition metals at B-site and 4d or 5d transition metals at B'-site have been extensively studied due to their interesting physical properties such as structural phase transitions, magnetic ordering or metal-insulator transition, that could be tuned by the partial substitution of the ions involved [1]. In this sense Ir based DPs are less investigated compared to Re or Os based ones. But its ability to display different oxidation states and structural constraints (distortion of bond angles) on the spatially more extended 5d orbitals promise interesting physical properties. The La<sub>2-*x*</sub>Sr<sub>*x*</sub>CoIrO<sub>6</sub> system has two degrees of freedom as the partial occupancy of Sr at the A-site reduces the electrons and at the same time the average ionic radii at the A-site determine the structure. La<sub>2-*x*</sub>Sr<sub>*x*</sub>CoIrO<sub>6</sub> was synthesized from La<sub>2</sub>O<sub>3</sub>, SrCO<sub>3</sub>, CoO and IrO<sub>2</sub> at 1200°C. Laboratory x-ray, synchrotron and neutron powder diffraction (NPD) techniques were combined to investigate the temperature and composition dependence of the crystal and magnetic structures for five different compositions *x* = 0, 0.5, 1, 1.5 and 2.

As the average size of the A-site cation increases, depending on the temperature, the following sequence of phases exists in this system: P21/n → P21/n+ I2/m → I2/m → I4/m → Fm-3m. The phase transition P21/n → I2/m is of the first order whereas I2/m → I4/m and I4/m → Fm-3m are second order in nature. The anti-ferromagnetic structure of this system (that exhibits non collinear magnetic ordering) depends on the composition. It varies from *k* = (0 0 0) for *x* = 0 to *k* = (0 1/2 1/2) for *x* = 1, 1.5 and 2. The (anti-ferromagnetic) component *m*AFM varies from (-0.7, 0, 1.5) μB for *x* = 0 to a value around (0, 0, 2.7) μB for *x* = 2.

[1] Q. Zhou, B. J. Kennedy and M. M. Elcombe, J. Solid State Chem. 180, 541 (2007).

## 12 Structural Dynamics

### P-64 Phonon lifetimes and superconductivity in Pb-Bi alloys

Nathalie Munnikes<sup>1</sup>, Pegor Aynajian<sup>1</sup>, Lilia Boeri<sup>1</sup>, Thomas Keller<sup>1</sup>, Bernhard Keimer<sup>1</sup>

<sup>1</sup>MPI für Festkörperforschung, Stuttgart, Germany

Previously, the resonance spin-echo mode on the triple-axis (TAS) spectrometer TRISP enabled measurements of the lifetimes of acoustic phonons in the pure elemental superconductors Nb and Pb with  $\mu\text{eV}$  resolution [1,2]. The width of the superconducting gap  $2\Delta(T)$  could be extracted directly from the lifetimes, since phonons with energy  $<2\Delta$  cannot break Cooper pairs and thus have a longer lifetime than phonons with an energy above  $2\Delta$ . Apart from this expected behavior, spin-echo and TAS measurements revealed anomalies in the momentum dependence of the phonon linewidth and related Kramers-Kronig consistent features in the dispersion along the high symmetry directions of transverse acoustic phonons in both Pb and Nb. These were identified as Kohn anomalies, originating from strong electron-phonon scattering at phonon momenta connecting parallel parts of the Fermi surface. Though Pb and Nb have a different structure and Fermi surface, the energy of the lowest Kohn anomaly unexpectedly converged with the low temperature limit of the superconducting energy gap  $2\Delta(0)$  in both materials. Thus, all indications are that the width of the superconducting gap is controlled by the location of normal state Kohn anomalies with similar energy in the acoustic phonon spectrum.

In order to deepen the insight on this apparent correlation between gap and Kohn feature, we proceeded with the investigation of Pb-Bi alloys, which possess higher  $2\Delta$  and  $T_c$  with increasing bismuth concentration, as known from tunneling measurements. Bismuth has one more electron than lead and thus the Fermi surface expands with doping. In fact, the two samples that were grown with 4% and 10% Bi concentration show a systematic shift of the Kohn anomaly to larger wave vectors. The energy of the Kohn anomaly increases in equal measure compared to the superconducting gap, so that they stay locked to each other.

[1] P. Aynajian, T. Keller, L. Boeri, S.M. Shapiro, K. Habicht, B. Keimer, *Science* 319, 1509 (2008).

[2] T. Keller, P. Aynajian, K. Habicht, L. Boeri, S.K. Bose, B. Keimer, *Phys. Rev. Lett.* 96, 225501 (2006).

### P-65 Tunnelling of methyl protons in poly-substituted benzenes

Jean Meinel<sup>1</sup>

<sup>1</sup>Université de Rennes 1, Sciences Chimique, France

In general in benzenes asymmetrically substituted with halogens and methyl groups, the methyl groups are highly hindered if for molecules packed in crystals, the tunneling gap being smaller than 30  $\mu\text{eV}$  and often widely spread. Particularly interesting exceptions are the 1,3-dihalogeno and 1,3,5-trihalogeno-2,4,6-trimethyl-benzenes (mesitylene derivatives). The crystal cell of 1,3-dibromo (DBM) is monoclinic  $P2_1/n$ , the methyls Me4 and Me6 are hindered, but unexpectedly, the Me2 between the two bromines is a quasi free rotor with a tunnelling gap of 390  $\mu\text{eV}$  if hydrogenated, and of 68  $\mu\text{eV}$  if deuterated. The hindering potential of Me2 is the same in the two cases: it has a main sixfold component equal to 18  $\text{meV}$  and a smaller threefold of 5  $\text{meV}$ . In triclinic tribromo (TBM) and triiodo-mesitylene (TIM), the three methyls are distinct and moderately hindered: gaps 49, 24 and 15 in TBM and 89, 25 and 15  $\mu\text{eV}$  in TIM.

For better understanding the relative influences of molecular symmetry and crystal packing we have synthesized 1,3-dibromo-5-iodo-mesitylene (dBIM) and 1-bromo-3,5-diiodo-mesitylene (BdIM). For these materials, the crystal cell is triclinic like TBM, there is a disorder in the position of the 1, 3, 5 halogens: molecules are jumping by  $120^\circ$  steps in the crystal at 293 K. A search of tunnelling peaks in the range -25+25  $\mu\text{eV}$  on SPHERES was unsuccessful.

The spectra on TOFTOF have revealed broad tunnelling contributions, with at least two components around 150 and 250  $\mu\text{eV}$ , for BdIM, around 150 and 300 for dBIM and widths larger than 50  $\mu\text{eV}$ . It has been tried calculations using atom-atom interactions to explain the different potentials seen by the Me groups.

## 13 Soft Matter

### P-66 A SANS investigation of sodium salt effects on dodecyl phosphocholine micelles

Epameinondas Leontidis<sup>1</sup>, Maria Christoforou<sup>1</sup>

<sup>1</sup>University of Cyprus, Chemistry, Nicosia, Cyprus

Understanding salt effects in appropriate model systems may solve the age-old puzzle of specific salt effects in Chemistry and Biology. Here we use the zwitterionic micelles of dodecyl phosphocholine (DPC) as such a system. DPC micelles are used as a membrane model to solubilize and examine membrane proteins using NMR and other solution-based methods. In our work we investigate the micelles with SANS in the presence of various concentrations of sodium salts with anions spanning the Hofmeister or lyotropic series (Cl, Br, NO<sub>3</sub>, ClO<sub>3</sub>, I, BF<sub>4</sub>, SCN, ClO<sub>4</sub>, PF<sub>6</sub>). The goal is to obtain the surface potential of the micelles and use it as a measure of ion binding. Fitting appropriate electrostatic models will allow to obtain the interaction constants of the ions with the micelle, and thus provide a quantitative measure for the Hofmeister effect in lipid systems. Such a measure has already been provided using phospholipid monolayers at the air-water surface as model systems.

[1] E. Leontidis et al., J. Phys. Chem. B 113, 1447 (2009). [2] E. Leontidis et al., J. Phys. Chem. B 113, 1460 (2009). [3] A. Aroti et al., Biophys. J. 93, 1580-1590 (2007). [4] E. Leontidis et al., Biophys. J. 93, 1591-1607 (2007). [5] Th. Zemb et al., Curr. Opin. Colloid Int. Sci. 9, 74-80 (2004).

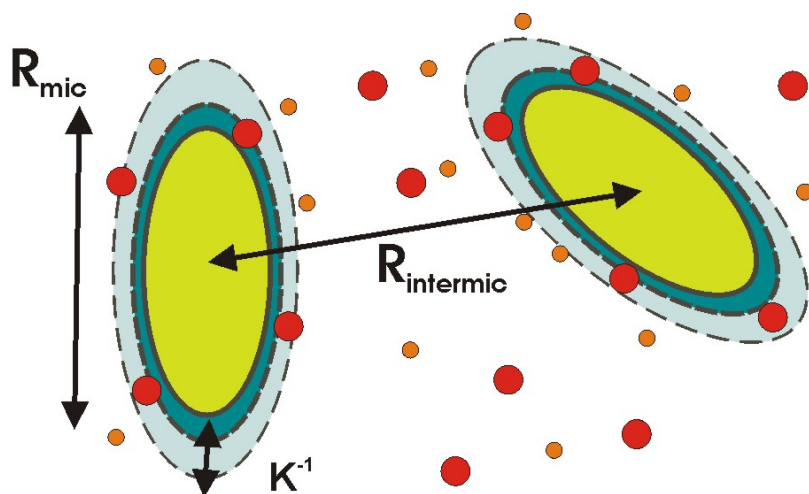


Figure 13.1: Ellipsoidal DPC micelles interacting in a solution containing an adsorbing salt

### P-67 Structural control of conjugated block copolymer films via addition of homopolymer

Matthias A. Ruderer<sup>1</sup>, Robert Meier<sup>1</sup>, Jan Perlich<sup>1</sup>, Gunar Kaune<sup>1</sup>, Robert Cubitt<sup>2</sup>, Martin Haese-Seiller<sup>3</sup>, Reinhard Kampmann<sup>3</sup>, Peter Müller-Buschbaum<sup>1</sup>

<sup>1</sup>TU München, Physik Department E13, Germany

<sup>2</sup>ILL, Grenoble, France

<sup>3</sup>GKSS-Forschungszentrum Geesthacht, Germany

Conjugated polymers have shown to be interesting candidates for organic photovoltaics due to their high absorption coefficient and easy processibility. Nevertheless there are stringent constraints in the morphology of the active layer due to the short exciton diffusion length (on the order of 10 nm). While polymer blends tend to form structure sizes in the range of hundred nanometers, one promising approach are conjugated block copolymers which generate nanostructures in the desired range due to micro-phase separation. [1] To adapt the morphology matching the desired spatial dimensions via the synthesis of block copolymers with different block lengths is therefore a tedious work. Instead of changing the composition of the block copolymer, an alternative approach is offered by blending the conducting block copolymer with a homopolymer which is equal to one of the blocks to adapt the morphology and match the desired spatial dimensions. A diblock copolymer P(S-b-P) with a rigid conjugated block of poly(para-phenylene) and a conventional coiled block of polystyrene is focused. We investigate the structural changes due to blending this block copolymer with deuterated polystyrene (d8-PS) of smaller degree of polymerization using the non destructive methods grazing incidence small angle neutron scattering (GISANS) and neutron reflectivity.[2] Due to deuteration the scattering contrast is increased. The detected lateral structure is independent of the fraction of d8-PS. We found that with increasing ratio of d8-PS an enrichment layer of d8-PS at the free interface is formed (see figure). In a photovoltaic device this will act as a blocking layer for one type of charge carrier. The investigations are completed with AFM and UV/Vis measurements. [3]

[1] S. Günes et al., Chem. Rev. 107, 1324 (2007). [2] P. Müller-Buschbaum et al., Langmuir 22, 9295 (2006) [3] M.A. Ruderer et al., in preparation.

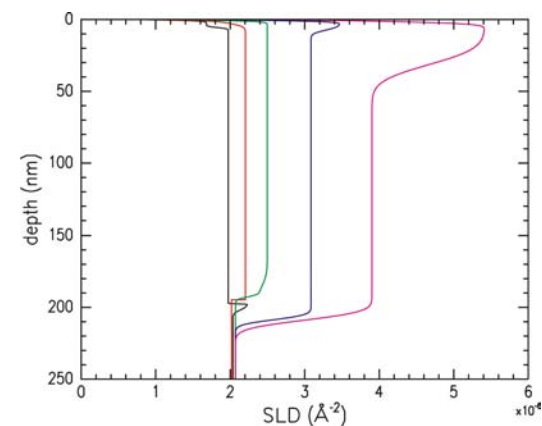


Figure 13.2: Scattering length density profile obtained from neutron reflectivity measurements of P(S-b-P):d8-PS films with different ratios of d8-PS. The ratio of d8-PS is increasing from 1 % (black solid line) to 50 % (magenta solid line). The ordinate represents the depth of the film, i.e. at 0 nm is the film surface.

## P-68 Characterization and swelling kinetics of PNIPAM based block copolymer films

Weinan Wang<sup>1</sup>, Jan Perlich<sup>1</sup>, Gunar Kaune<sup>1</sup>, Peter Müller-Buschbaum<sup>1</sup>, Christine M. Papadakis<sup>1</sup>, Achille Mayelle Bivigou Koumba<sup>2</sup>, André Laschewsky<sup>2</sup>

<sup>1</sup>TU München, Physik Department E13, Germany

<sup>2</sup>Universität Potsdam, Institut für Chemie, Germany

Poly(N-isopropylacrylamide) (PNIPAM) is one of the prominent stimuli-sensitive hydrogels for the construction of nanoscale sensors which are sensitive to water and to water vapour (humidity). To introduce an internal ordering and increase the mechanical stability in the films, the homopolymer is typically replaced by PNIPAM based block copolymers.

We focus on how the internal structures and the transition kinetics of such polymer films depend on the polymer composition and film thickness. The films are freshly made by spin coating. The surface and internal structure of the dry films are characterized with grazing incidence small angle neutron scattering (GISANS). The temperature dependent swelling and switching kinetics in water vapour of such sensor films is probed by in-situ neutron reflectometry. In addition, atomic force microscopy (AFM) and x-ray reflectivity are used for characterization.

The results of these experimental methods are in good agreement with each other.

[1] W. Wang, et al.; *Macromolecules* 41, 3209-3218 (2008) [2] W. Wang, et al.; *Macromol. Rap. Com.* 30, 114-119 (2009) [3] K. Troll, et al.; *Colloid Polym. Sci.* 286, 1079-1092 (2008)

## P-69 Structural investigation of diblock copolymer thin films using TOF-GISANS

Ezzeldin Metwalli<sup>1</sup>, Jean-François Moulin<sup>2</sup>, Markus Rauscher<sup>3</sup>, Gunar Kaune<sup>1</sup>, Matthias A. Ruderer<sup>1</sup>, Uwe van Bürck<sup>1</sup>, Martin Haese-Seiller<sup>2</sup>, Reinhard Kampmann<sup>2</sup>, Winfried Petry<sup>4</sup>, Peter Müller-Buschbaum<sup>1</sup>

<sup>1</sup>TU München, Physik Department E13, Germany

<sup>2</sup>GKSS-Forschungszentrum Geesthacht, Germany

<sup>3</sup>MPI für Metallforschung, Stuttgart, Germany

<sup>4</sup>Forschungs-Neutronenquelle Heinz Maier-Leibnitz (FRM II), München, Germany

The structure of a polystyrene (deuterated)-block-polyisoprene diblock copolymer thin film at various film depths, from the solid-polymer interface through the film bulk to the air-polymer interface, is simultaneously probed in a single measurement using the TOF-GISANS technique.

By utilizing the material characteristic Yoneda peak positions parallel to the normal of the polymer film, information about the enrichment at both interfaces with one or the other block is gained. For the polymer film attached to the low surface energy ( $36 \text{ mJ} \cdot \text{m}^{-2}$ ) amino-silane coated silicon substrate, a morphology transition from lamella to perforated lamella and finally to an ill-defined structure along the film normal is observed. The surface reconstruction of the polymer film does not seem to extend over the whole film thickness. Due to the competition between the stable cylinder morphology and the reorientation of the domains under the influence of the surface field, an ill-defined structure of the top most layers is observed. For the clean and untreated surface of silicon ( $63 \text{ mJ} \cdot \text{m}^{-2}$ ), a disordered pattern of the polymer film without any distinct morphology is mainly attributed to the absence of any specific interaction between the polymer components and the substrate.

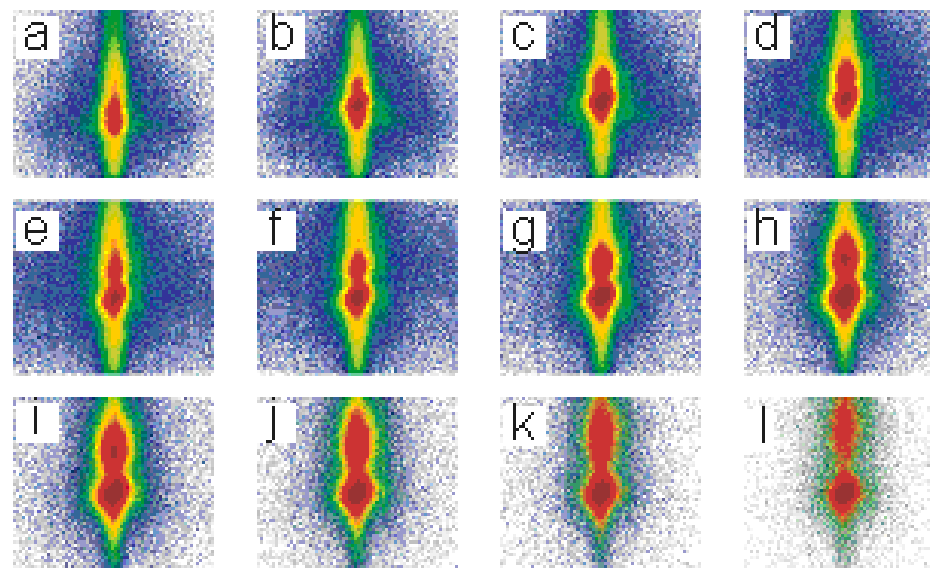


Figure 13.3:

## P-70 Experiments at the neutron reflectometer REFSANS to study supported phospholipid bilayers systems

Stefan Stanglmaier<sup>1</sup>

<sup>1</sup>LMU München, Fakultät für Physik, Experimentalphysik, Germany

An alignment strategy has been established, which allows verifying for sample parallelism respect to the incident beam, for detector-sample distance and for triggering of the chopper. Also first experiments confirm the flexibility of the choppersystem allowing for changing between high flux to high resolution.

For the reflectivity measurement of an extended  $q$ -range a silicon oxide film was used for the reflectometry at different incident-angles. Finally a solid supported lipid bilayer in  $D_2O$  was used as a benchmark for the signal-to-noise ratio.

First a bare Si wafer in  $D_2O$  and then a partly deuterated lipid bilayer in  $D_2O$  was measured. After this a glycolipid (GM1) was injected to the  $D_2O$  phase of the bilayer and after incubation time a neutron reflectometry measurement was started. previous measurement using hard x-rays have indicated that GM1 inserts spontaneously into the distal leaflet of the bilayer. The amount of GM1 intercalated into the distal leaflet is extracted from the observed scattering length density change in the neutron reflectivity measurement.

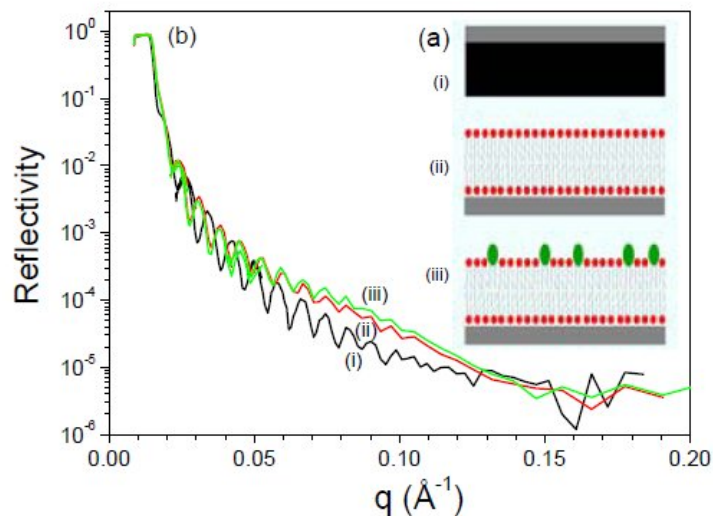


Figure 13.4: (a) Schematic of the sample states. (i) Bare wafer in  $D_2O$ . (ii) Supported bilayer in  $D_2O$ . (iii) Bilayer with GM1 incorporated. (b) Corresponding neutron reflectivity curves.

## P-71 Spinodal decomposition of PNIPAM solutions investigated with time-resolved SANS

Andreas Meier-Koll<sup>1</sup>, Anastasia Golosova<sup>1</sup>, Joseph Adelsberger<sup>1</sup>, Weinan Wang<sup>1</sup>, Peter Busch<sup>2</sup>, Vitaliy Pipich<sup>2</sup>, Peter Müller-Buschbaum<sup>1</sup>, Christine M. Papadakis<sup>1</sup>

<sup>1</sup>TU München, Physik Department E13, Germany

<sup>2</sup>Jülich Centre for Neutron Science, Outstation at FRM II, München, Germany

Aqueous poly(*N*-isopropylacrylamide) (PNIPAM) solutions show a phase separation transition at the lower critical solution temperature (LCST). Below this temperature the polymer binds water molecules into its network which leads to a swelling of the polymer. If the LCST is crossed, the polymer becomes hydrophobic and hence releases bounded water again. In highly concentrated polymer solutions the released water and the polymer form bicontinuous structures.

In the present study we investigated phase separation of a solution of a PNIPAM homopolymer and  $D_2O$  by SANS. In order to determine the characteristics of the phase transition, we performed temperature-dependent measurements in the temperature range from 15 to 45 °C (see figure). Below the LCST, the scattering profiles exhibit an Orstein-Zernicke (OZ) behavior. Both the OZ amplitude and the OZ correlation length show a power law behavior with a singularity at LCST. At the transition point, the curves are characterized by a Porod law typical for the formation of sharp interfaces between phase domains. The consecutive coarsening of the bicontinuous structure manifests itself in a decrease of the forward scattering. The kinetics of this process was investigated by performing deep temperature quenches from 20 to 45 °C. Time-resolved SANS curves show that the early stage of the decomposition with the creation of interfacing boundaries is finished within the first 2 min. The later coarsening can be subdivided into an intermediate (<10 min) and a late stage. In both time regimes the evolution of the interfaces follow power laws with exponents -1.03 and -1.87. These exponents correspond to a surface and a gravitation driven coarsening.

[1] H.G. Schild, Prog. Polym. Sci. 17, 163 (1992) [2] A. Meier-Koll, A. Golosova, P. Busch, V.Pipich, J. Wiedersich, C.M. Papadakis, P. Müller-Buschbaum; to be published

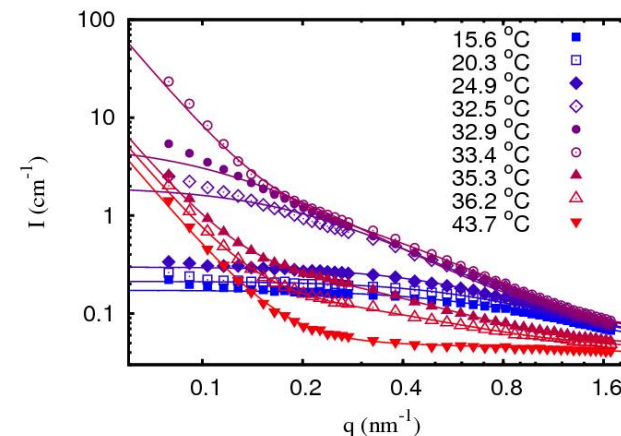


Figure 13.5: Temperature-dependent SANS curves in double-logarithmic representation. Continuous lines are fits.

## Index

- Adams, Tim, **69**  
 Adelsberger, Joseph, **15**, 96  
 Anwand, Wolfgang, 14, 87  
 Appavou, Marie-Sousai, **25**  
 Aynajian, Pegor, 64, 89
- Böni, Peter, 5, 10, 41, 46, 67–69  
 Bücherl, Thomas, 12, **42**  
 Büchner, Bernd, 63  
 Bauer, Ernst, 6  
 Baum, Max, **73**  
 Bayrakci, Sibel, 64  
 Becker-Bohaty, Petra, 73  
 Beddoe, Robin E., 80  
 Belgya, Tamás, 37  
 Berger, Rüdiger, 18  
 Bernlochner, Florian, 68  
 Binz, Benedikt, 10, 69  
 Birke, Michael, 19  
 Bivigou Koumba, Achille Mayelle, 15, 83, 93  
 Boehm, Martin, 8  
 Boeri, Lilia, 89  
 Boharty, Ladislav, 73  
 Bourges, Philippe, 7  
 Boysen, Hans, 35  
 Braden, Markus, 73  
 Bramwell, S.T., 71  
 Brandl, Georg, 46  
 Brauer, Gerhard, 14, 87  
 Brokmeyer, Heinz-Günter, 34, 58  
 Buchner, Kathrin, 38, 64  
 Busch, Peter, 15, 96  
 Busch, Sebastian, 49
- Calzada, Elbio, 5  
 Campbell, Stewart, **66**  
 Canella, Lea, **36**, 37, 51, 60  
 Ceeh, Hubert, 48  
 Chang, Johan, 8  
 Chow, K.H., 71  
 Christensen, Niels Bech, **8**  
 Christoforou, Maria, 91  
 Cizek, Jakob, **14**, **87**  
 Clancy, J.P., 71  
 Copley, J.R.D., 71  
 Cubitt, Robert, 92
- Dabkowska, H.A., 71  
 Danilyan, Gevorg, **54**  
 Davydov, Vadim, 85  
 De Beer, Frikkie, 75  
 de Souza, Nicolas R., 30  
 del Genovese, Dominique, 85  
 Dollinger, Günther, 48  
 Dosch, Helmut, 38, 45  
 Duine, Rembert, 67  
 Dunsiger, S.R., 68, **71**
- Eberth, Martin, 37  
 Egelhaaf, Stefan U., 17  
 Egger, Werner, 14, 48, 84, 87  
 Ehrenberg, Helmut, 88  
 Ener, Semih, 86  
 Ewert, Uwe, 12
- Faulhaber, Enrico, 65  
 Fernandez-Diaz, M. Teresa, 73  
 Festa, Giulia, 37  
 Franke, Joergen, 38  
 Franz, Christian, 5, 69, **70**  
 Frei, Gabriel, 17  
 Frey, Fritz, 44  
 Fritz, Kirstin, 23  
 Fueß, Hartmut, 4, 28, 35, 88
- Gan, W.M., 34  
 Gan, Weimin, **58**  
 Gardner, J.S., 71  
 Gaulin, B.D., 71  
 Gemma, Ryota, 14  
 Georgii, Robert, 10, **46**, 69  
 Gernhäuser, Roman, **3**  
 Gilles, Ralph, 11, **31**, 62, 85  
 Gobin, Oliver C., 28  
 Goerigk, Guenther, **43**  
 Golosova, Anastasia, 96  
 Grabmayr, Peter, 51  
 Grin, Juri, 69  
 Guo, Jimei, 42  
 Gutberlet, Tobias, **80**  
 Gutmann, Jochen S., 18
- Häußler, Wolfgang, 41  
 Haese-Seiller, Martin, 29, 59, 79, 83, 92, 94

- Hain, Karin, 48  
 Hamann Borrero, Jorge, 63  
 Hasenstab, Andreas, 12  
 Haug, Daniel, 7  
 Havranek, Vladimir, 87  
 Heger, Gernot, 40, 47, 72  
 Heim, Sabine, 61  
 Hellweg, Thomas, 15, **16**  
 Hermes, Helen E., **17**  
 Hertrich, Samira, 23, **24**  
 Hess, Christian, 63  
 Hiess, Arno, 8  
 Hilbig, Harald, 80  
 Hilger, André, 5  
 Hinkov, Vladimir, 7  
 Hinterstein, Manuel, **4**  
 Hoelzel, Markus, 4, 28, 32, **35**, 85  
 Hofmann, Michael, 11, 32, 34, 85  
 Holderer, Olaf, 15, **30**  
 Hradil, Klaudia, 7, 86  
 Hugenschmidt, Christoph, 14, **48**, 87  
 Hutanu, Vladimir, **40**, 47, 72  
 Huxley, Andrew, 6
- Ido, Masayuki, 8  
 Inosov, Dmytro, **7**
- Jünke, Norbert, 4, 35  
 Janoschek, Marc, **68**  
 Janus, Andreas, 28  
 Jechow, Mirko, 12  
 Jenkins, T., 71  
 Jentys, Andreas, 28  
 Jochum, Josef, 51  
 Jolie, Jan, 36, 37, 51  
 Jonietz, Florian, 10, **67**, 69  
 Jurisch, Anke, **61**
- Kästner, Anders, 17  
 Kögel, Gottfried, 48  
 Kampmann, Reinhard, 29, **59**, 79, 83, 92, 94  
 Kardjilov, Nikolay, 5  
 Katsavounis, Stefanos, 81  
 Kaune, Gunar, **79**, 92–94  
 Keimer, Bernhard, 7, 38, 64, 89  
 Keller, Thomas, 6, 38, **64**, 89  
 Kentzinger, Emmanuel, 43  
 Kenzelmann, Michel, 9  
 Khafizov, Rashid, **52**  
 Kiefl, R.F., 71  
 Kindervater, Jonas, 41  
 Kirchheim, Reiner, 14  
 Kirschner, Jürgen, 19  
 Kis, Zoltan, 37
- Klein, Wilhelm, 44  
 Klenke, Jens, **53**  
 Kolesnikov, Ivan, 52  
 Kolkhidashvili, Madlen, 52  
 Komarek, Alexander C., 73  
 Konorov, Igor, 52  
 Koutridou, Anastasia, 81  
 Kreuzpaintner, Wolfgang, **29**, 59  
 Krooss, Bernhard M., 61  
 Krsjak, Vladimir, 84  
 Kudejova, Petra, 36, 37, 51, 60
- Löwe, Benjamin, 48  
 Landee, Christopher, 9  
 Laschewsky, André, 15, 83, 93  
 Lefmann, Kim, 8  
 Lehmann, Eberhard, 17  
 Lenz, Sebastian, **18**  
 Leontidis, Epameinondas, **91**  
 Leps, Norman, 63  
 Lercher, Johannes A., 28  
 Lichtinger, Josef, 3  
 Lierse von Gostomski, Christoph, 42  
 Lin, Chengtian, 7  
 Link, Peter, 8, 9, 65, 68, 73, 86  
 Loewenhaupt, Michael, 65  
 Lott, Dieter, 29, 59
- Mühlbauer, Martin, 5  
 Mühlbauer, Sebastian, **10**, 67, 69  
 Müller, Martin, 34, 59  
 Müller-Buschbaum, Peter, 15, 59, 79, 83, 92–94, 96  
 Münzer, Wolfgang, 69  
 Major, Janos, 38, 45  
 Major, Marton, 45  
 Masalovich, Sergey, **33**  
 Mayer, Jakob, 48  
 McMorrow, Des, 8  
 Meier, Robert, 92  
 Meier-Koll, Andreas, 15, **96**  
 Meierhofer, Georg, **51**  
 Meinel, Jean, **90**  
 Melikhova, Oksana, 14, 87  
 Merkel, Casjen, **32**  
 Mesot, Joel, 8  
 Metwalli, Ezzeldin, **94**  
 Meven, Martin, 40, **47**, 63, 72, 73  
 Mikhailova, Daria, 88  
 Mohamed, Ashraf Elsayed, **57**  
 Mole, Richard A., 86  
 Momono, Naoki, 8  
 Monkenbusch, Michael, 30, 39  
 Morris, G.D., 71

Mottl,Rafael, 8  
 Moulin,Jean-François, 29, 59, 94  
 Moumtzi,Vasiliki-Fotis, 82  
 Mukherji,Debashis, **11**, 56, 62, 85  
 Munnikes,Nathalie, 64, **89**

Nülle,Max, 45  
 Narayanan,Narendrakumar, **88**  
 Neubauer,Andreas, 5, 10, 69  
 Neuhaus,Jürgen, 49, **86**  
 Nickel,Bert, **23**, 24, 59  
 Niedermayer,Christof, 8  
 Niewa,Rainer, 60  
 Niklowitz,Philipp, 6

Oda,Migaku, 8  
 Ohl,Manfred, 64  
 Osterloh,Kurt, **12**  
 Ostermann,Andreas, **39**, 44

Pailhes,Stephane, 8  
 Palacios Gómez,Jesús, **55**  
 Papadakis,Christine M., 15, 83, 93, 96  
 Park,Jitae, 7  
 Paul,Amitesh, **77**  
 Pedersen,Bjoern, **44**  
 Perlich,Jan, 92, 93  
 Petry,Winfried, 31, 39, 49, 86, 94  
 Pfeiffer,Franz, **76**  
 Pfeleiderer,Christian, 5, 6, 10, 64, 67–69  
 Pigozzi,Giancarlo, **62**  
 Pikart,Philip, 48  
 Piochacz,Christian, 48  
 Pipich,Vitaliy, 15, 96  
 Pomm,Matthias, 59  
 Price,A.N., 71  
 Prochazka,Ivan, 14, 87  
 Prokofiev,Andrej, 6  
 Pundt,Astrid, 14

Qiu,Y., 71  
 Qureshi,Navid, 73

Rädler,Joachim, 23  
 Rösler,Joachim, 11, 56, 85  
 Rühm,Adrian, 18, **38**, **45**  
 Rønnow,Henrik, 8, 9  
 Radebe,Mabuti, **75**  
 Rajewska,Aldona, **78**  
 Randau,Christian, **34**, 58  
 Rauscher,Markus, 94  
 Reitmeier,Stephan J., **28**  
 Richter,Dieter, 25, 30, 39  
 Ritz,Robert, **6**

Roessli,Bertrand, 68  
 Rosch,Achim, 10, 67–69  
 Roth,Georg, 63  
 Ruderer,Matthias A., **92**, 94  
 Ruff,J.P., 71

Söllradl,Stefan, **60**  
 Sandhofer,Mathias, **41**  
 Sazonov,Andrew, 40, 47, **72**  
 Schillinger,Burkhard, 17  
 Schmahl,Wolfgang, **13**, 28, 32, 35  
 Schmid,Martin, 69  
 Schmidt,Mathias, 45  
 Schmiele,Martin, 49  
 Schmitz,Fabian, **56**  
 Schneider,Gerald J., 27  
 Schneidewind,Astrid, 7–9, **65**, 73  
 Schreckenbach,Klaus, 48  
 Schreyer,Andreas, 29, 31, 34, 59  
 Schulz,Michael, **5**, 17  
 Schulze,Ralf, 36, **37**  
 Schumann,Frank Oliver, **19**  
 Schwikowski,Reinhard, 46  
 Seidl,Günther, 32  
 Senyshyn,Anatoliy, 35, 88  
 Sidis,Yvan, 7  
 Simeoni,Giovanna Giulia, **49**  
 Siouris,Ioannis, **81**, **82**  
 Slugen,Vladimir, **84**  
 Smuda,Christoph, 49  
 Sojak,Stanislav, 84  
 Sokolov,Dmitry, 6  
 Solovei,Valery, 52  
 Sonier,J.E., 71  
 Sparta,Karine, **63**  
 Sperr,Peter, 14, 48, 87  
 Störmer,Michael, 29  
 Stanglmaier,Stefan, 23, **95**  
 Stockert,Oliver, 65  
 Strunz,Pavel, 11, **85**  
 Sun,Dunlu, 7  
 Szentmiklósi,László, 37

Türler,Andreas, 36, 37, 60  
 Tekouo,William, 34  
 Tolokonnikov,Sergey, 52  
 Torokhov,Vladimir, 52  
 Trots,Dmytro, 88  
 Tsyruilin,Nikolay, **9**  
 Turnbull,Mark, 9

Unruh,Tobias, 49

van Bürck,Uwe, 94

van Riessen,Grant, 19

Wang,Jianli, 66  
 Wang,Weinan, 15, 83, **93**, 96  
 Winkler,Carsten, 19  
 Wizent,Nadja, 63  
 Woodward,Matthew, 9  
 Wuttke,Joachim, **27**

Xiao,Fan, 9

Zhong,Qi, 79, **83**  
 Zscherpel,Uwe, 12